UNIVERSIDADE FEDERAL DE ALAGOAS
INSTITUTO DE FÍSICA
PROGRAMA DE PÓS-GRADUAÇÃO EM FÍSICA – DOUTORADO

ELLENA JULIANA LINS DE OLIVEIRA

Surface and Electric Field Effects on Phase Transitions in Smectogenic Systems Involving the Smectic-C Phase

Maceió - 2021

ELLENA JULIANA LINS DE OLIVEIRA

Surface and Electric Field Effects on Phase Transitions in Smectogenic Systems Involving the Smectic-C Phase

Thesis submitted to the Physics Institute of the Federal University of Alagoas as a necessary requirement for obtaining the title of Doctor of Physics.

Advisor:
Prof. Dr. Italo Marcos Nunes de Oliveira
Co-advisor:
Prof. Dr. Maria Socorro Seixas Pereira

Maceió - 2021

Universidade Federal de Alagoas
Instituto de Física
Programa de Pós Graduação em Física

BR 104 km 14. Campus A.C. Simões
Cidade Universitária
Tabuleiro dos Martins
57072-970 Maceió - AL. Brasil
FONE : (82) 3214-1423/FAX 3214-1645

PARECER DA BANCA EXAMINADORA DE DEFESA DE

TESE DE DOUTORADO

"*Efeitos de superfícies e de campo elétrico sobre transições de fase em sistemas esmetogênicos envolvendo a fase esmética-C*"

por

Ellena Juliana Lins de Oliveira

A Banca Examinadora composta pelos professores Italo Marcos Nunes de Oliveira (orientador e presidente da banca), do Instituto de Física da Universidade Federal de Alagoas; Maria Socorro Seixas Pereira, do Instituto de Física da Universidade Federal de Alagoas; Solange Bessa Cavalcanti, do Instituto de Física da Universidade Federal de Alagoas; Fernanda Selingardi Matias, do Instituto de Física da Universidade Federal de Alagoas; Dora Izzo, da Universidade Federal do Rio de Janeiro; e Roberta Rarumy Ribeiro de Almeida, da Universidade Tecnológica Federal do Paraná, consideram a candidata **aprovada com grau " A ".**

Maceió, 22 de outubro de 2021.

Prof. Dr. Italo Marcos Nunes de Oliveira

gov.br
Documento assinado digitalmente
ITALO MARCOS NUNES DE OLIVEIRA
Data: 25/03/2024 11:32:18-0300
Verifique em https://validar.iti.gov.br

Profª. Drª. Maria Socorro Seixas Pereira

gov.br
Documento assinado digitalmente
MARIA SOCORRO SEIXAS PEREIRA
Data: 18/03/2024 10:16:51-0300
Verifique em https://validar.iti.gov.br

Profª. Drª. Solange Bessa Cavalcanti

gov.br
Documento assinado digitalmente
SOLANGE BESSA CAVALCANTI
Data: 17/03/2024 11:01:53-0300
Verifique em https://validar.iti.gov.br

Profª. Drª. Fernanda Selingardi Matias

gov.br
Documento assinado digitalmente
FERNANDA SELINGARDI MATIAS
Data: 15/03/2024 10:34:18-0300
Verifique em https://validar.iti.gov.br

Profª. Drª. Dora Izzo

gov.br
Documento assinado digitalmente
DORA IZZO
Data: 21/03/2024 15:05:35-0300
Verifique em https://validar.iti.gov.br

Profª. Drª. Roberta Rarumy Ribeiro de Almeida

gov.br
Documento assinado digitalmente
ROBERTA RARUMY RIBEIRO DE ALMEIDA
Data: 22/03/2024 09:23:22-0300
Verifique em https://validar.iti.gov.br

Acknowledgments

I don't know if I have reached the place that my past self hoped to reach, but I can say that my present self is very proud of the process that brought me here. Those who know me well enough are aware that I have always had a difficult relationship with physics. So I would like to thank all those who have been part of this journey. It has been a long journey, so it will be impossible to summarise all my gratitude in a few words. Nevertheless, I will try...

Thank you to my advisor, Italo, my 'papis' and above all, my friend. Thank you for everything you have taught me, as a professor, as an advisor and as a person. Thank you for encouraging and supporting me in these 10 years. Thank you for making me feel safe and welcome, especially during my outbreaks, which were not few. And most importantly, thank you for giving me a second family.

Thank you to my co-advisor, Socorro, for always being hardworking, understanding, kind, loving, and with such wonderful energy. You have always been an inspiration.

Thank you to the collaborator and also my friend, Evangelista, for the contributions to this work and above all for the always cheerful conversations.

Thank you to all the professors of the Institute of Physics who have contributed in some way to my development as a professional and as a person, whether inside or outside the classroom. I will not be able to do justice to all that I owe to you here. A special thanks to Professor Heber, aka Hebinho, for having introduced me to one of my passions, computing, through computational physics. This work would not have been the same without your training. And of course, for always arriving with an contagious smile and a 'Bom dia!' that really made that day good. Other special thanks here to (and I put them in alphabetical order because I just can't sort them): Fernanda, Iram, Marcelo, Maria Tereza, Sérgio, Solange, Thiago, Wagner, and Wandearley. Iram, thank you for thinking of me for ICTP's school a few years back, that trip changed my life in so many ways. Thank you, truly.

Thank you to my many course mates from IF-UFAL: Danilo, Eduardo, Luciano, Michele, Luan, Luís Felipe, Douglas, may you rest in peace, Henrique, Anderson. And the list goes on and on, that's what happens when you put down roots somewhere.

Thank you to my more recent physicists friends, but who I already consider special, Nicolas and Paulo. Thank you for the very pleasant conversations.

"But I don't want to go among mad people," Alice remarked.
"Oh, you can't help that," said the Cat. "We're all mad here. I'm mad. You're mad."
"How do you know I'm mad?" said Alice.
"You must be," said the Cat, "or you wouldn't have come here."

Alice in Wonderland
~ Lewis Carroll ~

Resumo

Esta tese investiga os efeitos da superfície e de tamanho finito nas transições de fase de filmes livremente suspensos e os efeitos de campo elétrico no bulk na fase esmética-C. Inicialmente, é feita uma revisão dos modelos microscópicos existentes e amplamente utilizados para a descrição das transições de fase em sistemas lineares apresentando fases nemática e esmética-A. Em seguida, revisamos o modelo desenvolvido por Govind e Madhusudana, descrevendo a transição de fase do esmética-C–esmética-A. Motivados por sua abordagem, propomos um novo modelo teórico para descrever as transições de fase em sistemas que apresentam a fase esmética-C. Usando um potencial de campo médio para uma partícula, mostramos que o diagrama de fase de compostos líquidos-cristalinos com um pequeno dipolo transversal pode ser razoavelmente descrito quando a contração das camadas esméticas induzida pela inclinação das moléculas é considerada e com um número reduzido de parâmetros do modelo. Com o objetivo de estender o modelo proposto para filmes livremente suspensos, o modelo de McMillan-Mirantsev para filmes livremente suspensos na fase esmética-A é revisado. O modelo introduzido por Mirantsev mostra que o ancoramento superficial estabiliza a fase esmética para temperaturas acima da temperatura de transição do bulk. Considerando um perfil do ângulo de inclinação e uma versão discreta do potencial de campo médio para uma partícula, a interação do ancoramento superficial e os efeitos de tamanho finito afetam o comportamento dos parâmetros de ordem nos filmes livremente suspensos na fase esmética-C. A temperatura de transição mostra-se dependente do ordenamento da superfície e da espessura do filme. A ordem orientacional imposta pelo ancoramento superficial estabiliza o parâmetro de ordem de inclinação na superfície do filme acima da temperatura de transição esmética-C–esmética-A do bulk. As camadas superficiais consequentemente permanecem na fase de esmética-C, enquanto as camadas centrais sofrem uma transição de fase de esmética-C–esmética-A. O efeito de um campo elétrico externo é considerado em amostras no bulk da fase esmética-C, induzindo uma reorientação do vetor diretor possibilitando a supressão da fase isotrópica e o aparecimento de fases nemáticas residuais e induzidas pelo campo.

Palavras-chave: 1. Cristais líquidos. 2. Fase esmética-C. 3. Efeitos de superfície. 4. Efeitos de campo elétrico. 5. Transições de fase. 6. Filmes livremente suspensos.

Abstract

This thesis investigates surface and finite size effects on the phase transitions of free-standing smectic-C films and electric field effects in the bulk. Initially, a review is given of existing and widely used microscopic models for the description of phase transitions in liquid-crystalline systems presenting nematic and smectic-A phases. We then review the model developed by Govind and Madhusudana, describing the smectic-C–smectic-A phase transition. Motivated by their approach, we propose a new theoretical model to describe phase transitions in systems presenting the smectic-C phase. Using a single-particle mean-field potential, we show that the phase diagram of liquid-crystalline compounds with a small transverse dipole can be reasonably described when the tilt-induced contraction of smectic layers is considered and with a reduced number of model parameters. Aiming to extend the proposed model for freely suspended films, McMillan-Mirantsev's model for free-standing smectic-A films is reviewed. The model introduced by Mirantsev shows that surface anchoring stabilises the smectic phase for temperatures above the bulk transition temperature. Considering a tilt angle profile and a discrete version of the single-particle mean-field potential, the interplay of surface anchoring and finite size effects affects the behaviour of the order parameters in free-standing smectic-C films. The transition temperature is shown to depend on surface ordering and film thickness. The orientational order imposed by surface anchoring is shown to stabilise the tilt order parameter in the film surface above the bulk smectic-C–smectic-A transition temperature. Surface layers therefore remain in the smectic-C phase, while the central layers undergo a smectic-C–smectic-A phase transition. The effect of an external electric field is considered in smectic-C bulk samples, inducing a re-orientation of the director vector and thus enabling the suppression of the isotropic phase and the appearance of residual and field-induced nematic phases.

Keywords: 1. Liquid crystals. 2. Smectic-C phase. 3. Surface effects. 4. Electric field effects. 5. Phase transitions. 6. Free-standing films.

LIST OF FIGURES

CONTENTS

I

INTRODUCTION

In everyday life, we encounter matter in three different states of aggregation[1]: solid, liquid and gaseous. The constituents of organic and inorganic compounds are organised differently for each state. Crystalline solids are three-dimensional periodic networks, with long-range positional and orientational order, whereas isotropic liquids and gases present short-range order. Consequently, the former tends to not deform under shear stresses, whereas the latter tends to flow. These states are qualitatively distinguished with respect to the substances' components interactions and, consequently, its global structure and mobility. Transitions between states are characterised by discontinuities in thermodynamic variables such as entropy and volume, however certain organic compounds can undergo multiple transitions, via intermediate states between the crystalline solid and isotropic liquid phases. Each phase presents distinct mechanical, optical and structural properties. Materials exhibiting these properties are called mesogens and are characterised by geometrical or chemical, molecular anisotropies. The phases found between solid and liquid states are called mesophases[2] or more commonly, liquid crystals.

To understand liquid crystals, the concept of 'ordering' is crucial. Solid crystalline phase constituents are all spatially organised in a well-defined configuration, therefore showing long-range positional and orientational order. Isotropic liquid phase constituents have short-range positional and orientational order, and therefore diffusely flow. Liquids are isotropic, meaning their properties are invariant under rotation. In contrast, anisotropic compounds possess both positional and orientational order, i.e., a measurement returns different values when performed along different axes. Solid crystalline phases show both long-range orientational and positional order.

---

[1] From the Latin *aggrego* - collect, assemble.
[2] From the Greek *mesos morphe* - between phases.

Liquid crystals are characterised by long-range orientational order coexisting with different degrees of positional ordering. Consequently, various molecular organisations exist, giving rise to different liquid-crystalline phases.

The main feature of liquid crystals is their geometrical anisotropy. As a result, their optical, electrical and magnetic properties resemble crystalline solids, while their mechanical properties resemble isotropic liquids. Furthermore, liquid crystals can be classified into mesophases, distinguished by differences in symmetry and order.

1.1   Liquid Crystals: History

The first observation of liquid-crystalline behaviour dates from 1850, when German chemist Wilhelm Heintz observed two partial melting points in natural fats. However, the discovery of liquid-crystalline phases is often attributed to Austrian botanist Friedrich Reinitzer who, while heating a sample of cholesteryl benzoate (an 'ester' derived from carrots) in 1888, realised that the compound presented two distinct melting points [1, 2]. At 145.5° C, the solid melts into a cloudy liquid, and at 178.5° C, the liquid turns transparent. In addition, the phenomenon appeared to be reversible and exhibited singular colorations for both transitions. Reinitzer sent samples to Otto Lehmann [3], a German physicist, who then studied the compound using polarised light microscopy. He discovered that, in the presence of polarised light, the compound becomes crystal-like, leading him to propose the name liquid crystals.

A few years after Reinitzer's discovery, experiments were already being carried out to understand why the properties of liquid crystals changed in the vicinity of surfaces. In 1904, Otto Lehmann [4] successfully suspended tiny drops of nematic liquid crystals in a viscous material. He was the first to document what is now known as the 'Memory Effect', where the properties of confined liquid crystals reappear, after being removed by heating, and then cooled to the initial temperature.

In 1907, the German chemist Daniel Vorländer [5, 6] discovered that a linear and elongated molecular structure was a prerequisite for mesophases. In 1922, French mineralogist Georges Friedel [7] proposed the classification of liquid-crystalline phases into nematic, smectic and cholesteric. Friedel suggested that liquid crystal molecules could be oriented by an electric field, and also discussed the presence of defects.

In 1929, Vsevolod Fréedericks [8] presented his work on the competition between confining and electromagnetic forces in liquid crystals. After, in 1933, the idea of treating liquid crystals as

elastic materials was proposed by Carl Oseen [9, 10] and Hans Zöcher [11] by considering the molecules from a mechanical point of view. In 1958, Frederick Charles Frank [12] reformulated Oseen's theory in the so-called Continuous Theory, describing the elastic properties of liquid crystals. In 1942, V. Tsevtkov [13] introduced the orientational parameter, s, defined with respect to the average angle between a component molecule's axis and the system's global orientation.

In 1961, the physicists Wilhelm Maier and Alfred Saupe [14–16] formulated a microscopic theory relating molecular characteristics to liquid-crystalline phases. In the same decade, French physicist Pierre-Gilles de Gennes began his work on liquid crystals and noticed their similarities with superconductors and magnetic materials, on which he had previously worked. In 1991, de Gennes received the Nobel Prize in Physics for discovering that methods used to study ordering in simpler systems can be generalised to more complex systems, such as liquid crystals.

Experimental work carried out by Dreyer [17], Sheng [18, 19], Pieranski [20] and Jerome [21–24] considered liquid crystal ordering near surfaces. In 1971, Dreyer reported that rubbed surfaces can induce orientation in the nematic phase, suggesting that the alignment induced by surfaces is geometric in origin, rather than chemical or intermolecular.

Liquid crystals remain, to this day, an object of much research, mainly due to the numerous applications of compounds that present these mesophases.

1.2 Applications

The discovery of liquid crystals has had a huge impact on science, engineering and technology, with an undying stream of new applications. Their anisotropy allows electric and magnetic fields to manipulate their optical properties. The basis of the technological applications of liquid crystals is the possibility of light modulation by changing their optical properties.

The principal application of liquid crystals is liquid crystal displays, LCDs. The LCD industry emerged in the 1970s with displays for digital devices such as wristwatches and calculators. With the development of touch-sensitive LCD screens, a new generation of portable devices emerged, such as smartphones and tablets. In addition to displays, liquid crystals can also be used to measure temperature through the selective reflection property of cholesteric liquid crystals [25]. These reflect light with a wavelength equal to the pitch of the material, a property defined in Chapter 2. Since the pitch depends on the temperature, the reflected colour is also dependent on the temperature. In this way, liquid crystals can be used as temperature sensors.

Disposable liquid crystal thermometers, which are safer than their mercury equivalents, have been developed for medical and domestic use.

Another area in which liquid crystals have been widely used is Cosmology. Cosmological models of the early universe have topological defects resulting from phase transitions that occurred in the early moments of the universe. The formation of topological defects in liquid crystals is similar to that observed in cosmological models, making nematic liquid crystals a great tool for the study of the primordial universe [26].

A recent application of liquid crystals is the manufacture of materials with a negative refractive index, known as metamaterials. Optical metamaterials are a new class of materials with the potential for a variety of applications, including invisibility devices. Nanostructured materials based on nanoparticles and liquid crystals allow the manufacture of tunable metamaterials through the reorientation of nanoparticles in response to applied external fields [27, 28].

Thermally induced optical storage and erasure of scattering centres in thin films of smectic liquid crystals have been studied and are believed to be the first to demonstrate contrast and response times suitable for practical devices. Using thermo-optical effects, high-resolution graphic images can be thermally recorded and erased by a focused X-Y deflected intensity-modulated infrared laser beam. The liquid crystal may be locally heated, and therefore written on by steering the focused laser beam across the cell. The image can be viewed either by the naked eye through crossed polarisers, or with a simple aperture-type schlieren projection system [29].

The potential for technological applications of mesogen compounds is enormous and is continually increasing with recent research on the characteristics of their mesophases.

1.3 Thesis Overview

This work studies surface and finite size effects in phase transitions of free-standing smectic-C films and effects of applying external electric field on bulk samples.

Chapter 2 presents the general properties of liquid crystals, including their classification and their most common phases. Order parameters are introduced and some liquid-crystalline phase transitions are reviewed. Finally, surface and external field effects in the liquid-crystalline order are discussed.

Chapter 3 presents the main mean-field theories describing liquid crystal phase transitions, including the well-established Maier-Saupe and McMillan theories, for those involving the nematic and smectic-A phases respectively. The Govind-Madhusudana model is furthermore presented for phase transitions involving the smectic-C phase, which accounts for the dipolar origin of molecular tilt. Finally, we propose a theoretical model similar to Govind-Madhusudana's, but which explicitly consider the layer contraction in the formation of the smectic-C phase. This model satisfactorily describes phase transitions with a reduced number of free parameters.

Chapter 4 presents a description of phase transitions in free-standing films of compounds with a lateral transverse dipole. The main characteristics of free-standing films are presented, as well as a brief review of the McMillan-Mirantsev model for smectic-A films. Finally, we present our extension of this model by introducing the discrete version of the tilting potential. The tilt angle profile and surface anchoring is shown to stabilise the smectic-C film above the bulk smectic-C–smectic-A transition temperature in the outermost layers.

Chapter 5 presents a description of phase transitions of compounds with a lateral transverse dipole and its response to external electric fields. The contributions of the field-dipole interaction and of the molecular polarisability anisotropy are considered. The electric field is shown to influence the tilt angle and the order parameters for negative and positive polarisabilities. The isotropic phase is shown to be suppressed along with the appearance of residual and field-induced nematic phases.

Finally, Chapter 6 reviews the main results obtained and discusses perspectives for possible extensions of the work presented. The papers resulting from this thesis are in the appendixes.

<div align="right">

II

</div>

FUNDAMENTAL PROPERTIES OF LIQUID CRYSTALS

As aforementioned, liquid crystals are a state of matter encompassing multiple intermediary phases between solid crystalline and liquid isotropic and whose molecular structure largely determines their transition temperatures, as well as their optical and electro-optical properties. In general, liquid crystalline materials possess different molecular structures despite always being anisotropic. This chapter aims to study the fundamental properties of liquid crystals necessary to understand the theories and results presented in the following chapters.

2.1 Classification of Liquid Crystals

To this day, thousands of organic and synthetic compounds are known to present liquid crystalline phases whose transitions can be classified by the properties and behaviour of various physical parameters as well as on the environment surrounding them. In this context, there are two main classifications: lyotropic and thermotropic.

2.1.1 Lyotropic Liquid Crystals

Lyotropic[1] liquid crystals were first identified by German pathologist Rudolf Virchow [30] who while studying myelin, a structure that covers nerve fibres, in water using polarised light, observed birefringent textures.

---

[1] From the Greek *lyo* - dissolve and *tropic* - change.

Lyotropic liquid crystals are formed by dissolving an amphiphilic[2] compound (e.g. surfactants) in a suitable solvent. Although variations in temperature and pressure are influential, the components' concentrations are mainly responsible for creating lyotropic liquid crystals.

Amphiphilic compounds possess a hydrophilic head, which is highly soluble in water and other polar solvents, attached to a hydrophobic tail, which are soluble in non-polar solvents. At concentrations above the critical micellar concentration (CMC), the amphiphilic molecules self-organise into ordered aggregates. When dissolved in a polar solvent, typically an aqueous solution, the hydrophilic heads interact strongly with the solvent, while the hydrophobic tails are repelled by the solvent, forming micelles as shown in figure 2.1(a). Conversely, if the solvent is non-polar, the hydrophobic tails interact more strongly with the solvent which causes the hydrophilic heads to cluster, thus producing so-called reverse micelles, shown in figure 2.1(b).

Figure 2.1: Cross-sections of amphiphilic molecule producing (a) micelles and (b) reverse micelles.

(a)   (b)   Hydrophobic tail

Hydrophilic head
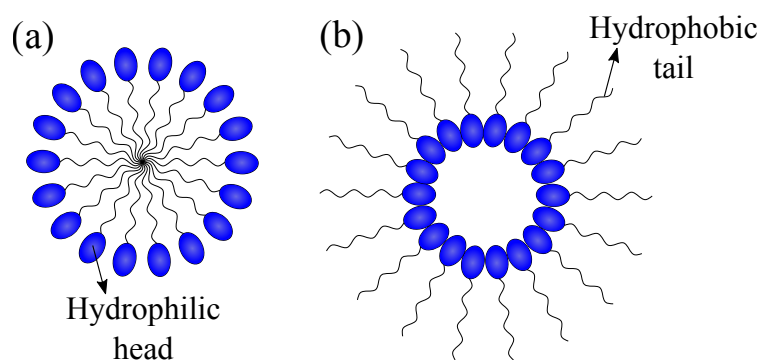
Source: Author, 2021.

Varying the concentration of amphiphilic molecules forms structures of varying complexity, of which some are shown in figure 2.2.

At low concentrations, only amphiphilic molecules are dispersed in a solvent. Above the CMC, the free amphiphilic molecules aggregate into spherical or cylindrical micelles. At yet higher concentrations, cylindrical micelles aggregate to a hexagonal lattice, presenting long-range orientational order. Cylindrical micelles can assume another spatial arrangement, where the micelles are located at the intersections of a square network. Sufficiently high concentrations of spherical micelles dispersed in a solvent packs them into a cubic structure possessing three-dimensional positional order. At even higher concentrations, amphiphilic molecules arrange themselves in bilayers, confining the solvent between lamellae, in what is called the lamellar phase. Additionally, depending on the type of solvent and the proportions of cylindrical micelles, inverted phases can also be observed, where the polar region of the molecule is inside the micelle.

[2]From the Greek *amphi* - both and *philic* - loves.

Figure 2.2: Phase diagram of lyotropic phases formed by amphiphilic molecules dissolved in a solvent, as a function of temperature and amphiphilic concentration.
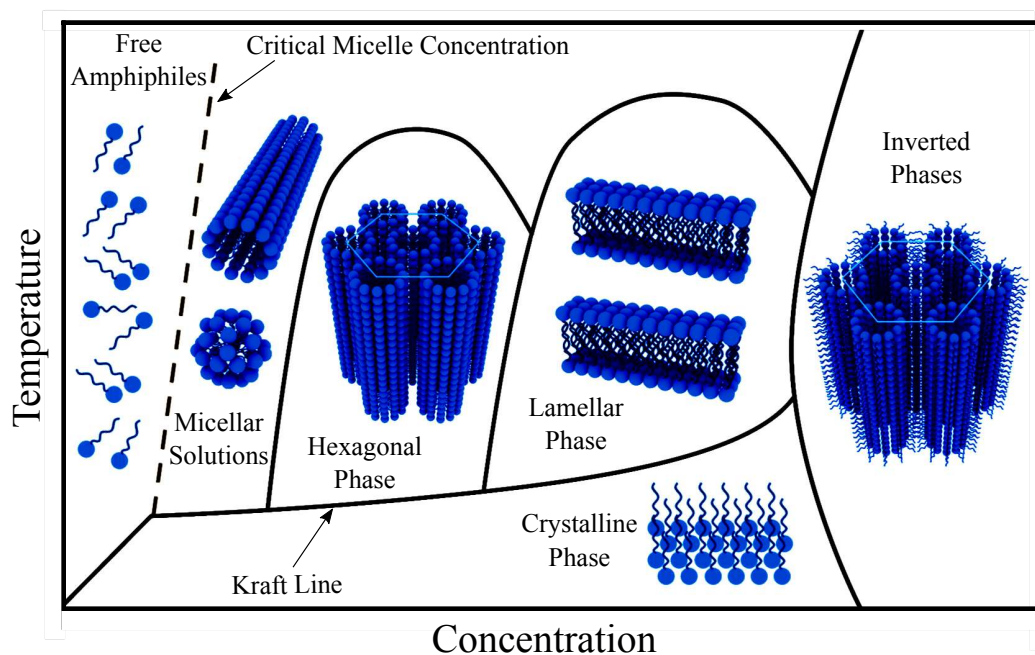
Source: Author, 2021. Adapted from Neto, 2021 [31].

It must be emphasised that although concentration is the determining factor for various lyotropic phases, each of these structures is only observed for temperatures above the Kraft line, shown in figure 2.2.

Lyotropic liquid crystals are abundant in nature, particularly biological systems. The structural similarity of lamellar phases to cell membranes creates a natural link to medical and biological research. Nonetheless, these systems are usually not suited for technological applications due to factors such as solvent evaporation and low dielectric anisotropy and birefringence.

2.1.2 Thermotropic Liquid Crystals

Thermotropic liquid crystals are the most commonly used and studied, especially for technological applications, due to their linear and non-linear optical properties. Their formation is principally determined by temperature variations. Therefore, within a defined temperature range, compounds exhibit liquid crystalline phases, as seen in figure 2.3. Below this range, known as the melting point, compounds present a solid crystalline phase. Above this range, known as the clearing point, compounds present a liquid isotropic phase.

As discussed in the previous chapter, phase transitions are characterised by a change in molecu-

Figure 2.3: Representative scheme of the ordering in the solid crystalline, liquid crystalline and liquid isotropic phases.
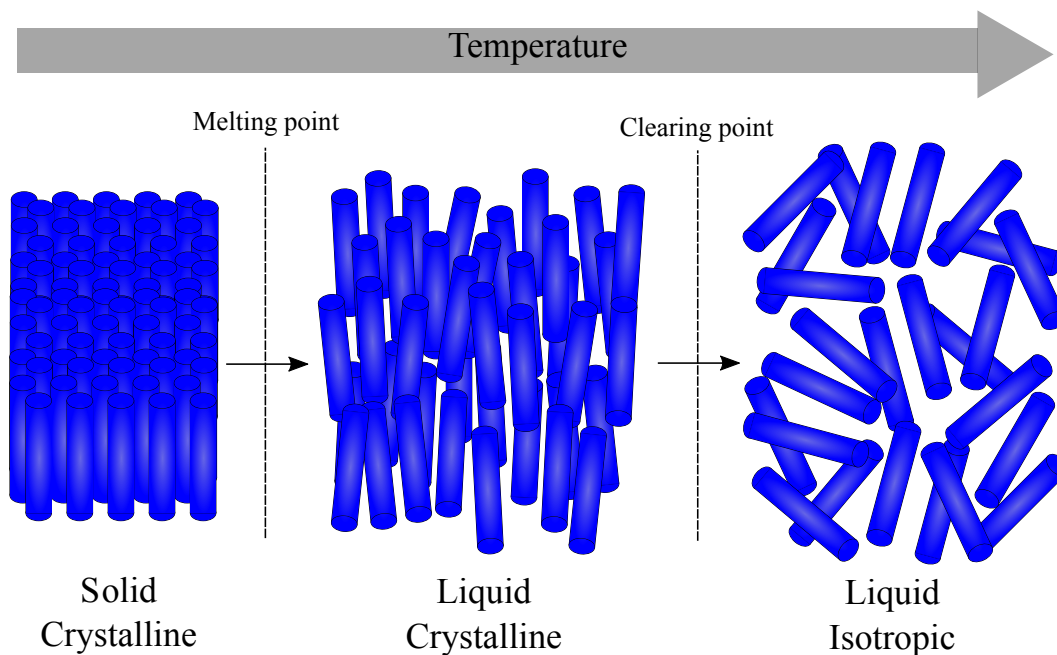
Source: Author, 2021.

lar order. Thermotropic liquid crystals transform from more ordered (or less symmetric) phases to relatively less ordered (or more symmetric) phases with increasing temperature, the sequence of which can be predicted. These materials exhibit a great variety of liquid crystalline phases, as will be discussed later. The exact number of liquid crystalline phases encountered between the solid and liquid phases depends on the mesogenic molecule.

Unlike for lyotropic liquid crystals, no change in concentration is required to form mesophases, and molecular aggregates do not form. Instead, as the constituent molecules are spatially anisotropic, their shape and rigidity favour anisotropic intermolecular interactions causing alignment. Next, we will discuss the main molecular properties of thermotropic compounds.

2.2   Molecular Structure of Thermotropic Liquid Crystals

Thermotropic liquid crystals can be further distinguished by their constituents' molecular shape, distinguished as calamitic, discotic, sanidic and bent-core, shown in figure 2.4. A common characteristic of these mesogenic[3] molecules is that they are rigid along their length, which favours collective alignment. Calamitic and discotic molecules are most commonly found. Calamitic

---

[3]i.e. show mesophases.

(figure 2.4(a)) liquid crystalline molecules are usually ellipsoidal or rod-like and present nematic and smectic phases. Discotic (figure 2.4(b)) liquid crystals are disk-like and present nematic and columnar phases. Less commonly, sanidic (figure 2.4(c)) and bent-core (figure 2.4(d)) molecules are brick-like and banana shaped respectively and can also form liquid-crystalline phases.

Figure 2.4: Geometric shape of different liquid crystalline molecules: (a) calamitic, (b) discotic, (c) sanidic and (d) bent-core.
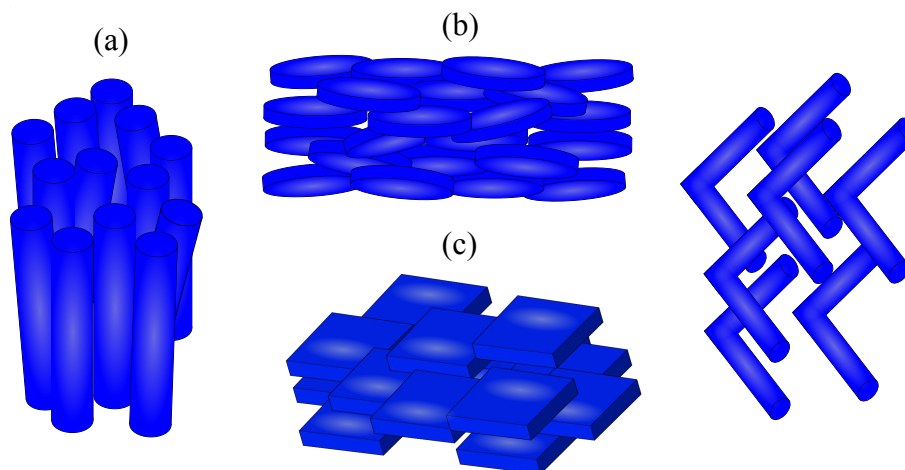
Source: Author, 2021.

The basic molecular structure of a thermotropic liquid crystalline compound, shown in figure 2.5, is divided into (i) a mesogenic group - composed of rings (also called a cyclic group or closed chain) and bridges - and (ii) side groups - composed of links and terminal groups [32].

Figure 2.5: Basic molecular structure of a mesogenic compound.
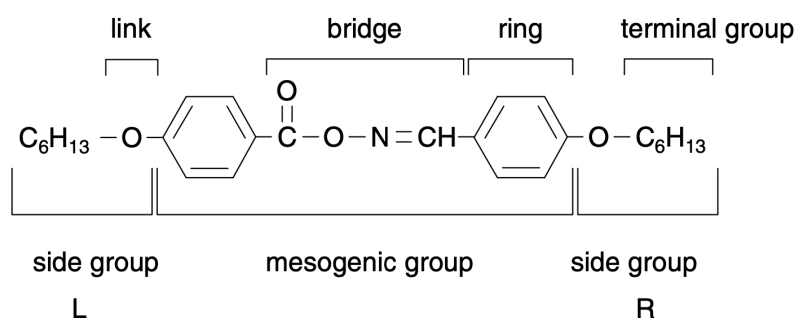
Source: Pestov, 2003 [32].

The cyclic groups, usually aromatic rings, determine the liquid crystal's electromagnetic properties. These rings are usually saturated[4] cyclohexane, unsaturated phenyl and biphenyl, or

---

[4]In organic chemistry, saturated means a compound contains only single carbon-carbon bonds, whereas unsaturated compounds contain double or triple carbon-carbon bonds. In other words, the more hydrogen atoms a molecule has, the more "saturated" it is.

some combination thereof. Usually, the clearing point increases with ring number.

The bridge, beyond elongating the molecule, plays an important role in determining the transition temperatures and physical properties of liquid crystals. Its elements determine the compound's chemical stability. A widely used nematic liquid crystal from the *n*-CB series, 5CB (figure 2.6(b)), is one of the most stable liquid crystals as it lacks a bridge connecting its aromatic rings.

Figure 2.6: Examples of compounds that present liquid crystalline phases and their respective molecular structures: (a) HOBA, (b) 5CB, (c) DOBAMBC, (d) 2M4P8BC, (e) MDW308, (f) CB - cholesteryl benzoate and (g) HET5.
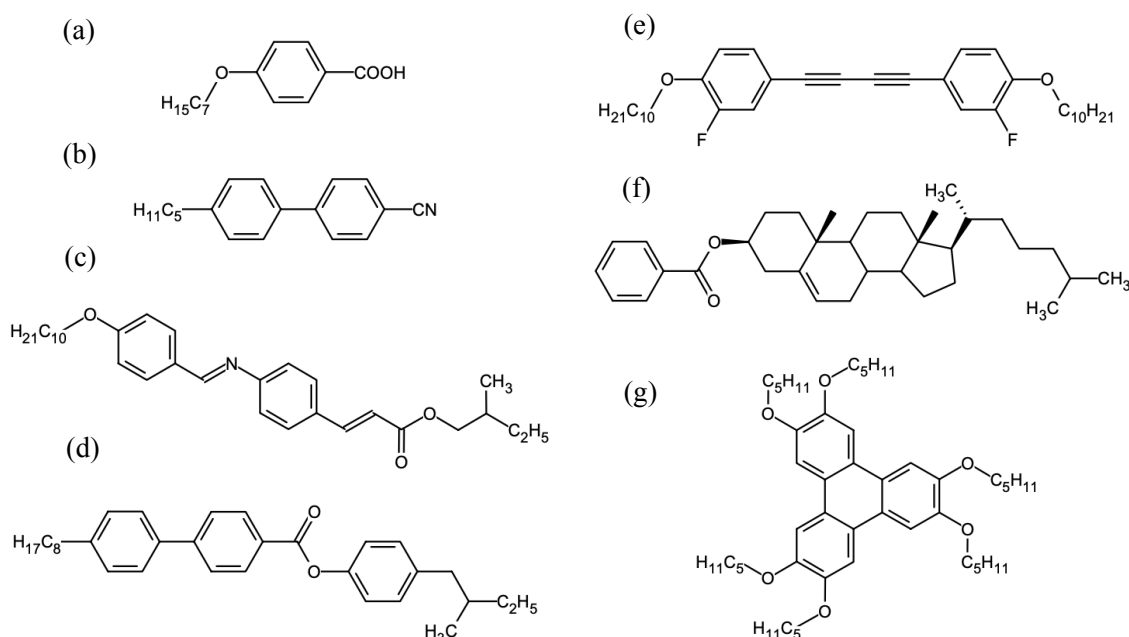
Source: Author, 2021. Adapted from: Pestov, 2003 [32].

Side groups are polar or apolar open organic chains, whose length and flexibility determine phase transition temperatures and the existence of a variety of mesophases, as detailed in figure 2.7 for the homologous series *n*-CB[5]. CB denotes cyanobiphenyl and *n* refers to the number of methylene ($-CH_2-$) units in the flexible chain spacer. $n = 1$ shows no mesogenic phase, yet $n \geq 3$ materials present at least one mesophase. Shorter side groups favour the nematic (N) phase, while longer side groups favour the smectic (Sm) phase. Cr and Iso denote crystal and isotropic phases, respectively. The groups most commonly used as side chains are: alkyl (C_nH_{2n+1}), alkoxy (an alkyl group singularly bonded to oxygen, OC_nH_{2n+1}), alkenyl (C_nH_{2n-1}) and alkenyloxy (OC_nH_{2n-1}) groups.

Finally, terminal groups contribute to the molecule's dielectric anisotropy. Compounds with

---

[5]Some compounds - as the ones from the n-CB series, with $n < 5$ - can supercool before recrystallising and then exhibit a metastable nematic phase below the melting point denominated monotropic nematic. In contrast, a thermodynamically stable mesophase, i.e. occurring above the melting point, is denominated enantiotropic.

Figure 2.7: Phase transition temperatures for compounds in the cyanobiphenyl homologous series.

Compounds	Mesophases
1CB	Cr $\xleftrightarrow{109°C}$ Iso
3CB	Cr $\xleftrightarrow{67.3°C}$ N $\xleftrightarrow{(30.3°C)}$ Iso
5CB	Cr $\xleftrightarrow{24°C}$ N $\xleftrightarrow{35.3°C}$ Iso
7CB	Cr $\xleftrightarrow{30°C}$ N $\xleftrightarrow{42.8°C}$ Iso
8CB	Cr $\xleftrightarrow{21.5°C}$ Sm-A $\xleftrightarrow{33.5°C}$ N $\xleftrightarrow{40.5°C}$ Iso
9CB	Cr $\xleftrightarrow{42°C}$ Sm-A $\xleftrightarrow{48°C}$ N $\xleftrightarrow{49.5°C}$ Iso
10CB	Cr $\xleftrightarrow{44°C}$ Sm-A $\xleftrightarrow{54.5°C}$ Iso
12CB	Cr $\xleftrightarrow{48°C}$ Sm-A $\xleftrightarrow{58.5°C}$ Iso

Source: Author, 2021. Data from: Pestov, 2003 [32].

apolar or weakly polar terminal groups - such as alkyl - have a weak dielectric anisotropy ($\Delta \varepsilon \sim 1$), whereas highly polar groups - such as cyano ($-C \equiv N$) - have a strong dielectric anisotropy ($\Delta \varepsilon \sim 10$).

Discotic compounds consist of a flat, rigid nucleus formed by several strongly bonded aromatic rings. Aliphatic chains that play a similar role as side chains in calamitic compounds are attached to the mesogenic core. The molecular structure of the discotic compound HET5 is shown in figure 2.6(g).

A detailed database of around 3000 mesogenic molecules can be found in reference [32]. Its richness of molecular structure permits an enormous quantity of compounds with different liquid-crystalline phases, of which the most important will be discussed below.

2.3 Liquid Crystalline Phases

Liquid-crystalline phases are characterised by two types of order. Orientational order, always present, quantifies how much the molecules orient along some preferential axis. Positional

order, sometimes present, quantifies the extent to which the molecules arrange in some kind of network, or at random.

As previously discussed, distinct mesophases correspond to different degrees of order, and are observed via external variables such as temperature and pressure. Compounds of anisotropic molecules (so-called thermotropic liquid crystals) present temperature-induced phase transitions. In contrast, for chemically anisotropic compounds, such as amphiphilic compounds, lyotropic liquid crystals undergo concentration-induced phase transitions. Some mesogenic compounds, known as amphotropic, may exhibit both lyotropic and thermotropic behaviours.

This thesis will focus on mesophases in thermotropic compounds. To this day, more than 20 thermotropic mesophases are known, and this number is growing. They can all be classified into three groups: nematic, cholesteric, and smectic.

2.3.1   Nematic Phase

The most common liquid-crystalline phase is the nematic[6] phase, observed in calamitic, discotic or banana shaped achiral molecular compounds. The molecules' centres of mass only display short-range positional order, meaning that compounds in this phase flow similarly to isotropic liquids. However, long-range orientational order is also present, i.e. on average the molecules align in a preferred direction, which is characterised by the director vector $\vec{n}$, as shown in figure 2.8(a).

Figure 2.8: (a) Representative scheme of the nematic phase. (b) Nematic thread-like texture.

(a)   (b)
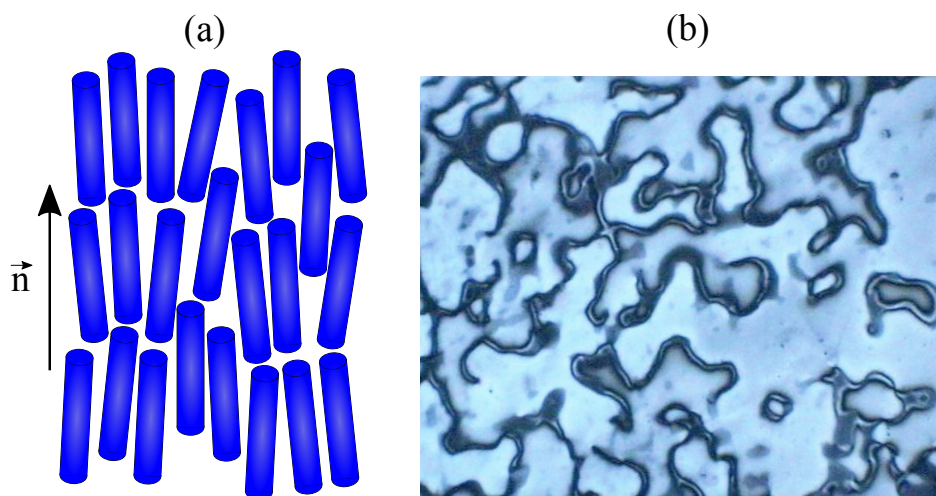
Source: Author, 2021. Adapted from: Dierking, 2003 [33].

---

[6]From the Greek *nematos* - thread-like.

This simplest liquid-crystalline phase is distinguished from isotropic liquids by its average molecular orientation. An important feature is that its directions $\vec{n}$ and $-\vec{n}$ are indistinguishable. Even if the molecules have permanent dipoles, their total dipole moment is nonetheless negligible [34]. For this reason, we say that the nematic phase is centrosymmetric[7]. Most nematic liquid crystals are uniaxial, i.e. they have one preferred direction. However, when biaxial, these molecules tend to orient themselves along some secondary axis in addition to the major axis.

Long-range orientational order causes the nematic phase to have characteristics typically found in crystalline solids, such as: birefringence, energy costs for deforming the optical axis and anisotropic responses to external electromagnetic fields. The fluidity of nematic liquid crystals is given by various coefficients of viscosity, defined by the angle between $\vec{n}$ and the flow direction, which have been widely explored in the manufacture of various electro-optical devices, such as digital displays [35], optical modulators [36] and optical filters [37].

The orientational order of nematic samples is defined by short range forces, such as molecular interactions with surfaces or impurities. When confined to sample holders that do not preset the director vector's orientation, nematic liquid crystals exhibit domains of different orientations which can be identified as light and dark regions on textures obtained from polarised light microscopy, as shown in figure 2.8(b). This type of texture is unique to the nematic phase, and is used to identify new compounds that exhibit it.

2.3.2 Cholesteric Phase

The cholesteric phase is created by adding chiral molecules to nematic liquid crystals, resulting in a stack of nematic planes with preferred molecular orientations, $\vec{n}$, following a helix defined by a *pitch*, P. The *pitch* is the distance measured along the helical axis in which the director completes a full rotation, as illustrated in figure 2.9(a).

Two compounds known to present the cholesteric phase are: hydroxypropyl cellulose (HPC) and 5-cholesten-3-yl benzoate, also known as cholesteryl benzoate. The latter was the first material discovered to present liquid crystalline properties, as discussed in the previous chapter. Unlike the light and dark textured regions of the nematic phase, cholesteric phases exhibit textures similar to fingerprints when the sample holder does not define the orientation of the helical axis, as shown in figure 2.9(b).

---

[7]A material is centrosymmetric when its physical properties are indistinguishable upon inverting its director.

Figure 2.9: (a) Representative scheme of the cholesteric phase, where P is the *pitch*. (b) Cholesteric polygonal (fingerprint) texture of a sample with a relatively long pitch.

(a)   (b)
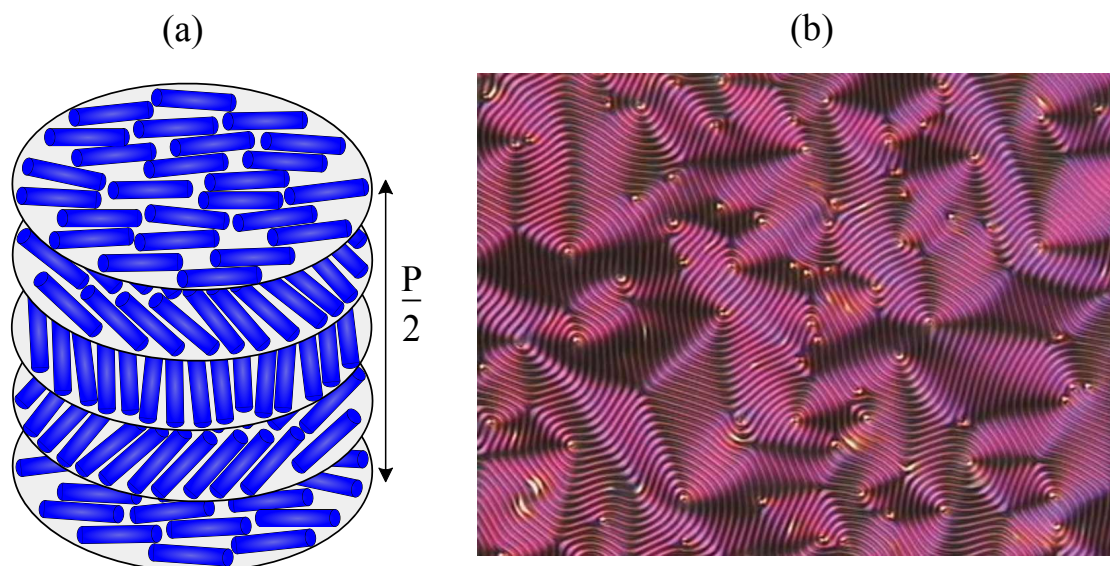
Source: Author, 2021. Adapted from: Dierking, 2003 [33].

The cholesteric phase has recently interested researchers by its selective reflection of light, acting as a photonic crystal for light with circular polarisation in the same direction as the director's helical distortion. This property has been explored in the manufacturing of low activation threshold lasers [38] and digital monitors that dispense the use of backlight [39].

2.3.3 Smectic Phases

Molecules in the smectic[8] phase tend to orient themselves along a director vector $\vec{n}$, like the nematic phase. However, an important distinguishing feature is the molecular stratification into layers [40]. The molecules are arranged in two-dimensional liquid layers, maintaining a well-defined spacing, yet the interactions between layers are weak when compared to the lateral intermolecular forces. Consequently, the layers slide freely over one another, explaining the phase's fluidity, despite being more viscous than the nematic phase. The smectic phase is more ordered than the nematic phase and usually occurs at lower temperatures. Different molecular arrangements within the layers determine the types of smectic phases, the most common being the smectic-A and smectic-C phases.

---

[8]From the Greek *smegma* - soap, ointment.

Smectic-A

The simplest of all smectic phases is the smectic-A phase. Consisting of non-chiral and non-polar molecules, this phase is characterised by the absence of positional order within the layers, i.e. each layer is a two-dimensional liquid. The average molecular orientation, $\vec{n}$, is perpendicular to the layers, as shown in figure 2.10(a). The layered stratification of the molecules causes the smectic-A phase to present a fan-like texture when observed by polarised light microscopy, as shown in figure 2.10(b). This type of texture is seen in all smectic phases, with slight differences in the patterns of each.

Figure 2.10: (a) Representative scheme of the smectic-A phase. (b) Typical fan-shaped texture of a smectic-A phase.
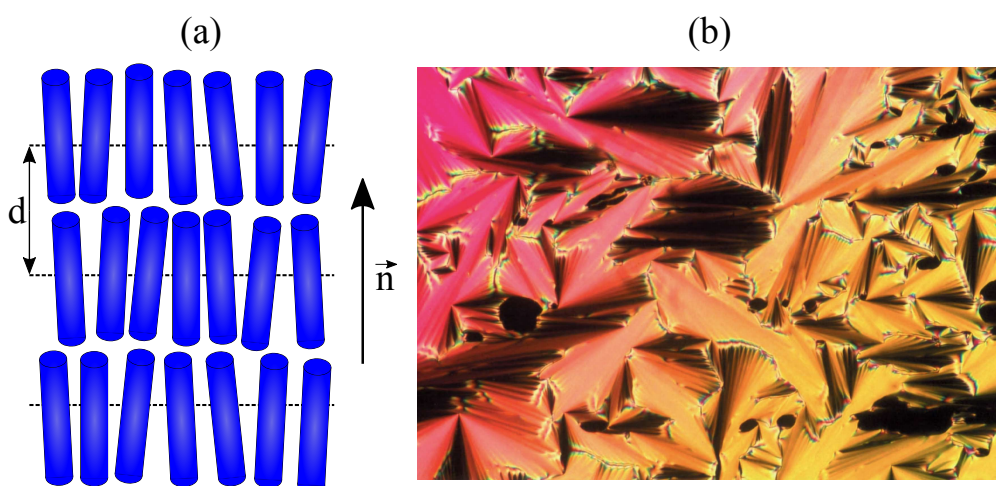
Source: Author, 2021. Adapted from: Dierking, 2003 [33].

The layers' thickness depends on the molecular structure of the material. Due to the molecular arrangement perpendicular to the layers' plane, the thickness is determined by the length of the rigid part of the molecule as well as by the flexibility of the side chain and the terminal group.

The smectic-A phase is uniaxial, with the optical axis determined by the axis normal to the plane of the layers. Due to its layered structure, such liquid crystalline phase is centrosymmetric, i.e. directions z and $-z$ are equivalent. The rotational symmetry around the z axis can be seen in the diffraction pattern shown in the figure 2.11. In this case, the incident beam is perpendicular to the layers' plane, making it possible to observe the plane's translational invariance.

Figure 2.11: Electron-diffraction pattern, a diffusive ring, of the smectic-A phase.

Source: Chao et al., 1997 [41].

Smectic-C

The smectic-C phase, as the smectic-A phase, is structured in layers, where each layer can be defined as a two-dimensional liquid. However, the molecules in each layer are oriented at an angle θ, known as smectic cone angle, defined relative to the normal to the plane of the layers. In non-chiral smectic liquid crystals, and in the absence of external influences, the director $\vec{n}$ is uniformly aligned, as shown in figure 2.12(a).

Figure 2.12: (a) Representative scheme of the smectic-C phase. (b) Transition to the broken fan-shaped texture of the smectic-C phase on cooling.

(a)   (b)
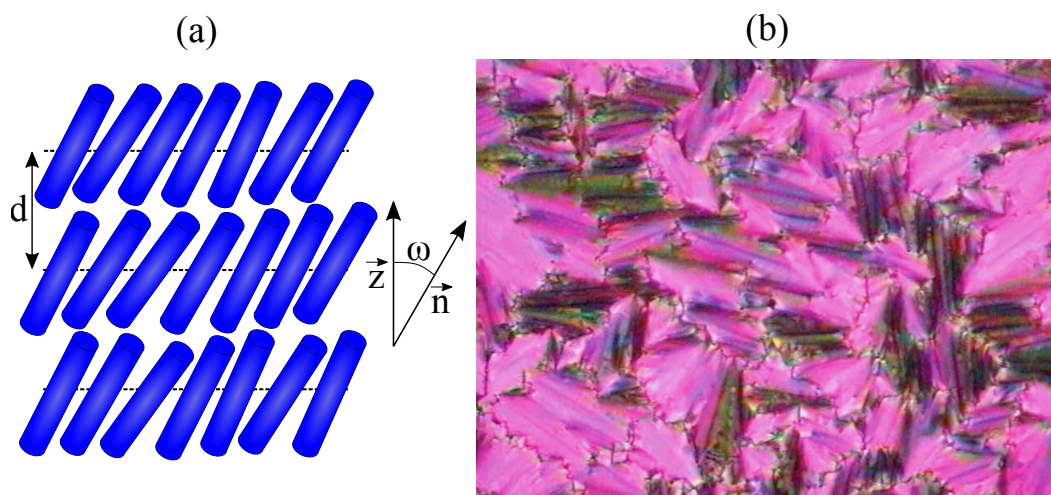
Source: Author, 2021. Adapted from: Dierking, 2003 [33].

The average tilt angle, $\omega \in [0°, 45°]$, is usually temperature-dependent and is therefore an order parameter for this phase. A consequence of the molecules' inclination is that this phase exhibits biaxial optical properties.

McMillan proposed a mean-field theory for smectic-C liquid crystals, relating the formation of a tilted phase to the presence of at least two outward pointing dipoles in the mesogenic molecule [42]. Although there is no consensus on the sufficient features to guarantee tilt; permanent or induced dipoles have been the key molecular ingredient of various theoretical investigations.

The work of van der Meer and Vertogen [43] considered the induction forces between transverse dipoles and neighbouring polarisable centres, while in a recent treatment by Govind and Madhusudana the off-axis position of a single transversal permanent dipole has been considered the key feature for tilt [44]. The alignment of these dipoles, and therefore the resulting tilt, tend to induce a layer contraction by a factor of $\cos\theta$.

Although it is known, since the work of Goodby et al. [45], that the presence of two or even one dipole is not a mandatory requirement, the vast majority of C smectogens are polar. A widely used compound presenting the smectic-C phase is p-decyloxybenzoic acid p-n-hexyphenyl ester (DOBHOP), as shown in figure 2.13, with a small transverse dipole moment. It is important to stress that phase transitions involving the smectic-C phase can be second or first-order, concepts we will discuss later on. However, dipole-dipole interactions are important in compounds that present a first-order transition.

Figure 2.13: Molecular structure of compound DOBHOP, presenting a small transverse dipole moment.
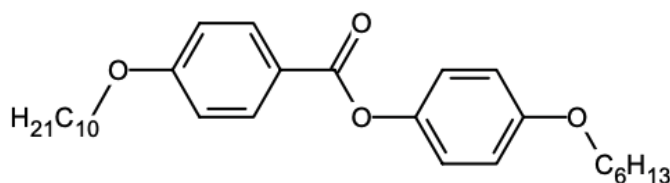
Source: Author, 2021.

2.4 Liquid Crystalline Order

As discussed in the previous sections, a fundamental feature of liquid crystals is the presence of a long-range orientational order combined with either no positional order, as in the nematic phase, or some degree of positional order, as in the smectic phases. Liquid crystalline phases are then distinguished by their symmetries and phase transitions correspond to symmetry breaking. These can be described with an order parameter, which represents how much the molecules' configuration differ from the less to more symmetrical phases.

2.4.1 Order Parameters

In general, the order parameter is a thermodynamic variable that can be measured experimentally, assuming non-zero values for temperatures below the transition temperature, T_C, $(T < T_C)$ and zero for temperatures above transition temperature $(T > T_C)$, i.e. some order parameter Q describing a phase transition satisfies the following requirements:

- $Q = 0$ in the most symmetrical, or least ordered, phase;

- $Q \neq 0$ in the less symmetrical, or more ordered, phase.

Order parameters can be microscopic or macroscopic. An order parameter built from a specific molecular model and giving a microscopic description of the system is therefore microscopic and represented by a scalar. In other situations, a microscopic description is not adequate and it is necessary to describe the system by a tensor order parameter representing macroscopic properties such as magnetic susceptibility. In this work, we will use a microscopic approach to phase transitions in liquid crystals.

Microscopic Order Parameters

The choice of order parameter can be made in several ways depending on the system studied. In some physical systems, the choice is quite intuitive, as for liquid-gas transitions, where the order parameter is the density difference between phases. For liquid crystals, the choice of order parameters is less trivial. For instance, the nematic phase is less symmetric, i.e. more ordered, than the isotropic phase. Thus, it is necessary to define an order parameter that is not null in the nematic phase, but that goes to zero with increasing symmetry at the nematic-isotropic phase transition.

In the nematic phase, the molecules are, on average, aligned along a preferential direction, defined by the previously introduced director vector $\vec{n}$. However, the average number of molecules aligned along $\vec{n}$ can vary with temperature, leading to a non-constant degree of order. This degree of order is described by a distribution function $f(\theta, \phi)d\Omega$ [46], giving the probability of encountering a molecule within a small solid angle $d\Omega = \sin\theta d\theta d\phi$ around the direction (θ, ϕ).

Since the nematic phase is centrosymmetric, the distribution function $f(\theta, \phi)$ must be independent of ϕ, i.e., the nematic phase possesses cylindrical symmetry around $\vec{n}$. Furthermore, $f(\theta) = f(\theta - \pi)$ accounts for the equivalence between $\vec{n}$ and $-\vec{n}$. In the nematic phase, the

distribution function must therefore be maximum at $\theta = 0$ and π and minimum at $\theta = \pi/2$ (figure 2.14). Moreover, it must be constant in the isotropic phase, to reflect the absence of orientational order.

Figure 2.14: Distribution function f(θ) for a system of rod-like molecules in the nematic phase.
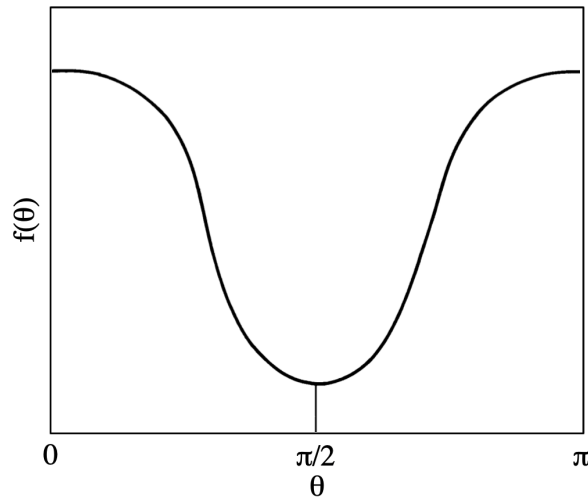
Source: Author, 2021. Adapted from de Gennes, 1993 [46].

Given a calamitic molecule, we consider a quantity measuring the dispersion of the major axis of the molecule, represented by the vector $\vec{a}$, around the director $\vec{n}$ (figure 2.15). At first sight, a possible candidate for the nematic order parameter would be a statistical average of the dipole moment expressed as:

$$\langle \cos\theta \rangle = \langle \vec{n} \cdot \vec{a} \rangle = \int \cos\theta f(\theta) d\Omega. \tag{2.1}$$

Figure 2.15: Coordinate system representing a calamitic molecule in relation to the director vector $\vec{n}$ of the nematic phase.
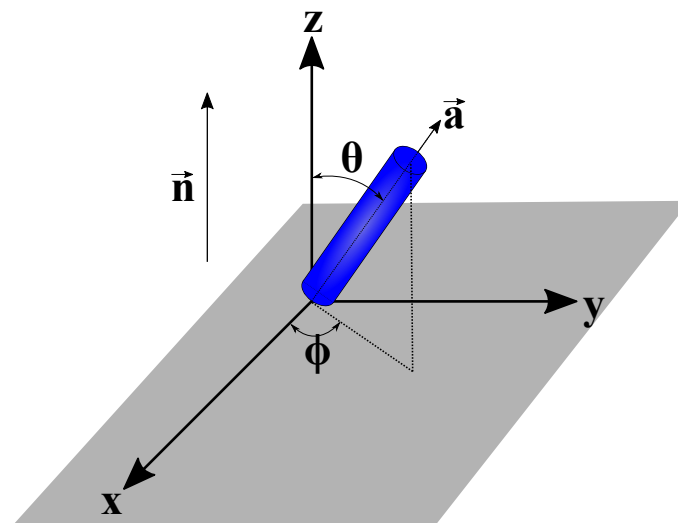
Source: Author, 2021.

Although this may appear a natural choice, it does not give a suitable description of the nematic phase because the molecules do not possess a net dipole moment in the preferred direction, i.e. $\langle \cos \theta \rangle = 0$. Furthermore, the function $\langle \vec{n} \cdot \vec{a} \rangle$ changes sign with $\vec{n} \to -\vec{n}$, which violates the centrosymmetric condition. As such, we must resort instead to the quadrupole term of the molecular interaction energy's multipole expansion, so that the order parameter is defined as:

$$s = \left\langle \frac{3}{2} cos^2 \theta - \frac{1}{2} \right\rangle = \int \left(\frac{3}{2} cos^2 \theta - \frac{1}{2} \right) f(\theta) d\Omega. \tag{2.2}$$

At low temperatures, $f(\theta)$ peaks around $\theta = 0$ and $\theta = \pi$, corresponding to a parallel molecular alignment, so that $cos^2 \theta = 1$ and $s = 1$. At high temperatures (isotropic phase) the molecules are randomly oriented, i.e., $f(\theta)$ is independent of θ, so that $\langle cos^2 \theta \rangle = \frac{1}{3}$ and $s = 0$.

The microscopic order parameter s is therefore a measure of average molecular alignment, with two different regimes:

- $s = 0$ in the isotropic phase;

- $s \neq 0$ in the liquid crystalline phase.

In addition to the orientational order of the smectic-A phase being similar to the nematic phase, there is also a one-dimensional order of almost long-range that originates from the formation of liquid layers that tend to maintain a well-defined spacing. Thus, another order parameter is required to measure the variation in layer density. Finally, for the smectic-C phase, we must introduce a third order parameter representing the molecules' average tilt angle inside the layers. The next chapter will detail how the order parameters for each of these liquid-crystalline phases are calculated.

2.5   Phase Transitions in Liquid Crystals

Since their discovery, transitions between various liquid crystalline phases have been extensively studied experimentally and theoretically. At equilibrium, these are identified by discontinuities or singularities of some thermodynamic function (e.g., volume, specific heat, susceptibility, etc) at the transition temperature [47, 48]. This behaviour is due to the microscopic interactions between their constituents. In compounds presenting liquid crystalline phases, the transitions are characterised by distinct changes in the structure's symmetry corresponding to intermediate transitions between the solid crystalline and liquid isotropic phases. In general,

a phase transition involves the transformation from an ordered phase to a relatively disordered phase as a function of temperature. Hence, it is possible to predict a sequence of transitions in which increasing temperature leads to the gradual destruction of molecular order, as shown in figure 2.16.

Figure 2.16: Possible progression of liquid crystalline phases with increasing temperature.

Cr – H – K – E – G – J – B – Sm-F – Sm-I – Sm-M – Sm-B – Sm-C – Sm-A – N – Iso

Temperature

Source: Author, 2021.

No known compound presents every phase, and many materials only exhibit a small proportion of them. Some of these transitions will now be detailed.

2.5.1 Types of Phase Transitions

The types of thermodynamic phase transitions can be classified using the Helmholtz free energy, defined as $F = U - TS$, where U is the system's internal energy, T is the temperature and S is the entropy. The behaviour of the order parameter Q depends the type of phase transition.

Zero-order Phase Transition

At a zeroth order phase transition, F is discontinuous at the transition temperature. This type of transition has been theoretically predicted for superfluidity and superconductivity.

First-order Phase Transition

In a first-order transition, F is continuous, while $\left(\frac{\partial F}{\partial T}\right)_V = -S$ is discontinuous at the transition temperature. In this type of transition, the order parameter is discontinuous at the transition temperature T_C, as shown in figure 2.17(a).

Figure 2.17: Representation of the dependence of the order parameter, Q, with temperature (a) first-order and (b) second-order phase transitions.
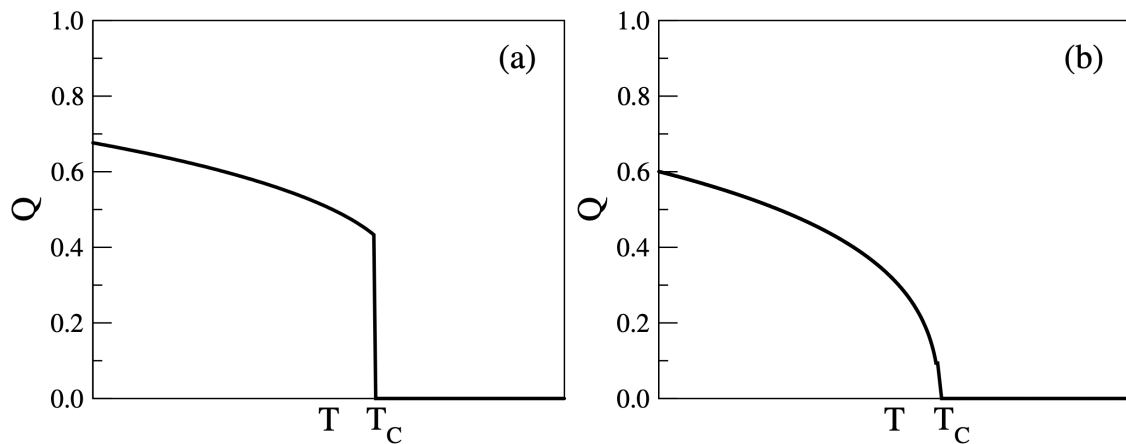
Source: Author, 2021.

Second-order Phase Transition

In a second-order phase transition, both F and $\left(\frac{\partial F}{\partial T}\right)_V$ are continuous, while $\left(\frac{\partial^2 F}{\partial T^2}\right)_V = -\frac{C_V}{T}$ is discontinuous at the transition temperature. In this transition, the order parameter is continuous and equals zero at the transition temperature T_C, as shown in figure 2.17(b).

2.5.2 Nematic–Isotropic Phase Transition

The isotropic–nematic transition involves spatial molecular reorientation. Although the molecules are initially distributed with the major axis at random, they orient themselves along a preferred direction, defined by the director vector $\vec{n}$. Experimental observations show that the order parameter abruptly drops to zero at the nematic–isotropic transition, i.e., it is a first-order transition. However, it is characterised by a loss of orientational order at a small latent heat of order of $1\text{kJ}\,\text{mol}^{-1}$. Thus, some authors classify this transition as being weakly first-order. However, even though the transition heat is small, the order parameter's discontinuity is always substantial.

Several theoretical approaches have described the nematic phase in the vicinity of its phase transitions. One of the best known approaches uses the phenomenological theory of Landau and de Gennes [49, 50], in which Helmholtz's free energy is expressed in terms of powers of the order parameter. The first version of a mean-field theory was proposed by Onsager [51], which attributed the origin of nematic ordering to the constituent molecule's anisotropic form, i.e., to repulsive interactions. In contrast, the well-known Maier-Saupe theory [14–16], attributed the

ordered phase formation to attractive anisotropic interactions, which will be covered in more detail in the next chapter.

2.5.3 Smectic-A–Nematic Phase Transition

The nematic–smectic-A transition involves the reorganisation of the molecules' centres of mass in equidistant planes, while maintaining the characteristic orientational order of the nematic phase. Molecules can move randomly within the layers as long as their director vector remains perpendicular to the plane. Consequently, the density shifts from periodic to homogeneous at the smectic-A–nematic transition. Just above the transition, one can expect small domains with a local smectic organisation [46].

Theoretical studies have shown that the order of the transition depends on the ratio T_{AN}/T_{NI}, where T_{AN} is the smectic-A–nematic transition temperature and T_{NI} is the nematic–isotropic transition temperature, and may be either first- or second-order. In some compounds, experimental results show a first-order transition at a latent heat of order $1\,\mathrm{kJ\,mol^{-1}}$. Conversely, measurements using differential calorimetry have demonstrated the absence of latent heat in the transition for several compounds, which characterises second-order transitions.

One of the most studied microscopic theoretical models for this transition was proposed by McMillan. His model is based on the molecular structure of compounds exhibiting the smectic-A phase. The nature of the phase transition is determined by the model parameter, which measures the strength of layering interactions. Two order parameters must be considered to represent both the long-range orientational order and the one-dimensional quasi-long-range translational order describing the phase transition. This model will also be further detailed in the next chapter.

2.5.4 Smectic-A–Isotropic Phase Transition

Theoretical studies and experimental measurements of optical reflectivity and calorimetry have shown that the smectic–isotropic transition is first-order, with a latent heat of the order of $6\,\mathrm{kJ\,mol^{-1}}$. This transition is determined by the side-chain length of the compounds. A typical example occurs with the nCB and nOCB homologous series. For short alkyl chains, these compounds exhibit nematic–isotropic transitions, while for long alkyl chains, these compounds exhibit smectic–isotropic transitions.

The smectic-A–isotropic transition allows the investigation of order induced by solid substrates and other surface effects. Various experiments studied the smectic-A order at the liquid-liquid and liquid-solid interfaces near the smectic-A–isotropic transition temperature revealing the presence of smectic layers for $T > T_{AI}$. This phenomenon is known as wetting, and is complete when the smectic layer's thickness diverges at the transition, or incomplete when it remains finite.

Furthermore, some materials exhibit a very peculiar phenomenon during this transition. By heating freely suspended films in the smectic phase, it is possible to observe a gradual reduction in film thickness, due to the melting of their central layers [52]. This phenomenon is known as the layer thinning transition. Several experiments have confirmed this unusual transition and many theoretical studies have been proposed in order to explain it [53–57].

2.5.5 Smectic-C–Smectic-A Phase Transition

The smectic-A–smectic-C transition is characterised by the one-dimensional tilting of the smectic layers. Reducing the temperature of a sample material in the smectic-A phase to T_{AC}, the smectic-A–smectic-C transition temperature, leads to strong light scattering due to fluctuations in the inclination angle of the smectic layer [46].

Experiments using different techniques such as calorimetric measurements and X-ray scattering have shown that the smectic-A–smectic-C transition is continuous, i.e., second-order. This transition is typically difficult to detect via latent heat, usually less than $300 \mathrm{J}\,\mathrm{mol}^{-1}$, however it can be detected by a singularity in specific heat. Other experiments, however, suggest that a change in the nature of the phase transition, from second- to first-order, is possible in the vicinity of the N–Sm-A–Sm-C and Iso–Sm-A–Sm-C triple points.

Several models have been proposed to describe the smectic-C phase. In the next chapter, we will review the model proposed by Govind and Madhusudana, which considers the molecular origin of the tilt and describe first- and second-order Sm-C–Sm-A phase transitions.

2.5.6 The Nematic–Smectic-A–Smectic-C Multicritical Point

In liquid-crystalline phase transitions, we observe the existence of multicritical points. The nematic–smectic-A–smectic-C (NAC) multicritical point represents the intersection of boundaries between NA, AC, and NC phase transitions in the thermodynamic plane. Phases are

indistinguishable at the multicritical point, and all nearby phase transitions are continuous.

The NAC multicritical point has been observed in the temperature *versus* concentration diagram of binary liquid crystal mixtures [58], and also in the pressure *versus* temperature diagram for single component systems [59], as illustrated in figure 2.18.

Figure 2.18: Phase diagrams in the vicinity of the NAC multicritical point. (a) Temperature *versus* concentration for a binary liquid crystal mixture and (b) pressure *versus* temperature for a single component system.
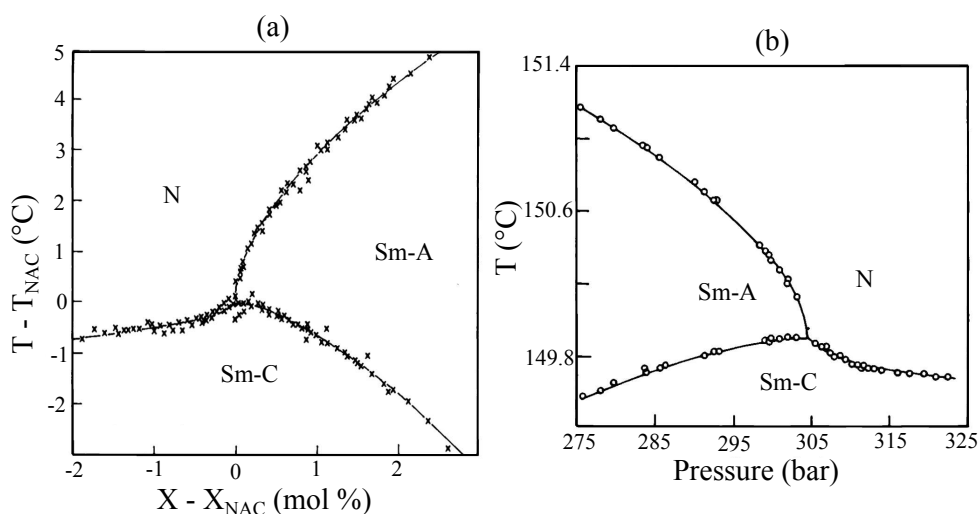
Source: Author, 2021. Adapted from: Chandrasekhar, 1992 [60].

As already discussed, liquid crystals exhibit a rich variety of phase transitions and are the subject of many theoretical and experimental studies. The study of phase transitions and critical phenomena in liquid crystals is directly related to surface and external field effects. The next section will discuss surface effects in liquid-crystalline ordering.

2.6 Surface Effects on Liquid Crystalline Order

Due to their structure, liquid-crystalline compounds are very sensitive to surface effects, leading to interesting and varied interfacial phenomena [23]. Surface effects depend on the mesophase in question. In this work, we will turn our attention to effects present in the nematic and smectic phases.

2.6.1   Surface Effects in the Nematic Phase

Surface effects are most studied in the nematic phase due to its structural simplicity and technological potential. Contact of the material with a surface or interface in a different phase (solid, liquid or gas) causes a disturbance in the nematic order, so that the orientation of the vector director is influenced by the presence of the surface. A transition region of length ξ, called the penetration length, is observed, with the nematic order being recovered for distances greater than ξ from the surface.

Thus, near the interface, the molecules have a fixed mean orientation. In the absence of external fields, this orientation is imposed by elastic forces that tend to orient the molecules near the interface, parallel to each other. This phenomenon of surface induced liquid crystal orientation is called surface anchoring.

The phenomenon of anchoring was discovered by Mauguin [61], when studying a nematic liquid crystal system deposited on a mica surface. Mauguin observed that the liquid crystal was oriented with its axis parallel to the substrate and made an angle of 60 degrees with the optical axis of the mica.

The equilibrium configuration of the director depends on the balance of forces involving the three basic deformations, namely splay, twist and bend (see figure 2.19). However, it is possible to artificially obtain a nematic monodomain using boundary conditions that previously defined the preferred direction, called the easy axis.

Figure 2.19: Types of liquid crystalline director deformations of samples between two flat surfaces: (a) splay, (b) twist and (c) bend.
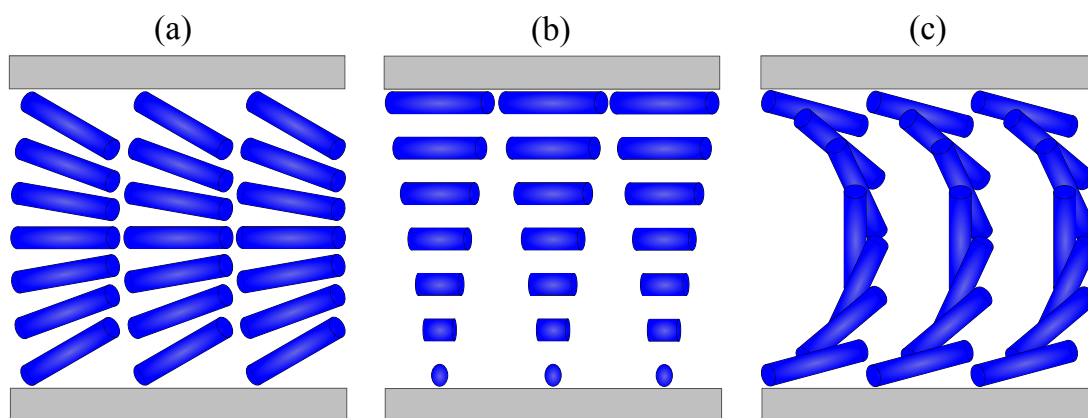
Source: Author, 2021.

The interfaces at which anchoring has been most extensively studied are those with solid substrates and treated glass surfaces. Treated surfaces allow for a better control of the induced

anchoring direction. The treatment of these surfaces can be mechanical (through rubbing mechanisms), chemical (by depositing a layer of surfactant, polymers, or inorganic substances), or a combination of both.

Surface anchoring can be planar, inclined or homeotropic (figure 2.20), depending on whether the anchoring direction is respectively parallel, inclined or perpendicular to the interface plane. Each of these anchoring types is obtained by chemically and/or mechanically treating the sample holder surface where the nematic liquid crystal is confined [62]. In planar anchoring, a thin polymer layer is deposited on the surfaces of the sample carrier, which is subsequently rubbed, which defines the easy axis direction. The homeotropic anchoring is obtained from the deposition of surfactants on the sample holder surfaces, so that their surface concentration is sufficient to prevent the deposited calamitic molecules of the liquid crystal from being parallel to the sample holder walls. In this way, the easy axis is normal to the surface of the sample holder.

Figure 2.20: Types of surface anchoring on a nematic sample between two flat surfaces. (a) Planar, (b) inclined and (c) homeotropic.
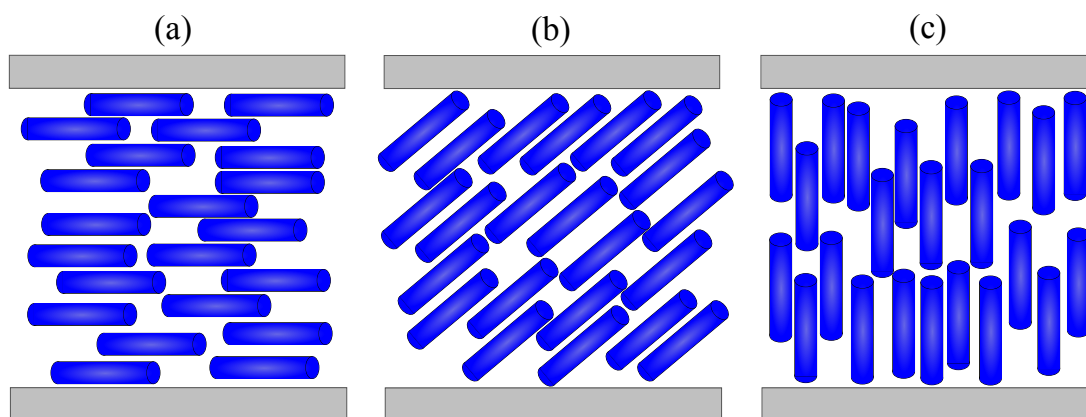
Source: Author, 2021.

Molecules close to the surface affect the orientation of molecules inside a liquid crystal cell, due to molecular interactions. These interactions can be strong or weak, giving rise to two anchoring regimes.

In many cases, the substrate surface's interaction with the liquid-crystalline molecules near the surface is very strong. As a result, external fields do not affect the orientational order in the vicinity of the boundary surface, and surface anchoring becomes the dominant factor. External field may be the dominant factor in bulk region, at a position far from the surface. Furthermore, when the field is removed, the liquid crystal returns to its initial condition. This is the strong anchoring regime. On the other hand, when the orientation of the liquid crystal after the removal of the field is different from its initial orientation, we have a weak anchoring regime.

The surface energy density describing the surface anchoring is given by [63]:

$$W = -W_0 \left[\frac{3}{2} (\vec{n} \cdot \vec{n_0})^2 - \frac{1}{2} \right], \tag{2.3}$$

where W_0 is the anchoring amplitude and its sign determines the type of anchoring; $\vec{n}$ is the director vector and $\vec{n_0}$ is the vector perpendicular to the surface. When $W_0 > 0$, the minimum surface energy occurs when $\vec{n}$ and $\vec{n_0}$ are parallel, so that the anchoring is homeotropic. If $W_0 < 0$, the surface energy minimum occurs when $\vec{n}$ and $\vec{n_0}$ are perpendicular, so that the anchoring is planar degenerate. The degenerate term reflects that the equation 2.3 does not specify the direction of the easy axis, but only that the director must be perpendicular to $\vec{n_0}$.

2.6.2 Surface Effects in the Smectic Phase

Usually, smectic layers lie parallel to the substrate, with the molecules arranged homeotropically (figure 2.21(a)). However, it is possible that an oblique structure is formed in a planar cell with an antiparallel alignment treatment [64] (figure 2.21(b)). Additionally, X-ray measurements showed that a smectic-C sample under parallel alignment conditions displays a structure of layers inclined in a chevron shape [65] (figure 2.21(c)).

Figure 2.21: Smectic layer structures in different alignments: (a) homeotropic, (b) oblique and (c) chevron.

(a)   (b)   (c)
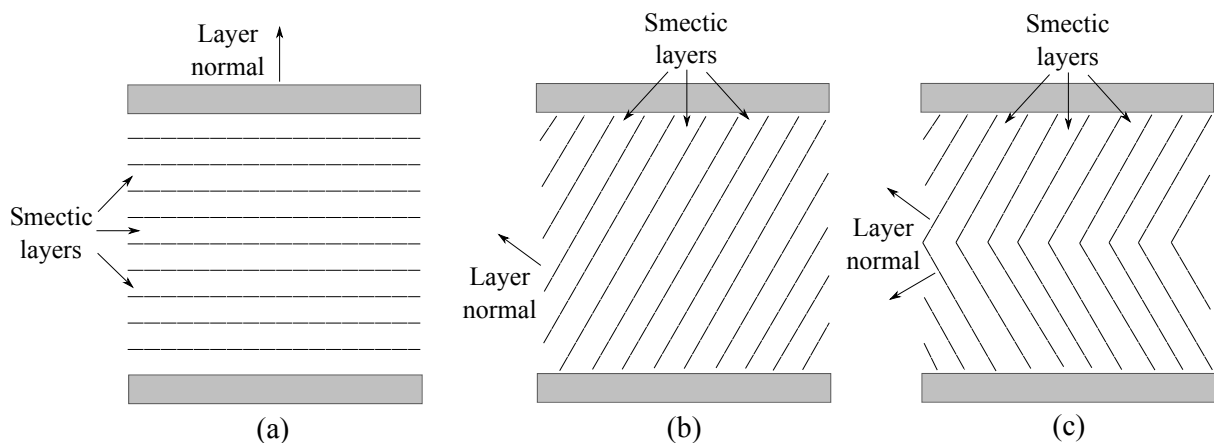
Source: Author, 2021.

2.6.3 Surface Effects and Phase Transitions

Several investigations were performed to determine how surface effects influence phase transitions in liquid-crystalline systems. This explains different phenomena, such as layer thinning transitions in thin smectic films [52] and the emergence of ordered surface phases above the sample's transition temperature (wetting phenomenon) [66–68].

Phase transition investigation in a nematic sample anchored under a substrate showed that the nematic order parameter is greater at the surface than at the centre of the sample with the anchored layer presenting a higher nematic-isotropic transition temperature [19]. The existence of a local order parameter for the nematic phase was predicted via different means [69, 70]. The existence of a profile in the smectic order parameter was proposed in order to explain the smectic wetting phenomenon on the free surface of samples in nematic and isotropic phases [71]. It was shown that the nematic and smectic order parameters are not uniform, but vary continuously across the sample [72]. Near the surface, for a distance up to the surface penetration length, nematic and/or smectic order remains stable even for $T > T_{NI/SI}$, i.e., in the isotropic phase.

Surface effects on liquid-crystalline phase transitions are quite complex. More detailed studies of these effects can be found in references [23, 73]. In Chapter 4, we will turn our attention to surface and finite size effects in freely suspended films in the smectic-C phase.

2.7 External Field Effects on Liquid Crystalline Order

Liquid crystals exhibit anisotropic responses to applied external fields. As a result, the director vector can reorient depending on its relative orientation to the applied field. Such orientations occur when the electric field's energy contribution overcomes the elastic deformation of the director vector.

The external field can increase or decrease the system's energy density depending on its dielectric anisotropy, as well as its relative orientation with the director vector. The energy density with respect to an external electric field is given by:

$$F_e = -\frac{\varepsilon_a}{2}(\vec{E} \cdot \vec{n})^2. \tag{2.4}$$

$\varepsilon_a = \varepsilon_\parallel - \varepsilon_\perp$ is the material's dielectric anisotropy, where $\varepsilon_\parallel$ is the electric susceptibility in the direction of $\vec{n}$ and $\varepsilon_\perp$ to its perpendicular. If $\varepsilon_a > 0$, the external field tends to reorient the director vector along its direction, with $\vec{n}$ parallel to $\vec{E}$. When $\varepsilon_a < 0$, the energy is minimised

when $\vec{n}$ is perpendicular to $\vec{E}$. The dielectric anisotropy can be positive ($\varepsilon_\parallel > \varepsilon_\perp$), or negative ($\varepsilon_\parallel < \varepsilon_\perp$), usually with $\varepsilon_a \in [-5, +30]$ for nematic liquid crystals.

Figure 2.22: Nematic liquid crystal with strong homeotropic alignment in (a) absence of external field and (b) presence of external field.
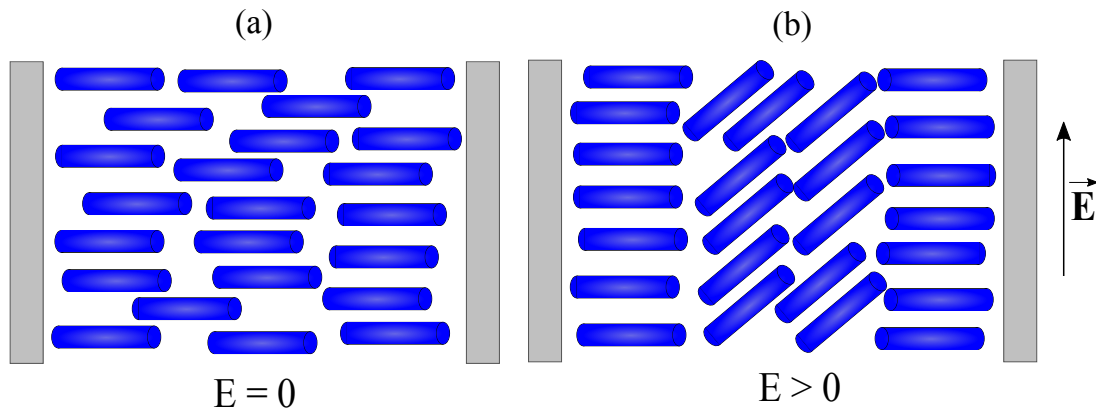
Source: Author, 2021. Adapted from: Khoo, 2007 [34]).

In a strong anchoring regime as shown in figure 2.22, the applied field does not change alignment near the surface. This type of situation is useful in most applications involving liquid crystals. However, a weak anchoring regime is also observed experimentally, where the presence of external field alters the alignment near the surfaces, as shown in figure 2.23.

Figure 2.23: Nematic liquid crystal with weak homeotropic alignment in the presence of external field.
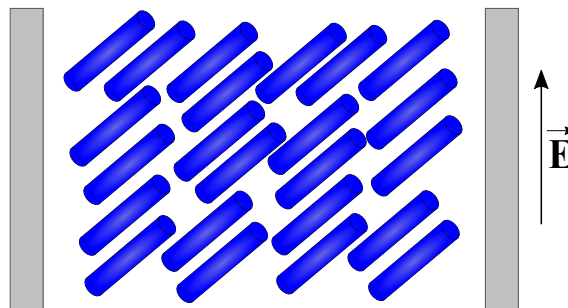
Source: Author, 2021. Adapted from: Khoo, 2007 [34]).

Chapter 5 will focus on electric field effects in the smectic-C phase.

III

MICROSCOPIC THEORIES FOR BULK TRANSITIONS IN LIQUID CRYSTALLINE SYSTEMS

In recent decades, remarkable interest has developed towards understanding phase transitions involving smectic liquid crystals with a tilted molecular alignment [59, 74–82]. Different experimental techniques helped determine the nature of smectic-C–smectic-A (Sm-C–Sm-A) and smectic-C–nematic (Sm-C–N) phase transitions [59, 74, 76, 77, 79, 83–86]. In rod-like compounds with a small or moderate transverse dipole moment ($P \leq 20$ nC/cm^2), it has been verified that the Sm-C–Sm-A phase transition is a second order transition [74, 77], while the Sm-C–N phase transition exhibits first order behaviour with low latent heat [74]. Moreover, the analysis of heat-capacity measurements in several compounds revealed that the temperature range of the Sm-A phase plays an important role to the behaviour of continuous Sm-C–Sm-A phase transition [83], delimiting the crossover between the mean-field tricritical and the ordinary mean-field character of this transition [79]. However, a first order Sm-C–Sm-A phase transition has been reported in smectogenic compounds with a large transverse dipole moment ($P > 50$ nC/cm^2) [84], over a large smectic-A temperature range [79]. nematic–smectic-A–smectic-C (NAC) multicritical points have been reported in both binary liquid crystal mixtures [58] and single component systems under high pressures [59].

Motivated by the rich phenomenology of experimental results, several theoretical studies better described smectic-C liquid crystal phase transitions [44, 87–93]. In fact, a large variety of microscopic models have been introduced to characterise intermolecular interactions in smectogenic systems. Assuming a bilinear mean-field potential for the tilt angle distribution, Gieβelman and Zugenmeier provided an equation of state for the smectic-C phase [88], consisting of a Langevin function of the reduced tilt angle and reduced temperature. Despite

well describing the tilt angle's dependence on temperature, such oversimplified models cannot reproduce the full variety of experimental phase diagrams. Considering a system of rod-like molecules with a perfect orientational order, van deer Meer and Vertogen analysed how a dipole-induced interaction leads to the emergence of a tilted smectic phase [43], in which the Sm-C–Sm-A transition is not the usual order-disorder type. Based on molecular interactions between rod-like molecules with off-axis dipoles, Govind and Madhusudana developed a modified version of McMillan's model for Sm-A–N–Iso systems, being successful in the description of experimental phase diagrams presenting the smectic-C phase [44, 89]. However, such a model requires the introduction of an excluded-volume contribution which stabilises the Sm-A phase, thus leading to a large number of free parameters. Using a complete set of orientational and translational order parameters, recent studies introduced different pair-interaction potentials for polar and nonpolar molecules, reproducing phase diagrams containing conventional or "de Vries-type" smectic-C phases [91, 92, 94–96]. Nevertheless, the use of a complete set of order parameters implies a large number of free parameters in the molecular models, which makes their comparison with typical characteristics of liquid-crystalline compounds difficult.

3.1 Microscopic Theories of Liquid Crystalline Phase Transitions: A Review

As already discussed, liquid crystals are characterised by long-range orientational order that can coexist with some degree of positional order. Ever since the discovery of liquid-crystalline phases, several theoretical approaches have sought to understand the long-range orientational order and properties of the nematic phase, as well as other types of order in more complex phases. As we will see, molecular theories can successfully address the physical behaviour of these materials during phase transitions and, consequently, in the vicinity of transition temperatures.

3.1.1 Maier-Saupe Theory

The molecular theory of liquid crystals aims to understand the physical behaviour of these materials during phase changes and in the vicinity of the transition temperature. Theories of the nematic phase's behaviour in the vicinity of its phase transitions have followed several directions. One of the most applied approaches uses the phenomenological theory of Landau-de Gennes, in which the Helmholtz free energy is expressed in terms of powers and gradients of the order parameters. In this model, five or more adjustable parameters, associated with the symmetry of the system and physical processes, are determined experimentally.

One useful approach in developing a long-range orientational order theory related to nematic phase properties is molecular field theory, the first for the nematic phase was proposed by Born in 1916. In this theory, Born treated the medium as a set of permanent electric dipoles and demonstrated the possibility of transition from an isotropic phase to an anisotropic phase with decreasing temperature.

The best known theory based on the molecular field approximation was devised by Maier and Saupe in the late 1960s. In the Maier-Saupe formalism, each molecule is subject to an internal mean field that is independent of any local variation or short-range ordering. The individual intermolecular forces need not be specified for the development of the theory. However, in the original work, Maier and Saupe assume that the stability of the nematic phase arises from the anisotropic part of dispersion forces.

In the Maier-Saupe theory, the anisotropic shape of molecules is ignored and Coulombian dipole-dipole interactions are considered. Thus, if we consider a pair of molecules, the interaction between them is

$$V_{12}(\theta_{12}) = -\frac{V_0}{N}\left(\frac{3}{2}\cos^2\theta_{12} - \frac{1}{2}\right) = -\frac{V_0}{N}P_2(\cos\theta_{12}), \tag{3.1}$$

where V_0 is a constant or characteristic potential, N represents the number of molecules, P_2 is the second Legendre polynomial and θ_{12} is the angle between the major axes, $\vec{a}_1$ and $\vec{a}_2$, of the molecules 1 and 2 (see figure 3.1).

Figure 3.1: Representative scheme of the angle between two rod-like molecules interacting according to the Maier-Saupe potential.
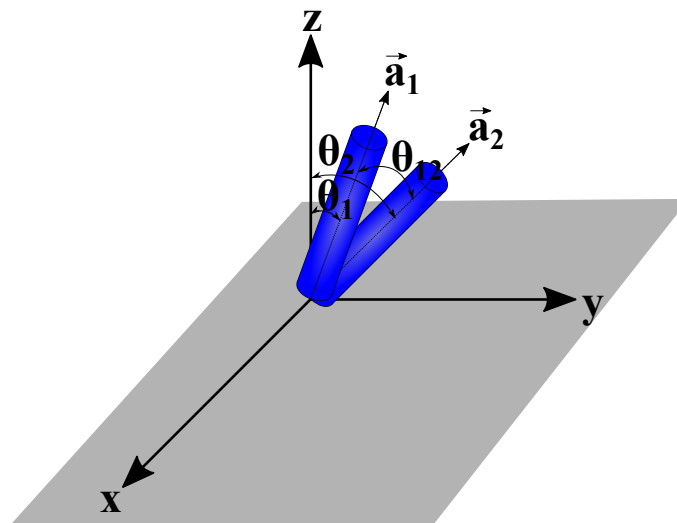
Source: Author, 2021.

The addition theorem for spherical harmonics states that

$$P_2\left(\cos\theta_{12}\right) = P_2\left(\cos\theta_1\right)P_2\left(\cos\theta_2\right) + 2\sum_{m=-2}^{2}P_2^m\left(\cos\theta_1\right)P_2^m\left(\cos\theta_2\right)\cos\left[m\left(\phi_1 - \phi_2\right)\right], \quad (3.2)$$

where θ_1 and θ_2 are the angles between the major axis of each molecule and the preferred axis, and θ_{12} is therefore their difference. In the nematic phase, the system has azimuthal symmetry, so that $m = 0$, leaving only one term in the addition theorem. Thus, the interaction potential between the molecules is

$$V_{12}(\theta_1,\theta_2) = -\frac{V_0}{N}P_2(\cos\theta_1)P_2(\cos\theta_2). \tag{3.3}$$

In a mean-field approximation, each molecule is subject to a field due to its interaction with all other molecules in the medium. Thus the following integral determine the interaction potential between two molecules:

$$V_1(\theta_1) = \frac{N\int d^3\vec{r_2}V_{12}(\theta_1,\theta_2)e^{-\frac{V_{12}}{k_BT}}d\Omega_2}{\int d^3\vec{r_2}e^{-\frac{V_{12}}{k_BT}}d\Omega_2}, \tag{3.4}$$

where the integral in r_2 refers to the position, while the integral in the solid angle Ω_2 refers to the possible orientations of molecule 2.

After some algebra, it is possible to show that the potential of a single molecule is

$$V_i = -V_0\left(\frac{3}{2}\cos^2\theta_i - \frac{1}{2}\right)s, \tag{3.5}$$

where $s = \left\langle \frac{3}{2}\cos^2\theta - \frac{1}{2}\right\rangle$ is the order parameter that describes average molecular alignment.

Considering a system of N particles in the Maier-Saupe approximation, the internal energy per molecule is defined as

$$U = \frac{N}{2}\bar{V_i}, \tag{3.6}$$

where $\bar{V_i}$ is the average value of the interaction potential of one particle. Thus, the internal energy of the nematic phase is:

$$U = -\frac{NV_0s^2}{2}. \tag{3.7}$$

Entropy is defined as $S = N\left(k_B\ln Z + \frac{\bar{V_i}}{T}\right)$, where Z is the one-particle partition function, given by

$$Z = \int e^{-\frac{V_i}{k_BT}}d(\cos\theta_i). \tag{3.8}$$

Thus, the entropy reads

$$S = Nk_B \left[\ln \int_0^1 e^{\frac{-V_i}{k_B T}} d(\cos \theta_i) - \frac{V_0 s^2}{k_B T} \right].$$

(3.9)

The Helmholtz free energy, defined as $F = U - TS$, is given by:

$$F = \frac{NV_0 s^2}{2} - Nk_B T \ln \int_0^1 e^{\frac{-V_i}{k_B T}} d(\cos \theta_i).$$

(3.10)

The condition for equilibrium is:

$$\left(\frac{\partial F}{\partial s} \right)_{V,T} = 0.$$

(3.11)

This condition is satisfied when all molecules are aligned on average in the same preferential direction, with the nematic order parameter given by:

$$s = \frac{\int_0^1 P_2(\cos \theta) e^{\frac{-V}{k_B T}} d(\cos \theta)}{\int_0^1 e^{\frac{-V}{k_B T}} d(\cos \theta)}.$$

(3.12)

Note that this is a self-consistent equation, given that the interaction potential depends on the value of the order parameter s that minimises the Helmholtz free energy.

Figure 3.2: Variation of free energy with the order parameter as calculated by Maier-Saupe theory, for different temperatures.
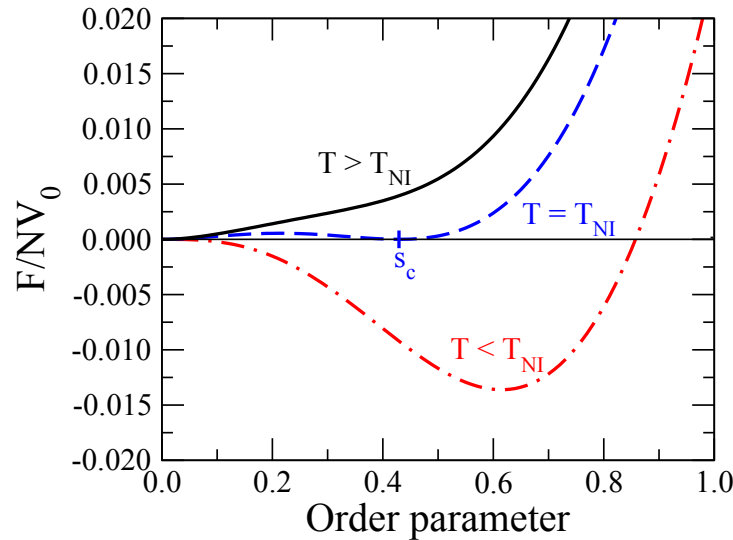
Source: Author, 2021.

Figure 3.2 shows the temperature dependence of the Helmholtz free energy on the order parameter s. The free energy minimum, therefore, occurs at the value of s that satisfies the self-consistent equation. Let T_{NI} be the nematic-isotropic transition temperature. For $T < T_{NI}$, there is only one minimum with $s > 0$ corresponding to the ordered phase, that is, the nematic phase. For $T = T_{NI}$, there are two minima: one at $s = 0$ and the other at $s = s_c$. However, these two

states have the same energy. At this temperature, therefore, a discontinuous transition occurs
without change in volume, but with an abrupt change in the order parameter, with the coexis-
tence of nematic and isotropic phases. For $T > T_{NI}$, there is only one minimum that corresponds
to the disordered phase, that is, the isotropic phase with $s = 0$.

By setting $F = 0$, we obtain the order parameter at the transition, $s_c = 0.4292$. This value is very
close to the experimental value observed in N–Iso transitions, which demonstrates the success
of the Maier-Saupe theory in this context.

Figure 3.3 shows the dependence of the nematic order parameter s with the reduced temperature,
where the order parameter, and entropy are discontinuous, and specific heat diverges at the
transition temperature.

Figure 3.3: Order parameter, entropy, and specific heat as a function of the reduced temperature for
Maier-Saupe theory, showing the first-order nematic-isotropic phase transition.
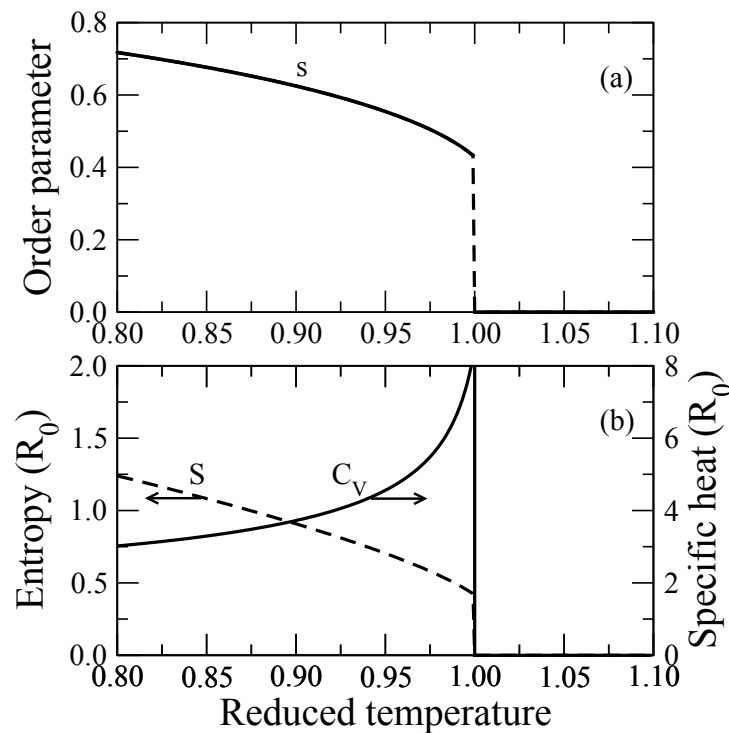
Source: Author, 2021.

Despite describing the nematic phase, this theory is unable to predict phase transitions including
other liquid-crystalline phases, such as the smectic phases. In the following section, we will
present a model that extends the Maier-Saupe theory to liquid-crystalline systems presenting
the smectic-A phase.

3.1.2   McMillan Model

Different models have proposed how interactions between calamitic molecules induce the formation of smectic layers. These models show that short-range interactions between the molecules can favour the modulation in the density of the sample, characteristic of the smectic phase.

Within this context, McMillan [42] proposed a simple but elegant description of the smectic phase A. This model, which is an extension of the Maier-Saupe theory for the nematic-isotropic transition, includes an additional order parameter that characterises the one-dimensional translational periodicity of a layered structure.

We must remember that calamitic molecules are formed by a rigid structure, consisting of aromatic rings joined or not by a linking chain. Flexible alkyl chains are attached to this rigid structure. The central aromatic region of the molecule has a high polarizability, causing such regions of neighbouring molecules to interact strongly. Thus, the formation of the smectic layers depends on the size of the alkyl chain, which must be large enough to separate the central aromatic regions, allowing the layers to form.

In McMillan's model, molecules interact according to a short-range potential that depends on the position and relative orientation of the molecules (figure 3.4).

Figure 3.4: Representative scheme of the relative position of two rod-like molecules.
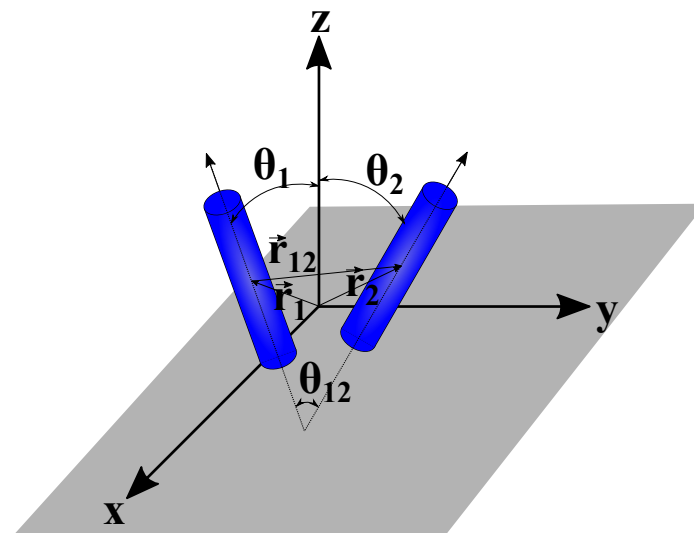
Source: Author, 2021.

The anisotropic part of this potential is given as:

$$V_{12}(r_{12}, \theta_{12}) = -\left(\frac{V_0}{N r_0^3 \pi^{\frac{3}{2}}}\right) e^{-\left(\frac{r_{12}}{r_0}\right)^2} P_2(\cos \theta_{12}), \tag{3.13}$$

where r_0 is on the order of the length of the rigid part of the molecule, r_{12} is the distance
between the molecules' centres, θ_{12} is the angle between the principal molecular axes and N is
the number of molecules per unit volume. P_2 is the Legendre polynomial of second order, V_0 is
the amplitude of interaction. The Gaussian term characterises the interaction as short-range.

The smectic phase is characterised by the existence of a well-defined distance, d, separating the
layers. Considering that the molecular alignment is in the z direction, normal to the plane of the
layers, the Gaussian term can be expanded in Fourier series. If keeping only the first term of the
series and considering that, by the addition theorem, $P_2(\cos\theta_{12}) = P_2(\cos\theta_1)P_2(\cos\theta_2)$, it is
possible to show that the effective potential for a particle inside a mean field approximation is;

$$V(z, \theta) = -V_0 \left[s + \alpha\sigma\cos\left(\frac{2\pi z}{d}\right) \right] P_2(\cos\theta), \quad \alpha = 2e^{-\left(\frac{\pi r_0}{d}\right)^2}. \tag{3.14}$$

Here s and σ are the nematic and smectic order parameters respectively. The potential min-
imises the free energy when its molecule lies in the plane of the smectic layer along the z axis.

The distribution function for a single particle is;

$$f(z, \theta) = exp[-V(z, \theta)/k_B T], \tag{3.15}$$

where k_B is the Boltzmann constant and T is the temperature. The order parameters are defined
as:

$$s = \left\langle \frac{3\cos^2\theta - 1}{2} \right\rangle, \tag{3.16}$$

and

$$\sigma = \left\langle \left(\frac{3\cos^2\theta - 1}{2}\right)\cos\left(\frac{2\pi z}{d}\right) \right\rangle. \tag{3.17}$$

Here, $\langle A \rangle$ denotes the statistical mean over the distribution function. s defines the orientational
order, as in the Maier-Saupe model. σ is a new parameter that represents the measure of the
amplitude of the density wave describing the layered structure. The order parameters are defined
by the self-consistency relations, since the effective potential depends on s and σ. The equations
for the order parameters can be solved numerically to give three possible solutions:

- if $s = \sigma = 0 \rightarrow$ isotropic phase;

- if $s \neq \sigma$ and $\sigma = 0 \rightarrow$ nematic phase;

- if $s \neq \sigma$ and $\sigma \neq 0 \rightarrow$ smectic-A phase.

These solutions are obtained by adjusting the two free parameters of the model: V_0 and α. For

this model, the Helmholtz free energy can be written as

$$ F = \frac{NV_0}{2} \left(s^2 + \alpha \sigma^2 \right) - N k_B T \ln \left[\frac{1}{d} \int_0^1 dz \int_0^1 d(\cos \theta) f(z, \theta) \right]. \qquad (3.18) $$

The material is characterised by two parameters: V_0 determines the nematic-isotropic transition temperature and $\alpha \in [0, 2)$ establishes the intensity of the interaction that induces the formation of the smectic layers. α also depends on the ratio between the length of the rigid part of the molecule and the layer thickness. Experimentally, d is of the order of the molecular length. In general, the energy associated with smectic ordering tends to increase with α. Therefore, α increases with the length of the alkyl chain.

Figure 3.5: (a) Nematic and smectic order parameters, (b) entropy and specific heat *versus* reduced temperature for $\alpha = 0.60$.
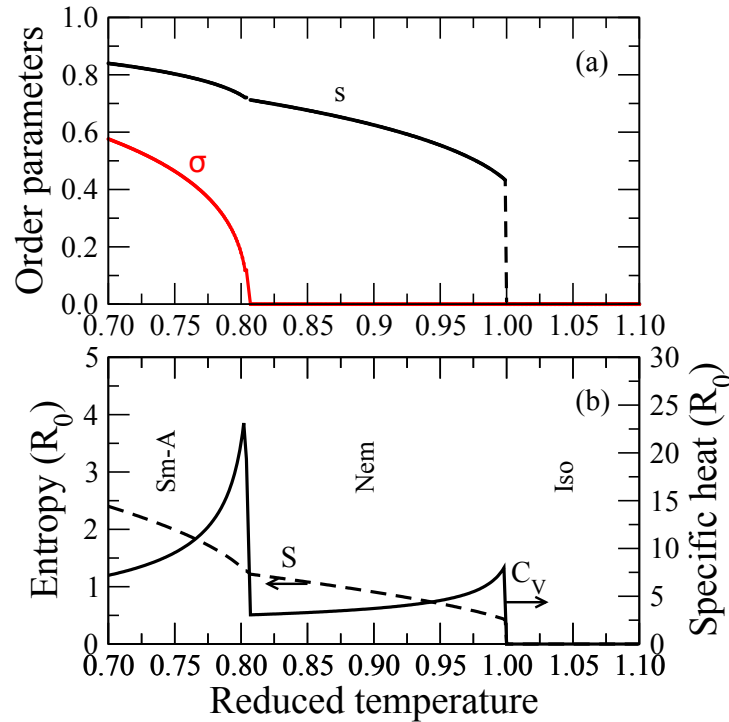
Source: Author, 2021.

We show the temperature dependence of the order parameters, entropy and specific heat for increasing values of α, the model parameter. For $\alpha = 0.60$ (figure 3.5), the behaviour of the order parameters, entropy change and specific heat shows that the Sm-A–N transition is second-order, and the N–Iso transition is first-order. For $\alpha = 0.85$ (figure 3.6), we have first-order Sm-A–N and N–Iso transitions. Finally, for $\alpha = 1.10$ (figure 3.7), we can note that there is only the first-order Sm-A–Iso transition, with the nematic phase totally suppressed.

From the $T - \alpha$ phase diagram obtained by McMillan (figure 3.8), we note that, for $\alpha > 0.98$, the smectic phase can transform directly into the isotropic phase, while for $\alpha < 0.98$ there is

Figure 3.6: (a) Nematic and smectic order parameters, (b) entropy and specific heat *versus* reduced temperature for $\alpha = 0.85$.
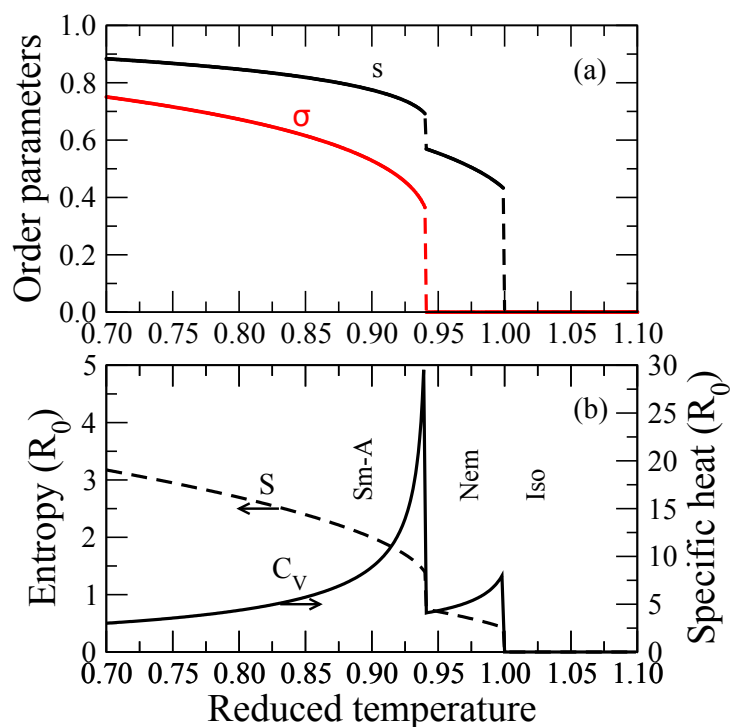
Source: Author, 2021.

Figure 3.7: (a) Nematic and smectic order parameters, (b) entropy and specific heat *versus* reduced temperature for $\alpha = 1.10$.
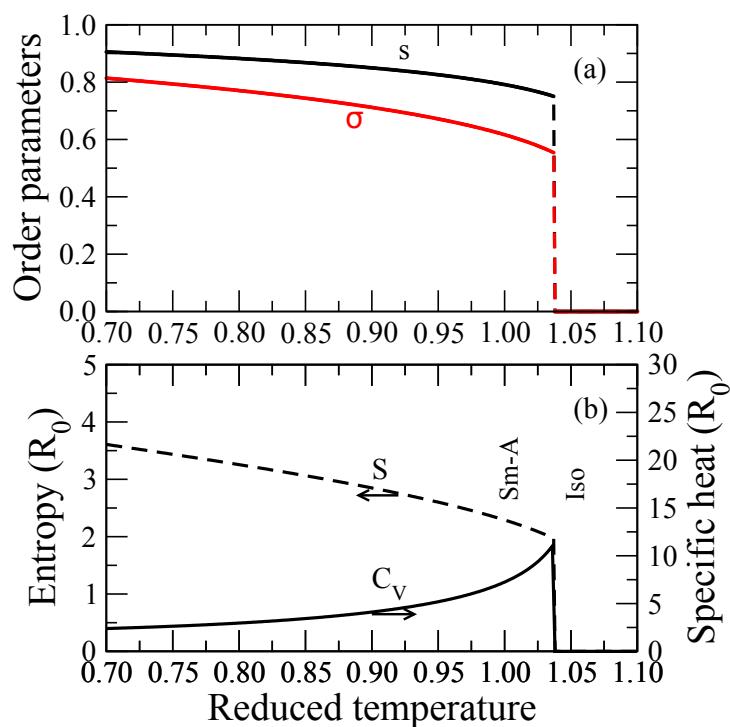
Source: Author, 2021.

a Sm-A–N transition followed by a N–Iso transition at higher temperatures. Furthermore, for $\alpha < 0.70$, the model predicts a second-order Sm-A–N transition, whereas for $\alpha > 0.70$ it is predicted to be first-order. Thus, $\alpha = 0.70$ corresponds to a tricritical point, in which a first-order transition line meets a second-order transition line.

Figure 3.8: Phase diagram for McMillan's theoretical model, transition temperature *versus* the model parameter α. The dashed (solid) line indicates a second-order (first-order) transition.
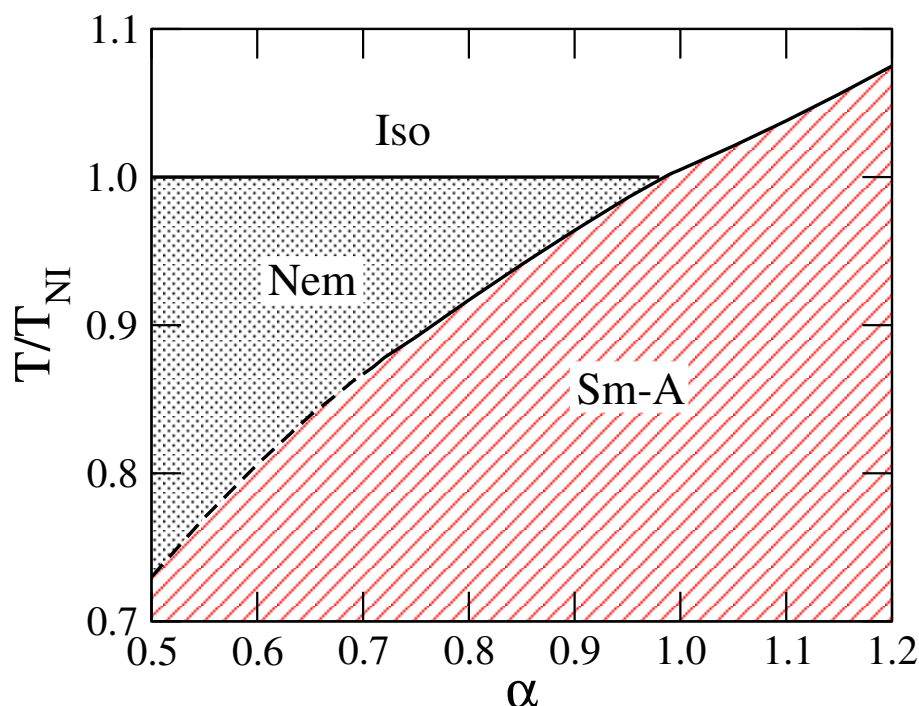
Source: Author, 2021.

Thus, McMillan's model satisfactorily describes some aspects of experimentally observed phase transitions in liquid crystals, such as the dependence of different transitions on homologous series. However, McMillan's model neglects surfaces, so it cannot describe freely suspended thin films. These systems will be discussed in chapter 4. Another limitation is that the model does not allow us to distinguish different smectic phases. This originates from the spatial part of the potential being spherically symmetrical, thus preventing the preferential direction of the molecules to emerge naturally from the model. Next, we will revise a model proposed to address this limitation.

3.1.3 Govind-Madhusudana Model

Organic compounds that exhibit the smectic-C phase are made of rod-shaped molecules with a lateral dipole moment. Govind and Madhusudana proposed descriptions of smectic-C phase transitions by arguing that a proper molecular theory for the smectic-C phase must include

the phase's intrinsic biaxiality. Furthermore, it is assumed that its molecular tilt is due to the compounds' lateral dipolar components, and that the molecular potential used should be derived from their proposed tilt mechanism.

Figure 3.9: Proposed off-axis dipolar mechanism tilt in smectic-C layers. The repulsive interactions from the antiparallel configuration of dipoles as in (a) is much larger than the attractive interaction of the parallel configuration (b), or the repulsive interaction shown in configuration (c) resulting in a relative shift of the molecules (d).
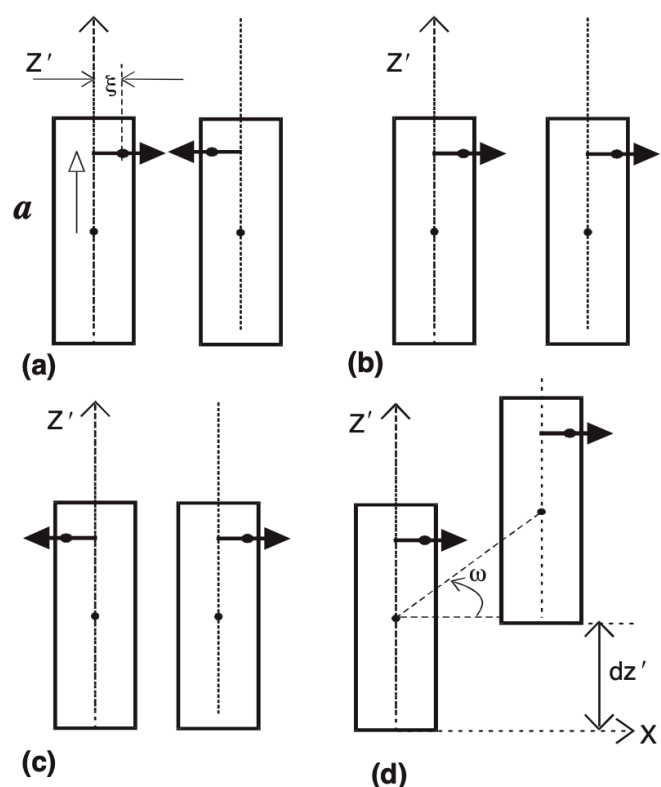
Source: Govind and Madhusudana, 2002 [89].

While neighbouring molecules in a smectic layer rotate freely about their major axes in a preferred average direction, the lateral dipoles face each other in close spatial proximity. This contributes to a large repulsive interaction, especially when the molecular centres are at the same z' coordinate. In the configuration shown in figure 3.9(b), the dipole interaction is attractive. If the dipoles are along the molecular major axis, the average energy would be zero when both molecules rotate freely about their major axes. Since the dipoles are off-axis, their separation decreases, shown in figure 3.9(a). The dipoles also lie antiparallel when they are more distant (figure 3.9(c)), but the corresponding repulsive interaction is quite small. The net contribution when averaged over molecular rotations is repulsive. In the smectic-C phase, the angle of inclination with respect to the normal plane of the layers is equivalent to having neighbouring molecules displaced along dz' in the inclination plane (figure 3.10).

Govind and Madhusudana took the following into account in their model:

Figure 3.10: The relative shift of molecules along Z' shown in (a) is equivalent to a tilting of the molecules in the layers with the layer normal along Z (b).
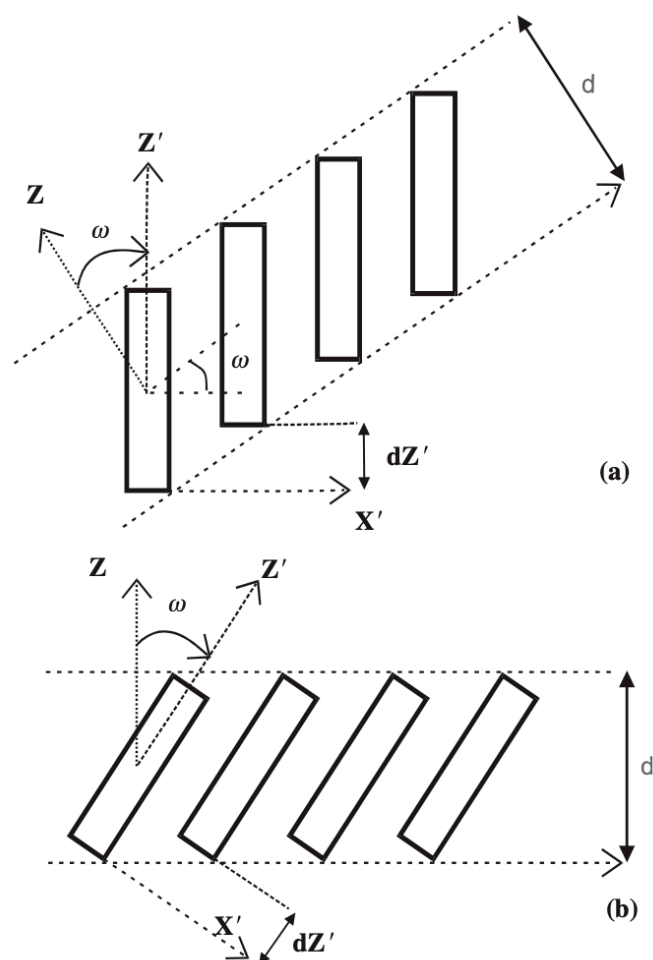
Source: Govind and Madhusudana, 2002 [89].

- the molecules are rod-shaped with an off-axis lateral dipole, and can rotate freely along the molecular major axis;

- the molecules tilt only in one plane, and the displacement is zero in a plane orthogonal to the tilting plane;

- the molecules experience an attractive potential due to dispersion interactions between the aromatic nuclei.

Experimental studies indicate that the stability of the Sm-C phase strongly depends on the molecular structure. In general, molecules with stronger dipoles lead to larger tilt angles, and the addition of a terminal dipole increases the stability of the Sm-C phase. It can be seen that the theoretical trends are reflecting the experimental ones, and the assumption that the tilt is a consequence of lateral off-axis dipoles seems reasonable.

The authors proposed a single-particle tilt potential considering the following facts:

- The molecular tilt is only possible with layer ordering. Since the sign of the relevant order parameter τ only depends on the choice of origin, by symmetry, the tilt potential only depends on τ^2. So, $U_C \propto \tau^2$.

- The strength and number of minima in the inclination potential depend on the detailed molecular structure. Thus, $U_C(\theta_i) \propto -\sum_n \beta_n \sin 2n\theta_i$, where β_n depends on the strength and geometric arrangement of the dipoles.

- Their calculations assumed perfectly ordered molecules ($S = 1$). However, in reality $S \neq 1$ and therefore angles θ and ϕ must vary according to an appropriate distribution function. Therefore, U must be coupled to S. However, the direct coupling of U_C with S was not considered.

- The inclination potential depends on ϕ, as the Sm-C phase is biaxial. So, $U_C(\phi_i) \propto \cos\phi_i$.

- As in any mean-field theory, the single-particle potential depends on the extent of the relevant ordering in the medium. Considering η the order parameter of the Sm-C phase, one should have $U_C \propto \eta$.

Under these conditions, the one-particle tilting potential, consistent with biaxial symmetry, is written as

$$U_C(\theta_i, \phi_i) \propto -\sum_n \beta_n \eta_n \tau^2 \sin 2n\theta_i \cos\phi_i, \tag{3.19}$$

where β_n depends on the strength and geometrical arrangement of the molecule's dipoles. $\tau = \langle \cos(2\pi z/d) \rangle$ is the translational order parameter, where z is the position of the centre of the molecule along the axis normal to the layer plane, $\vec{z}$ and d is the layer spacing. $\eta_n = \langle \sin 2n\theta \cos\phi \rangle$ gives the tilting order parameter, with θ_i and ϕ_i the polar and azimuthal angles of the major axis of the i-th molecule with respect to the coordinate axis. For simplicity, the calculations were restricted to $n = 1$, allowing a maximum tilt of $45°$.

The layering potential considered was proposed by McMillan for the smectic-A phase. However, Govind and Madhusudana chose the decoupled form of the potential, following Katriel and Kventsel:

$$U_M(\psi_i, z_i) = -U_0 \left[1 + \alpha\eta \cos\left(\frac{2\pi z_i}{d}\right) \right] S \left(\frac{3\cos^2\psi_i - 1}{2} \right), \tag{3.20}$$

where $S = \langle 3\cos^2\psi - 1 \rangle / 2$ is the nematic order parameter and α is McMillan's model parameter for the formation of smectic layers.

As aforementioned, this layering potential neither specifies the relative orientation between the director nor the layer normal. In order to ensure that the smectic-A phase exists, an excluded-volume contribution must be considered. To do so, elongated right circular cylinders are considered, with an excluded area of $4\pi R^2/$ in the smectic-A phase, where R is the radius of cross-section of the cylinders. In the smectic-C phase, a small tilt angle ω increases the excluded area by $\Delta A \propto \sin^2 \omega$.

In hard-rod models, the increase in the free energy due to the hard-core interaction is proportional to the excluded volume, and so to ΔA. It also depends on τ^2, given the argument used earlier, that the molecular tilt only exists in the presence of a layering order. Goossens shows that, for ellipsoids, the proportionality factor must be a function of the orientational order. Govind and Madhusudana, however, argue that this dependence can be neglected. The increase in the free energy due to excluded volume effects is then given by

$$\delta F_{hr} = \gamma K_B T \tau^2 \sin^2 \omega, \tag{3.21}$$

where $\gamma > 0$ is a parameter dependent on the ellipsoid's dimensions.

The molar Helmholtz free energy is given by

$$
\begin{aligned}
F &= -\frac{NU_0}{2}\left[(1+\alpha\tau^2)S^2 + \alpha\beta\tau^2\eta^2\right] \\
&+ Nk_BT\left[\frac{1}{2\pi d}\int_{-1}^{+1} d\cos\theta \int_0^\pi d\phi \int_{+d/2}^{-d/2} dzf\ln f + \gamma\tau^2\sin^2\omega\right],
\end{aligned}
\tag{3.22}
$$

where $f(\theta, \phi, z)$ is the single-particle distribution function:

$$
\begin{aligned}
f &= Z^{-1}exp\left\{\left(\frac{U_0}{k_BT}\right)\left[(1+\alpha\tau^2)S\left(\frac{3\cos^2\psi - 1}{2}\right) + \alpha\beta\tau^2\eta\sin 2\theta\cos\phi\right]\right. \\
&+ \left.\left[\left(\frac{U_0}{k_BT}\right)\alpha(S^2 + \beta\eta^2) - 2\gamma\sin^2\omega\right]\tau\cos\left(\frac{2\pi z}{d}\right)\right\},
\end{aligned}
\tag{3.23}
$$

and Z is the normalising integral.

The order parameters, obtained as the averages over the distribution function are:

$$S = \frac{1}{2\pi d}\int_{-1}^{+1} d\cos\theta \int_0^\pi d\phi \int_{-d/2}^{+d/2} dzf\left(\frac{3\cos^2\psi - 1}{2}\right), \tag{3.24}$$

$$\tau = \frac{1}{2\pi d}\int_{-1}^{+1} d\cos\theta \int_0^\pi d\phi \int_{-d/2}^{+d/2} dzf\cos\left(\frac{2\pi z}{d}\right), \tag{3.25}$$

$$\eta = \frac{1}{2\pi d} \int_{-1}^{+1} d\cos\theta \int_{0}^{\pi} d\phi \int_{-d/2}^{+d/2} dz f \sin 2\theta \cos \phi. \tag{3.26}$$

These self-consistency equations also minimise the free energy.

In the model, the tilt angle ω, which is the average of all molecular tilt angles θ, appears explicitly, so that the free energy must be minimised with respect to ω. Its variation closely follows η, so that for small values, one can expect $\omega \approx \eta/2$ (see figure 3.11). The temperature dependence on the order parameters s, τ and η is also shown in figure 3.11, for the model parameters $\alpha = 0.95$, $\beta = 0.4$ and $\gamma = 3$. As expected, we can see a second-order Sm-C–Sm-A followed by first-order Sm-A–N and N–Iso phase transitions.

Figure 3.11: Temperature variations of the order parameters S, τ and η and the tilt angle ω for $\alpha = 0.95$, $\beta = 0.4$ and $\gamma = 3$.
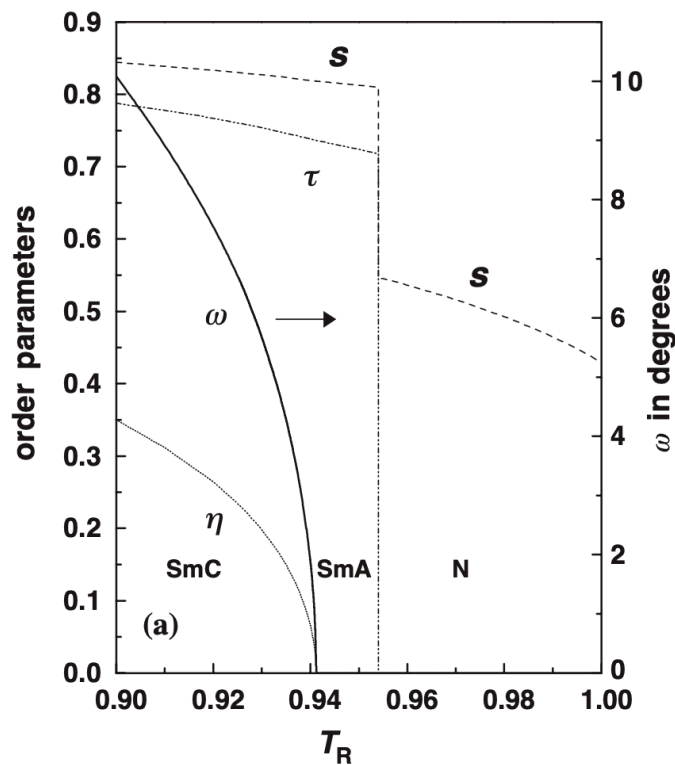
Source: Govind and Madhusudana, 2002 [89].

The phase diagram $T - \alpha$ is shown in figure 3.12 for $\gamma = 3$ and $\beta = 0.42$. As α is increased, the Sm-A range decreases to zero, giving rise to a first-order Sm-C–N transition. Despite not being immediately evident, there is a small increase in slope between the N–Sm-A and N–Sm-C transition lines.

Figure 3.12: Calculated phase diagram $T - \alpha$ for $\gamma = 3$ and $\beta = 0.42$. The dashed line indicates a second-order transition and the solid line indicates a first-order transition. The jump in η at the first-order Sm-C–N transition decreases to zero as the N–Sm-A–Sm-C point is reached.
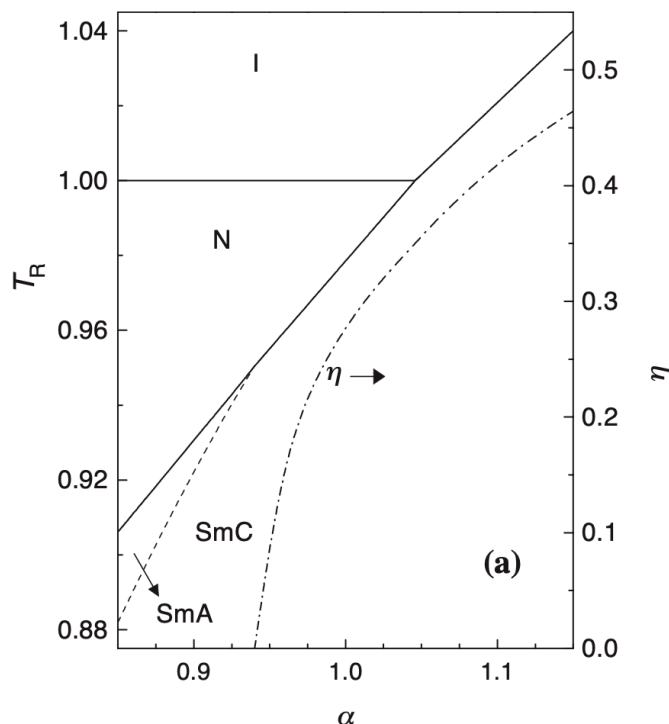
Source: Govind and Madhusudana, 2002 [89].

3.2 Microscopic Model for Bulk Transitions of Smectogenic Systems in the Smectic-C Phase

As discussed in the previous section, it is possible to create microscopic models of liquid crystalline systems by considering the interaction potential between molecules. However, the description of phase transitions involving liquid-crystalline phases with more ordering degrees requires a larger number of free parameters in these models. We have seen that the model proposed by Govind and Madhusudana can adequately describe phase transitions involving liquid crystals in the smectic-C phase. However, a high number of free parameters and an additional excluded-volume contribution is needed to satisfactorily describe these systems. In order to extend the model to freely suspended smectic-C films in the next chapter, we will first introduce a model similar to that of Govind and Madhusudana, but with fewer free parameters.

We investigate a single component smectogenic system of rod-like molecules with a small or moderate transverse dipole moment [89], which presents a layer contraction in the tilted smectic phase. In order to characterise the average molecular orientation inside the smectic layers, the relative orientation of the director $\vec{n}$ ($|\vec{n}| = 1$) to the smectic wave vectors $\vec{q}$, given by the

average tilt angle ω, is considered. These are shown in figure 3.13(a), where $\vec{q}$ is assumed to be normal to the smectic layer plane ($x - y$ plane), whose magnitude depends on the layer spacing d ($|\vec{q}| = 2\pi/d$).

Figure 3.13: (a) Schematic representation of the long molecular axis $\vec{a}$ in the Sm-C phase, for a Cartesian coordinate system, with the z-axis normal to the smectic layer plane. (b) Representation of the layer contraction induced by the molecular tilt, with d_0 the layer spacing in the Sm-A phase.
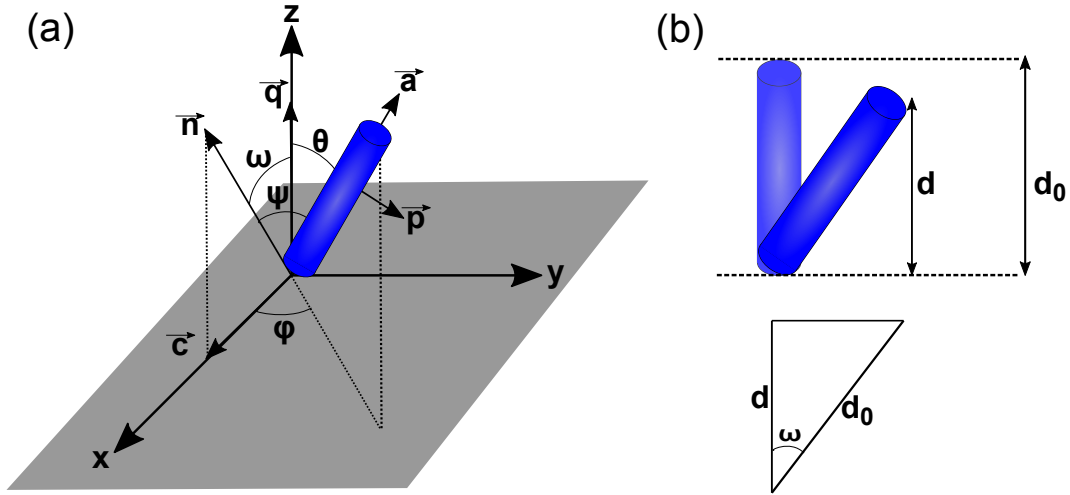
Source: Author, 2021.

For convenience, the director $\vec{n}$ is fixed in the $z - x$ plane in a Cartesian system with the z axis parallel to $\vec{q}$, the orientation of the molecular long axis $\vec{a}$ is defined using polar and azimuthal angles θ and ϕ, respectively. The orientation of the molecular long axis with respect to the director is represented by the angle ψ, which satisfies;

$$\cos\psi = \cos\theta\cos\omega + \sin\theta\sin\omega\sin\phi. \qquad (3.27)$$

In what follows, the average tilt direction is assumed invariant for all smectic layers and that all molecular centres are randomly distributed within the layer's plane. Furthermore, a non-null average tilt leads to a contraction of the layer spacing, defined by $d = d_0\cos\omega$, with d_0 denoting the layer spacing in the smectic-A phase, as represented in figure 3.13(b).

3.2.1 Our Model and Formalism

Using Govind and Madhusudana's approach [44, 89], a single-particle mean-field potential that corresponds to an extension of McMillan's model with the inclusion of a tilting term is written

as

$$V = -V_0 \left\{ \left[s + \alpha\sigma\cos\left(\frac{2\pi z}{d}\right) \right] P_2(\cos\psi) + \alpha\beta\sigma^2\eta\sin 2\theta\cos\phi \right\}. \tag{3.28}$$

In equation 3.28, V_0 is a typical interaction potential that determines the bulk nematic–isotropic transition temperature. $P_2(\cos\psi)$ is the second order Legendre polynomial, where ψ is the angle between the molecular long axis and the director $\vec{n}$. s, σ and η are orientational, translational and tilt order parameters, respectively. β is a constant associated with the geometrical arrangement and the dipole strength in rod-like molecules. The quantity α is given by

$$\alpha = 2\left(\frac{\alpha_0}{2}\right)^{\sec^2\omega}, \tag{3.29}$$

in which α_0 is the geometric parameter related to the length of alkyl chains of rod-like molecules, through the expression $\alpha_0 = 2\exp\left[-(\pi r_0/d_0)^2\right]$. r_0 is a characteristic length associated with the molecular rigid part.

The order parameters s, σ and η are defined by

$$s = \langle P_2(\cos\psi) \rangle, \tag{3.30}$$

$$\sigma = \left\langle P_2(\cos\psi)\cos\left(\frac{2\pi z}{d}\right) \right\rangle, \tag{3.31}$$

and

$$\eta = \langle \sin 2\theta\cos\phi \rangle. \tag{3.32}$$

The thermodynamical averages, $\langle \cdots \rangle$, are computed using the one-particle distribution function;

$$\mathscr{Z}(z,\theta,\phi) \propto \exp[-V/k_B T], \tag{3.33}$$

in which k_B is the Boltzmann constant and T is the temperature. The equilibrium order parameters are solutions of the self-consistent equations, corresponding to the extreme values of the Helmholtz free energy, given by;

$$
\begin{aligned}
\frac{F}{N_0 V_0} &= \frac{1}{2}\left(s^2 + \alpha\sigma^2 + \alpha\beta\sigma^2\eta^2\right) \\
&- \frac{k_B T}{V_0}\ln\left[\frac{1}{2\pi d}\int_{-1}^{1}d\cos\theta\int_0^{\pi}d\phi\int_0^{d}dz\mathscr{Z}\right],
\end{aligned}
\tag{3.34}
$$

where N_0 is the number of molecules. The equilibrium state is determined by the Helmholtz free energy's global minimum. The solutions corresponding to the different phases are

- $s = \sigma = \eta = 0 \rightarrow$ Isotropic;

- $s \neq 0$ and $\sigma = \eta = 0 \to$ Nematic;

- $s \neq 0$, $\sigma \neq 0$ and $\eta = 0 \to$ Smectic-A;

- $s \neq 0$, $\sigma \neq 0$ and $\eta \neq 0 \to$ Smectic-C.

In the present model, the order parameters are numerically determined by the self-consistent equations for different values of tilt angle ω, and for fixed values of T, α_0 and β. The equilibrium configuration is determined by the Helmholtz free energy minimum with respect to ω.

3.2.2   Results

Figure 3.14 shows the Helmholtz free energy as a function of the average tilt angle, in the vicinity of the Sm-C–Sm-A transition temperature T_{CA}, for $\alpha_0 = 0.80$ and $\beta = 0.40$. For $T > T_{CA}$, the null tilt angle corresponds to the only Helmholtz free energy minimum, which excludes the possibility of coexisting Sm-C and Sm-A phases at $T = T_{CA}$. Such a scenario is typical of a second order phase transition, where the energy minimum in the disordered phase becomes a local maximum in the ordered one. When $T < T_{CA}$, the Helmholtz free energy is minimized at a non-null value of tilt angle.

Figure 3.14: Helmholtz free energy with respect to tilt angle ω for $\alpha_0 = 0.80$ and $\beta = 0.40$ and for temperatures: $T = 0.94T_{CA}$ (solid black line), $T = 1.00T_{CA}$ (dashed red line) and $T = 1.01T_{CA}$ (dotted blue line), where T_{CA} is the Sm-C–Sm-A transition temperature. Notice that a non-null tilt angle corresponds to a minimum of the Helmholtz free energy for $T < T_{CA}$.
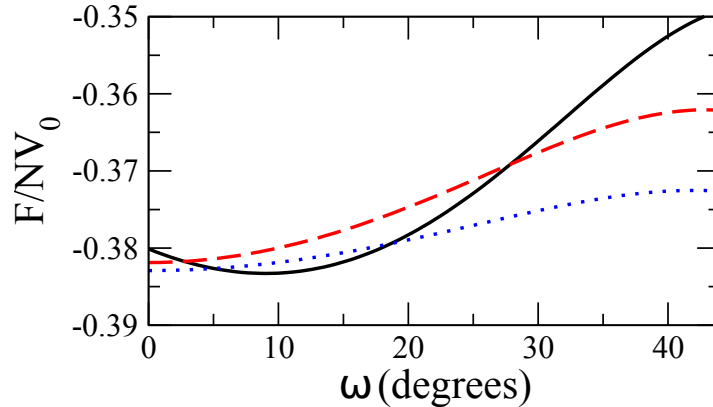
Source: Author, 2021.

We show the temperature dependence of s, σ and η order parameters for $\beta = 0.33$ and different values of α_0. For simplicity, we use a reduced temperature, where the system's temperature is normalised by the nematic–isotropic transition temperature, $T_{NI} = 0.2202V_0/k_B$. For $\alpha_0 = 0.70$,

the tilt order parameter η decays continuously with increasing temperature, while the orientational and translational order parameters stay finite, characterising a second order Sm-C–Sm-A phase transition at $T/T_{NI} = 0.729$ (figure 3.15(a)). At $\eta = 0$, the single particle potential is of McMillan's model, which predicts a second-order Sm-A–N phase transition for $\alpha_0 \leq 0.70$. The translational order parameter σ continuously goes to zero at $T/T_{NI} = 0.867$, signalling a second order Sm-A–N phase transition, as predicted by McMillan's model. Finally, the orientational order parameter s is discontinuous at $T/T_{NI} = 1$, signalling a first order N–Iso phase transition, as predicted by both the Maier-Saupe theory and McMillan's model.

Figure 3.15(b) shows the entropy change and specific heat as a function of the temperature. At $T = T_{CA}$. The entropy change is continuous, while the specific heat has a small discontinuity, characterising a second-order transition. At $T = T_{AN}$, we notice a slope change in the entropy. However, this change is still continuous at the transition, presenting a more pronounced discontinuity in the specific heat, also characterising a second-order transition. Finally, at $T = T_{NI}$, the entropy change is discontinuous, which is typical of a first-order phase transition.

Figure 3.15: Temperature dependence of (a) orientational, s, translational, σ, and tilt, η, order parameters and (b) entropy and specific heat for $\beta = 0.33$ and $\alpha_0 = 0.70$.
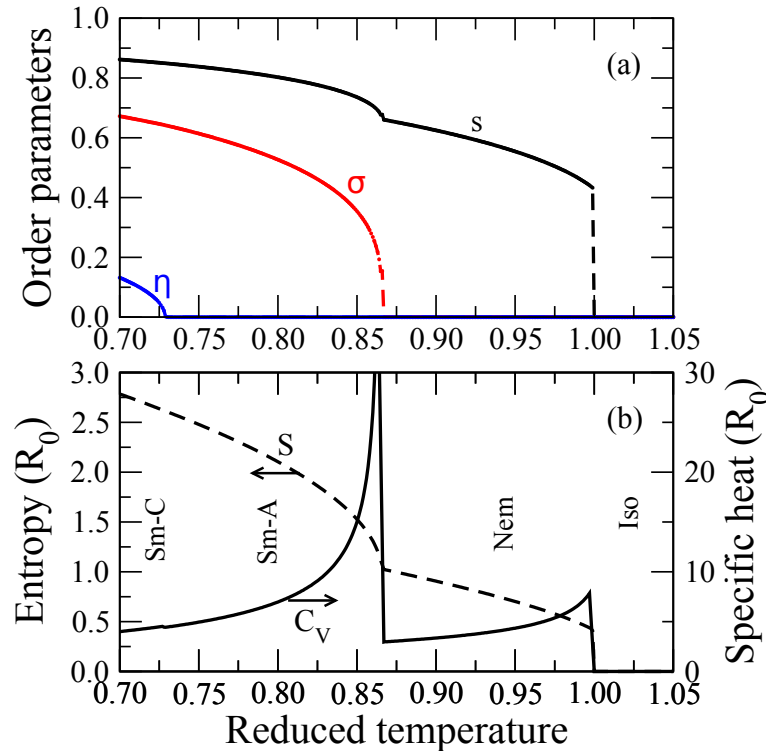
Source: Author, 2021.

McMillan's model predicts a first-order Sm-A–N phase transition for $\alpha_0 > 0.70$. In figure 3.16, we notice that when $\alpha_0 = 0.75$, the translational order parameter σ develops a discontinuity at $T/T_{NI} = 0.892$, which is accompanied by an abrupt reduction of the orientational order parameter s, signalling a first order Sm-A–N phase transition.

Figure 3.16: Temperature dependence of (a) orientational, s, translational, σ, and tilt, η, order parameters and (b) entropy and specific heat for $\beta = 0.33$ and $\alpha_0 = 0.75$.
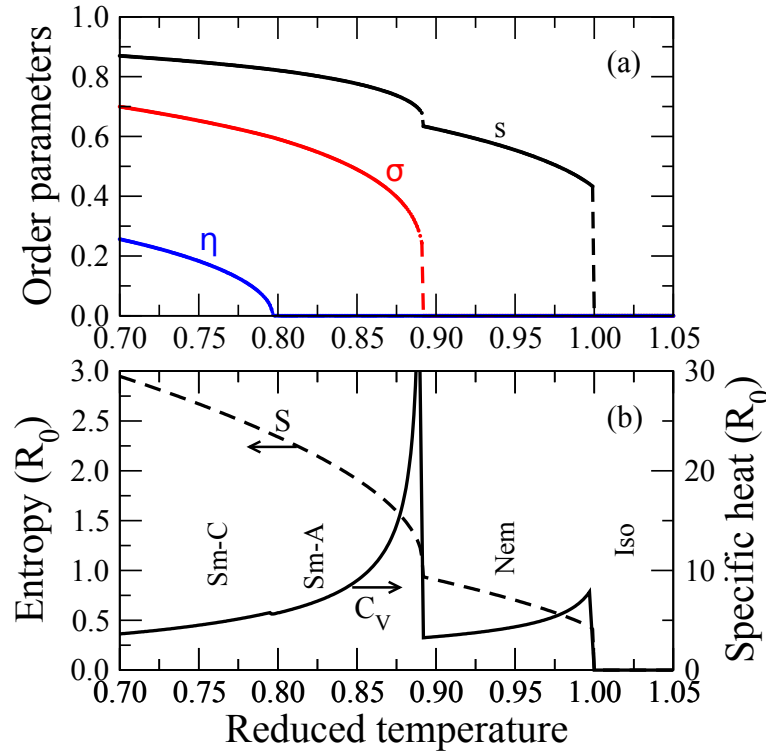
Source: Author, 2021.

Furthermore, we notice that increasing α_0 alone favours molecular tilting, and therefore the smectic-C phase (see figures 3.15 and 3.16). This is because molecular tilting is only relevant in the presence of layering, and the strength of the tilting potential is proportional to both β and $\alpha = \alpha(\alpha_0, \omega)$. Since the nematic–isotropic transition temperature only depends on the interaction potential's amplitude, V_0, favouring the smectic-C phase causes the temperature range of the smectic-A and nematic phases to decrease with increasing α_0.

Moreover, we can use T_{CA}/T_{NI} and T_{AN}/T_{NI} to compare these results with experimental findings for smectogenic compounds with a small transverse dipole moment. Recall that the nonchiral liquid crystalline compound p-decyloxybenzoic acid p-n-hexyphenyl ester (DOBHOP) exhibits a second order Sm-C–Sm-A phase transition, followed by a first order Sm-A–N phase transition, with $T_{CA}/T_{NI} = 0.872$ and $T_{AN}/T_{NI} = 0.937$ [32]. As the DOBHOP molecules present a small transverse dipole moment ($P \approx 4$ nC/cm^2) [97], the present results indicate that the single-particle molecular potential of equation 3.28 provides a reasonable description of the phase sequence of DOBHOP compound with model parameter values of $\beta = 0.33$ and $\alpha_0 = 0.85$ (figure 3.17).

To characterise the effects of molecular structure on the tilt behaviour of the smectic-C phase, the tilt angle's temperature dependence for $\beta = 0.33$ and distinct values of α_0 are shown in

Figure 3.17: Temperature dependence of (a) orientational, s, translational, σ, and tilt, η, order parameters and (b) entropy and specific heat for $\beta = 0.33$ and $\alpha_0 = 0.85$.
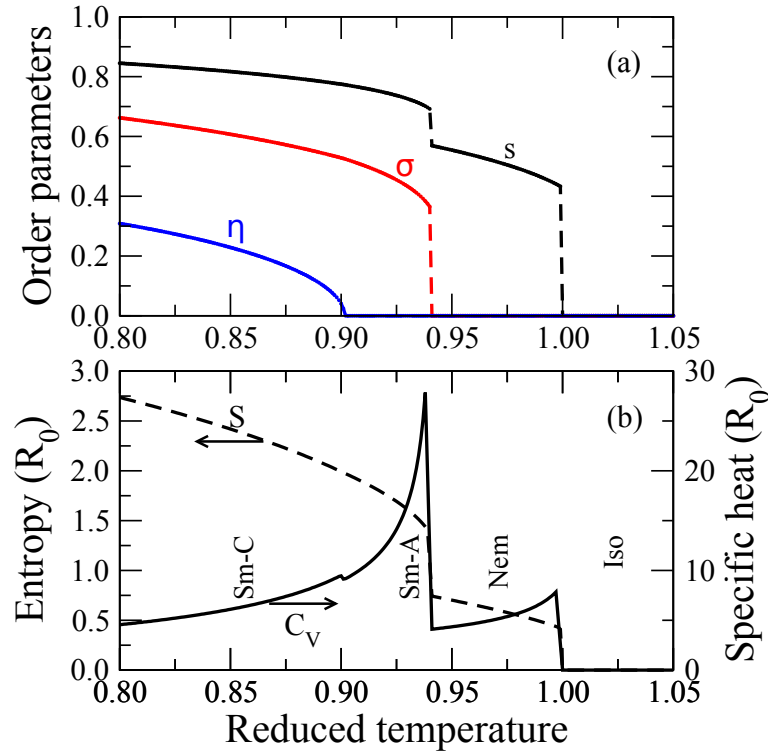
Source: Author, 2021.

figure 3.18.

Figure 3.18: The tilt angle as a function of T/T_C for $\beta = 0.33$ and three representative values of the geometric parameter α_0: $\alpha_0 = 0.75$ (solid black line), $\alpha_0 = 0.85$ (dashed red line), and $\alpha_0 = 0.98$ (dotted blue line).
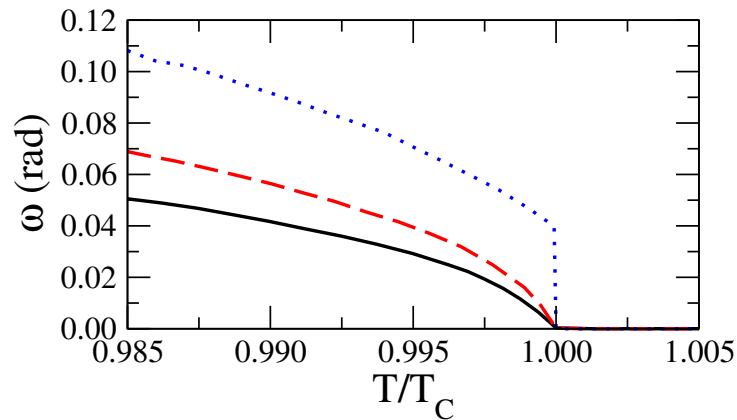
Source: Author, 2021.

For convenience, the system's temperature was rescaled by T_C, which vanishes the η order parameter. As α_0 increases, the continuous decay of the tilt angle is replaced by a discontinuous jump at $T = T_C$. This suggests that α_0 affects the nature of the phase transitions involving the

smectic-C phase, despite a constant β. Since α_0 is associated with the length of alkyl-chains in
rod-like molecules, this result corresponds with experimental findings for different homologous
series [74, 98], where the molecular rigid part is kept constant and the alkyl-chain's length is
varied. For $T < T_C$, the tilt angle is favoured with increasing α_0, and the layer contraction
becomes more pronounced.

Figure 3.19 shows both the geometric parameter α and layer spacing d against temperature and
thereof, the tilt angle ω. The layer contraction increases with model parameters α_0 and β.

Figure 3.19: Temperature dependence of the geometric parameter α and the layer spacing d for (a)
$\beta = 0.33$; $\alpha_0 = 0.85$ and (b) $\beta = 0.70$; $\alpha_0 = 0.95$.
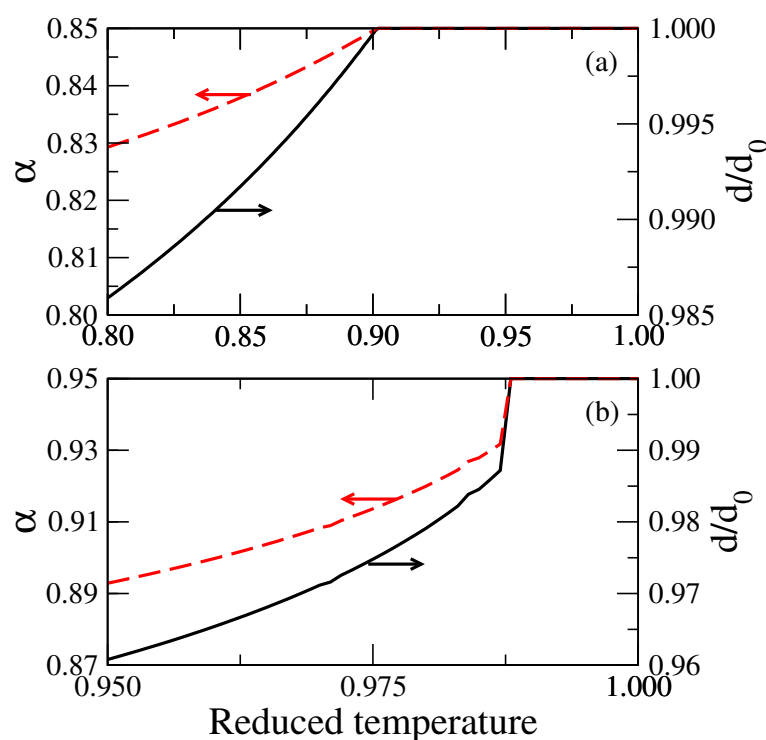
Source: Author, 2021.

The model also predicts phase transitions involving smectic-C beyond the Sm-C–Sm-A tran-
sition. Figure 3.20 shows the order parameters for $\beta = 0.70$ and different values of α_0. For
$\alpha_0 = 0.65$, we observe a second-order Sm-C–N transition followed by a first-order N–Iso tran-
sition. For $\alpha_0 = 0.95$, a sequence of first-order Sm-C–N and N–Iso transitions take place. At
$\alpha_0 = 1.05$, only a first-order Sm-C–Iso phase transition occurs.

Finally, figure 3.21 gives a better understanding of phase transitions involving the smectic-C
phase. We show the phase diagrams of temperature *versus* α, for various β. The temperature
is rescaled by the nematic–isotropic transition temperature, T_{NI}. For $\beta = 0.30$, we observe a
second order Sm-C–Sm-A phase transition for $\alpha_0 < 1.01$, while a first order Sm-C–Iso phase
transition takes place for $\alpha_0 > 1.01$, as shown in figure 3.21(a). This indicates that $\alpha_0 = 1.01$

Figure 3.20: Temperature dependence of orientational, s, translational, σ, and tilt, η, order parameters, entropy and specific heat for $\beta = 0.70$ and $\alpha_0 = $ (a) 0.65, (b) 0.95 and (c) 1.05.
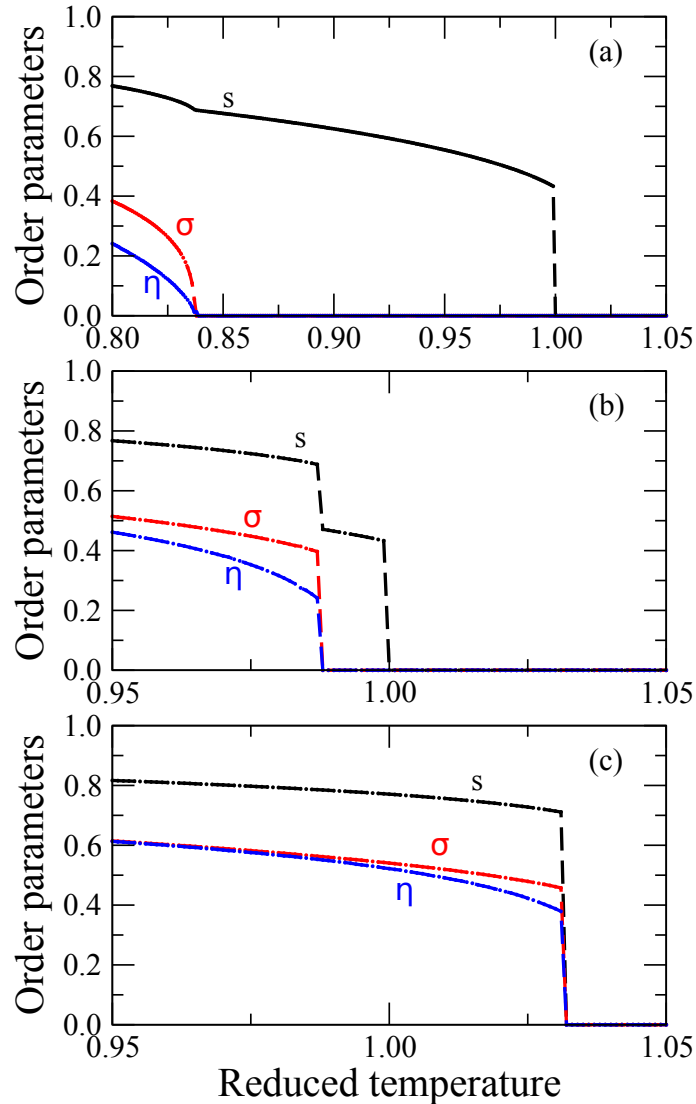
Source: Author, 2021.

is a critical end point, which corresponds to the position where the line of continuous Sm-C–Sm-A transition encounters the coexistence line between the smectic-C and the isotropic phase. Similarly to McMillan's model [99], we observe a tricritical point at $\alpha_0 = 0.70$, delimiting the regions of continuous and discontinuous Sm-A–N transitions. Moreover, one can note the triple point at $\alpha_0 = 0.98$, which determines the coexistence of nematic, smectic-A and isotropic phases. This phase behaviour is in agreement with experimental findings for terephthal-bis-(4n)-alkylaniline (TBnA) [74] and 2-(4-alkyloxyphenyl)-5-alkyloxypyrimidines (PhPn) [98] homologous series.

Figure 3.21(b), shows the $T - \alpha_0$ phase diagram for $\beta = 0.33$, where a critical end point is observed at $\alpha_0 = 0.96$. However, the line of continuous Sm-C–Sm-A transition reaches the

Figure 3.21: The phase diagram in the reduced temperature *vs* α_0 plane for $\beta =$ (a) 0.30, (b) 0.33, (c) 0.40 and (d) 0.70. Solid (dotted) lines corresponds to first-order (second-order) transitions. As the parameter β increases, the smectic-A phase disappears.
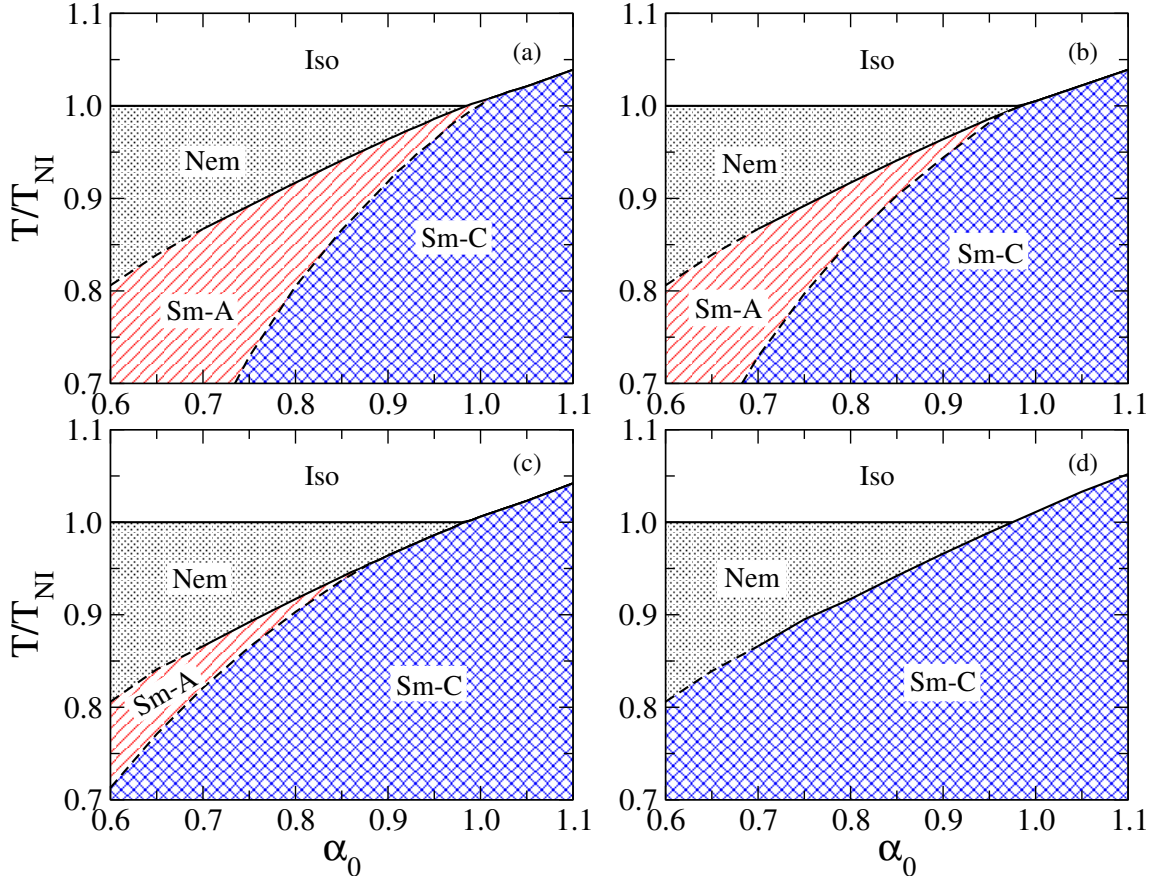
Source: Author, 2021.

coexistence line of discontinuous Sm-A–N transition, thus corresponding to a NAC critical end point. A similar scenario is observed for $\beta = 0.40$, as presented in figure 3.21(c). It is remarkable that the NAC critical end point is displaced to lower values of α_0 as β is increased, which is accompanied by a reduction in the Sm-A temperature range.

For $\beta = 0.70$, the smectic-A phase is suppressed and a tricritical point at $\alpha_0 = 0.70$ delimits the regions of continuous and discontinuous Sm-C–N transitions, as shown in figure 3.21(d). We notice that the NA tricritical point and the NAC critical end point merge with increasing β, giving rise to a NC tricritical point. It is important to emphasise that the smectic-A phase is stabilised by the layer contraction, without an excluded-volume contribution, as suggested by Govind and Madhusudana [44, 89]. The single-particle mean-field potential introduced in equation 3.28 captures the main features of the phase transitions involving Sm-C phase, with a reduced number of free parameters.

IV

SURFACE AND FINITE SIZE EFFECTS ON PHASE TRANSITIONS IN FREE-STANDING SMECTIC-C FILMS

Smectic liquid crystal phase transitions are phenomenologically very rich due to their interplay of anisotropic critical behaviour [75, 100], surface ordering [68, 101, 102], finite size effects [78, 103], and external fields [104–106]. In particular, smectic samples have a unique ability of forming freely suspended films, also termed as free-standing films, which correspond to a stack of smectic layers confined in a surrounding gas [107]. Due to the absence of a solid substrate, the equilibrium configuration is determined by the film holder, with the surface tension reducing thermal fluctuations at the film's surface [108]. In fact, surface anchoring conditions at the gas/film interface can lead to the stabilisation of the smectic ordering even above the bulk transition temperatures [109]. A large variety of unusual physical phenomena can consequently be observed in free-standing smectic films, such as layer thinning and thickening transitions [52, 110, 111], specific heat anomalies [75, 79, 80], thickness dependence on the transition temperature [103], as well as surface-induced biaxiliaty [102]. Since the film thickness can vary from a few nanometres to several micrometres, free-standing films constitute a suitable experimental setup for understanding how changes in the system's dimensionality affect the thermodynamic behaviour of the smectic phase [109, 112].

Tilting transitions in free-standing smectic films may exhibit different behaviour to those observed in bulk systems [76, 78, 81, 84, 113–116]. In fact, surface anchoring conditions and finite size effects tend to affect the thermal behaviour of both orientational and translational order parameters in thin free-standing smectic films. From monitoring the transmittance of such systems close to a second order Sm-C–Sm-A phase transition, an unusual thickness dependence has been reported for the thermal behaviour of the average tilt angle [76], with the transition

temperature in thin films being higher than of bulk system's. Optical ellipsometry revealed a finite average tilt in the surface layers of free-standing films well above the bulk transition temperature [84]. Such a scenario has been supported by electron diffraction measurements in thin film [81], where a surface-induced phase sequence is identified. Moreover, surface effects may lead to changes in the nature of Sm-C–Sm-A phase transition [84, 116], especially in films of a few layers. For compounds presenting a first order Sm-C–Sm-A bulk phase transition, the discontinuous jump in the tilt angle is replaced by a continuous behaviour at the transition temperature, when the film thickness is lower than a characteristic thickness [84, 116]. Furthermore, surface anchoring and finite size effects give rise to a non-uniform tilt profile in free-standing smectic-C films [115], with the outermost layers most tilted. In chiral smectic samples, a series of discrete transitions has been reported [78], where a reentrant synclinic-anticlinic-synclinic ordering sequence takes place at the surface film in the presence of an external electric field.

Although several studies have been devoted to the theoretical description of phase transitions in bulk smectic-C systems, microscopic models for free-standing films have not been extensively explored so far. We investigate nematic–smectic-A–smectic-C phase transitions by using an extended version of the mean-field theory for smectic-C liquid crystals. The interplay of surface anchoring and finite size effects is shown to affect the thermal behaviour of the order parameters in free-standing smectic films. In particular, the additional orientational order imposed by the surface anchoring may lead to a stabilisation of order parameters in central layers, thus modifying the nature of the phase transitions. The results are compared against experimental findings for typical thermotropic compounds presenting a nematic–smectic-A–smectic-C phase sequence.

4.1 Free-Standing Films

Due to their layered structure, smectic liquid crystals form films similar to soap bubbles. This property of smectic mesophases has been known to George Friedel [7] since the beginning of the 20th century. Such films have been considered very convenient and highly perfect samples for structural X-ray studies of smectic liquid crystals. However, systematic studies of the structure and physical properties of these films were only carried out in the early 1970s, by Young et al [117].

Smectic free-standing films are two-dimensional liquid layers surrounded by a gaseous environment that tend to maintain a well-defined spacing (see figure 4.1). These films are denominated 'free-standing' due to the absence of stabilising solid substrates. Other nomenclatures used to describe these systems include freely suspended films or membranes. In his study of how and why such systems exist, Pieranski [118] used the term 'membranes' to reflect that surface

Figure 4.1: Representative scheme of a free-standing smectic film, with layers surrounded by a gaseous environment, where d is the distance between layers.
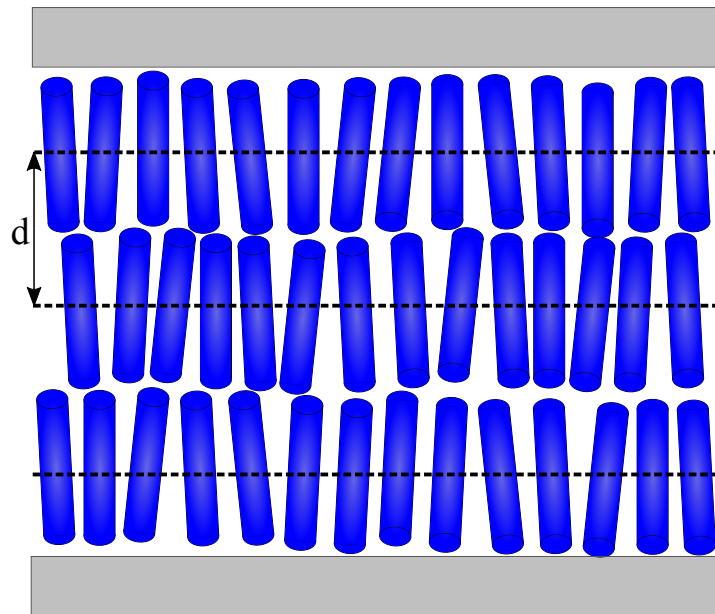
Source: Author, 2021.

tension is a requirement for the existence of such films. In order to stay flat, the film must be subject to a surface tension τ, like a drum's skin. If the tension were to be released, the film would thicken due to new layers being formed. Furthermore, if a hole were made in the film its tension would drop to zero, causing a rupture. Within a hydrodynamic approach, the surface tension represents the coupling between the film and the gaseous environment and is responsible for reducing fluctuations close to the film's surface.

In general, free-standing films are formed by depositing material in the smectic phase on a flat surface with a hole, as shown in figure 4.2. Then the material is heated and spread over the hole, with a few millimetres in diameter. The larger the hole's diameter of the hole, the thinner the film. The lateral extension of these films is usually of the order of millimetres or centimetres, while their thickness is of the order of a few nanometres or micrometres.

The film's existence depends on the presence of the frame on which it is spanned. The film is connected to the frame via the meniscus, whose volume is much larger than the film's, and so can be considered a reservoir of molecules (see figures 4.3 and 4.4(a)). Changes in the film's surface area requires a transfer of molecules between the film and the meniscus. During this process, molecules flow both between and within layers.

To determine the film's thickness, the reflected intensity of a low-power laser on the film's surface [119] is measured. The shape of the meniscus can also be deduced from the interference fringes. Films can contain textures involving any of the in-plane ordering of molecules that are

Figure 4.2: Representative scheme of the formation process of a free-standing smectic film. A sample of smectic liquid crystal is spread over a circular opening in a flat surface. The film is connected to the frame by a meniscus.
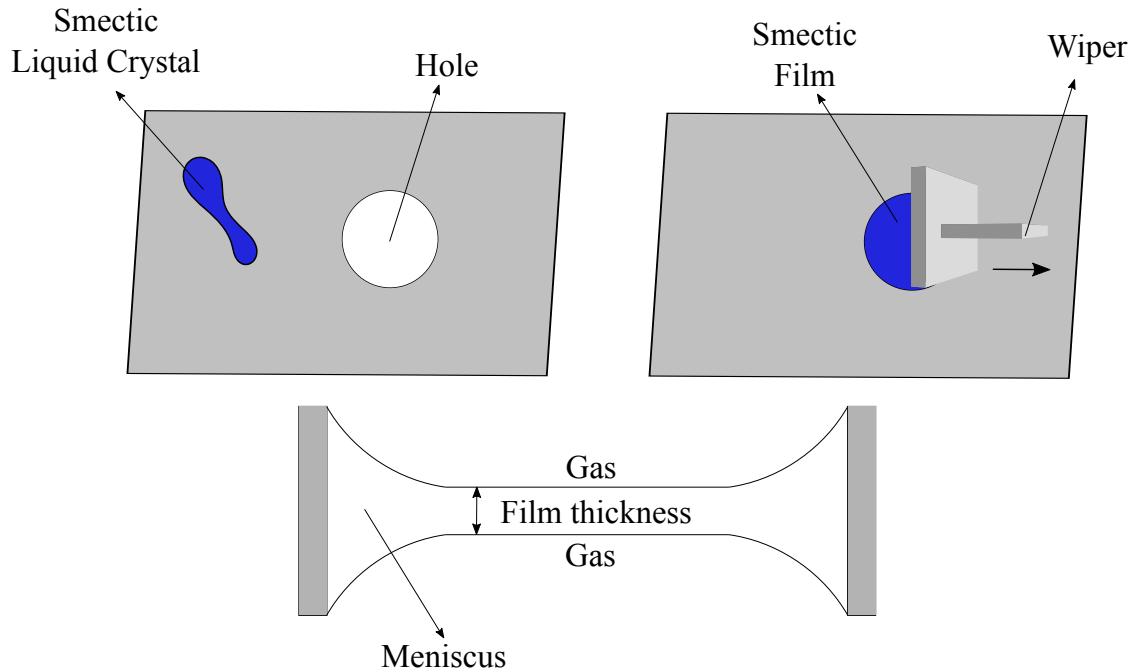
Source: Author, 2021.

Figure 4.3: Idealised structure of the meniscus.
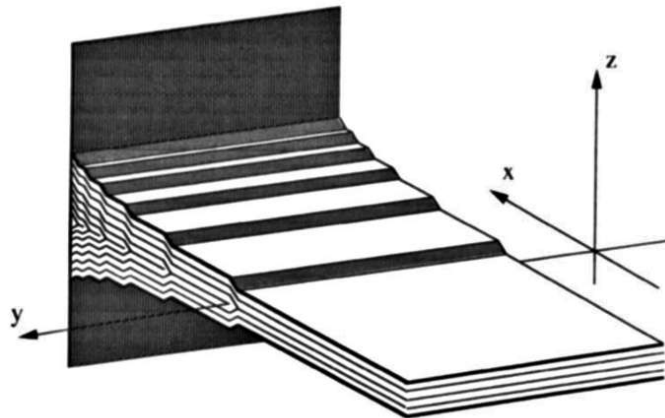
Source: Pieranski, 1993 [118].

characteristic for smectic phases other than the usual smectic-A phase. In figure 4.4(b), we see a hedgehog singularity characteristic of smectic phases with tilted molecules. In the smectic-C phase, the hedgehog singularity exists in any closed loop-like step.

As in soap bubbles, gravitational effects in free-standing films are negligible when compared to intrinsic elastic forces. These films are stable for days and even weeks which is due to the surface tension at the film/gas interface that suppresses variations at the film's surface area. The

Figure 4.4: (a) Nucleation of the film as seen in the reflecting microscope under illumination from a monochromatic light. A circular membrane of small diameter is surrounded by the meniscus. (b) Hedgehog singularity in a smectic-C* film as seen in the reflecting microscope under a polarised monochromatic illumination. The orientation $\vec{n}$ of molecules can be deduced from the fringe's configuration.
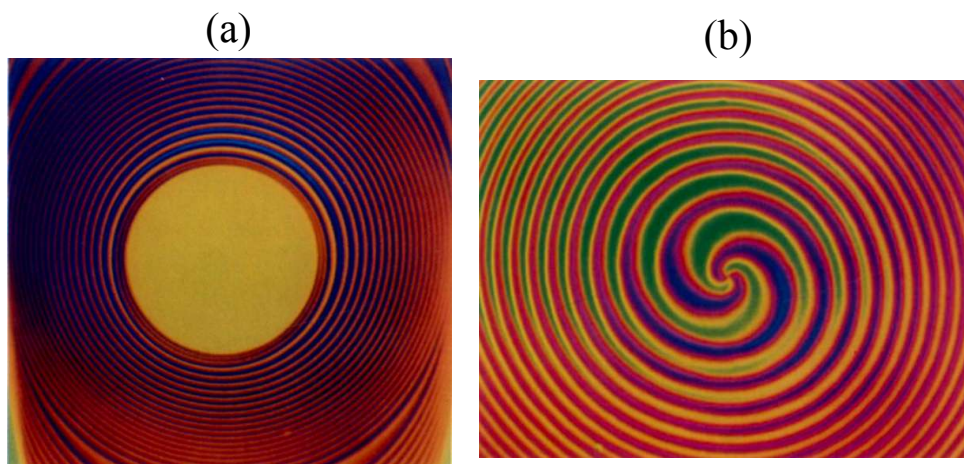
Source: Pieranski, 1993 [118].

surface tension is directly related to interactions close to the surface [120]. It is possible to distinguish two regimes of surface tension: strong surface anchoring, where the surface tension induces a greater organisation in the vicinity of the surface than in the film's centre, and a regime of weak surface anchoring, where the centre of the film is more organised than its surface. Therefore, free-standing films are interesting for investigating surface effects [121].

An interesting aspect of free-standing films is that surface effects can stabilise the smectic order at temperatures above the sample's transition temperature [52, 109]. Several unusual phenomena can be observed depending on the superficial anchoring intensity. In particular, a transition by layer reduction, induced by the surface, can take place, reducing the film's thickness layer by layer with increasing temperature [55]. Layer-thickening transition can also take place in free-standing films, whose first clear observation by de Jeu et al. [122], attributed by local heating at one side of the film. A change - thinning or thickening - in the number of layers is discontinuous and can be seen as a first-order transition.

4.2 Extension of McMillan's Model for Free-Standing Films: McMillan-Mirantsev Model

With the purpose of studying phase transitions in thin films, Mirantsev proposed an extension of McMillan's model to transitions involving the smectic phase A. In his work, the author

considered a freely suspended smectic film consisting of N discrete liquid-crystalline layers
with thickness d of the order of the molecular length. Moreover, the film is homeotropically
oriented, i.e. the director $\vec{n}$ lies along the normal to the plane of the layers. In this model,
each layer has a pair of order parameters (nematic and smectic) that are coupled to the pair of
parameters of the neighbouring layers. Thus, the molecules in each layer can interact only with
molecules of the same and the two closest neighbouring layers.

The interaction between the liquid crystal molecules and the boundary surface is simulated by a
short-range orientational field that acts directly and solely on the first and last layers of the film.
The anchoring potential can be written as follows

$$W_1(\theta_1) = -W_0 \left(\frac{3}{2} \cos^2 \theta_1 - \frac{1}{2} \right), \tag{4.1}$$

and

$$W_N(\theta_N) = -W_0 \left(\frac{3}{2} \cos^2 \theta_N - \frac{1}{2} \right), \tag{4.2}$$

where θ_1 and θ_N are the angles between the major axes of the molecules in the first and last
layer, respectively, and the normal to the boundary surface. W_0 is the interaction amplitude,
which also incorporates excluded volume effects. As the molecules in the i-th layer only interact
with molecules in that and in neighbouring layers, it is possible to associate the interaction with
the following pseudopotential $V_i(z_i, \theta_i)$:

$$V_1(z_1, \theta_1) = -\frac{V_0}{3} \left(\frac{3}{2} \cos^2 \theta_1 - \frac{1}{2} \right) \left[s_1 + s_2 + \frac{3W_0}{V_0} + \alpha \cos \left(\frac{2\pi z_1}{d} \right) (\sigma_1 + \sigma_2) \right],$$

$$V_{2 \leq i \leq N-1}(z_i, \theta_i) = -\frac{V_0}{3} \left(\frac{3}{2} \cos^2 \theta_i - \frac{1}{2} \right) \left[\sum_{j=i-1}^{i+1} s_j + \alpha \cos \left(\frac{2\pi z_i}{d} \right) \sum_{j=i-1}^{i+1} \sigma_j \right], \tag{4.3}$$

and

$$V_N(z_N, \theta_N) = -\frac{V_0}{3} \left(\frac{3}{2} \cos^2 \theta_N - \frac{1}{2} \right) \left[s_{N-1} + s_N + \frac{3W_0}{V_0} + \alpha \cos \left(\frac{2\pi z_N}{d} \right) (\sigma_{N-1} + \sigma_N) \right],$$

where $\alpha = 2e^{-(\pi r_0/d)^2}$. s_i and σ_i are the nematic and smectic order parameters, respectively, for
the i-th layer, determined by the following self-consistent relations:

$$s_i = \left\langle \frac{3}{2} \cos^2 \theta_i - \frac{1}{2} \right\rangle_i, \tag{4.4}$$

$$\sigma_i = \left\langle \left(\frac{3}{2} \cos^2 \theta_i - \frac{1}{2} \right) \cos \left(\frac{2\pi z_i}{d} \right) \right\rangle_i. \tag{4.5}$$

To obtain equations 4.3 the system is assumed to be axially symmetric and the average number

of molecules in each layer is constant. The mean value of a physical quantity A is given by

$$\langle A \rangle_i = \frac{\int_{(i-1)d}^{id} dz_i \int_{-1}^{1} A_i(z_i, \theta_i) e^{\frac{-V_i}{k_B T}} d(\cos \theta_i)}{\int_{(i-1)d}^{id} dz_i \int_{-1}^{1} e^{\frac{-V_i}{k_B T}} d(\cos \theta_i)}. \tag{4.6}$$

The Helmholtz free energy for a film of discrete layers is:

$$
\begin{aligned}
F_1 &= N_0 V_0 \left[\frac{1}{6} s_1 (s_1 + s_2) + \frac{1}{6} \alpha \sigma_1 (\sigma_1 + \sigma_2) \right. \\
&\quad - \left. \frac{k_B T}{V_0} \ln \left(\frac{1}{2d} \int_{-1}^{1} d\cos \theta_1 \int_{0}^{d} dz_1 \mathscr{Z}_1 \right) \right],
\end{aligned}
$$

$$
\begin{aligned}
F_{2 \leq i \leq N-1} &= N_0 V_0 \left[\frac{1}{6} s_i \sum_{j=i-1}^{i+1} s_j + \frac{1}{6} \alpha \sigma_i \sum_{j=i-1}^{i+1} \sigma_j \right. \\
&\quad - \left. \frac{k_B T}{V_0} \ln \left(\frac{1}{2d} \int_{-1}^{1} d\cos \theta_i \int_{(i-1)d}^{id} dz_i \mathscr{Z}_i \right) \right], \tag{4.7}
\end{aligned}
$$

$$
\begin{aligned}
F_N &= N_0 V_0 \left[\frac{1}{6} s_N (s_{N-1} + s_N) + \frac{1}{6} \alpha \sigma_N (\sigma_{N-1} + \sigma_N) \right. \\
&\quad - \left. \frac{k_B T}{V_0} \ln \left(\frac{1}{2d} \int_{-1}^{1} d\cos \theta_N \int_{(N-1)d}^{Nd} dz_N \mathscr{Z}_N \right) \right],
\end{aligned}
$$

where N_0 is the number of molecules inside a single layer. The total free energy F of an N-layer film is then

$$F = \sum_{i=1}^{N} F_i. \tag{4.8}$$

In his work, Mirantsev used $\alpha \geq 1$, corresponding to Sm-A–Iso transitions according to McMillan's theory. Moreover, the interaction between the liquid crystal molecules and the surface, W_0, was taken as greater than the intermolecular interaction, V_0.

Figure 4.5 shows the profiles of the orientational (s) and translational (σ) order parameters for $\alpha = 1.05$, which shows a first-order Sm-A–Iso phase transition at $T_{AI}^{bulk} = 1.021 T_{NI}$ in the bulk. For $T < T_{AI}^{bulk}$ (black circles), both order parameters are non-null and are larger in the surface layers. For $T > T_{AI}^{bulk}$ (red squares and blue diamonds), the smectic-A phase becomes unstable, and the system undergoes a discontinuous transition to a quasi-smectic-A phase, where the order parameters are non-zero at the surface and drop to zero rapidly at the centre of the film. For $T \gg T_{AI}^{bulk}$ (green triangles), the whole film becomes unstable, with the smectic order parameter going to zero even in the surface layers.

Figure 4.5: Profiles of (a) orientational and (b) translational order parameters for a free-standing smectic-A film with $\alpha = 1.05$ and $N = 25$, at different temperatures: $T = 1.000T_{NI}$ (black circles), $T = 1.040T_{NI}$ (red squares), $T = 1.060T_{NI}$ (blue diamonds) and $T = 1.100T_{NI}$ (green triangles). We use $W_0/V_0 = 3.00$, corresponding to the strong anchoring regime.
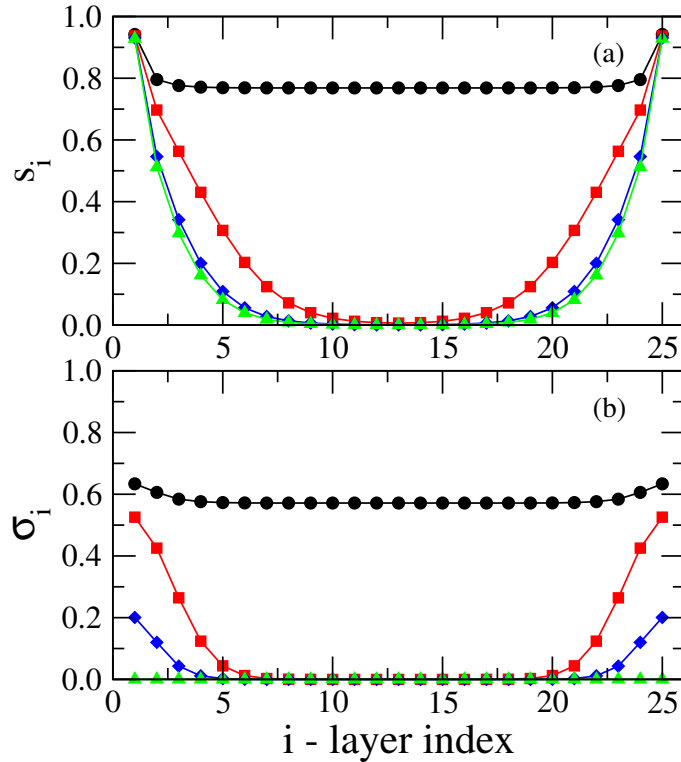
Source: Author, 2021.

We also show the order parameter profiles for $\alpha < 1$, corresponding to a system presenting the Sm-A–N–Iso phase transition sequence, in figure 4.6. Consider the example of $\alpha = 0.85$ with the following bulk transition temperatures: $T_{AN}^{bulk} = 0.941T_{NI}$ and $T_{NI}^{bulk} = T_{NI}$. We consider a film of $N = 25$ layers and use $W_0/V_0 = 2.5$, configuring a strong anchoring regime. For $T > T_{AN}^{bulk}$, the smectic order parameter goes to zero at the centre of the film, with $\sigma \neq 0$ in the outer layers. However, the nematic order parameter is non-null across the entire film, which indicates that the interior layers don't transition to the isotropic phase, as for $\alpha > 1$, and instead the entire film becomes unstable. This suggests that a layer thinning transition can only occur for compounds already presenting the Sm-A–Iso phase transition in the bulk.

Figure 4.6: Profiles of (a) orientational and (b) translational order parameters for a free-standing smectic-A film with $\alpha = 0.85$ and $N = 25$, at different temperatures: $T = 0.900T_{NI}$ (black circles), $T = 0.940T_{NI}$ (red squares), $T = 0.960T_{NI}$ (blue diamonds) and $T = 0.980T_{NI}$ (green triangles). We use $W_0/V_0 = 2.50$, corresponding to the regime of strong anchoring condition.
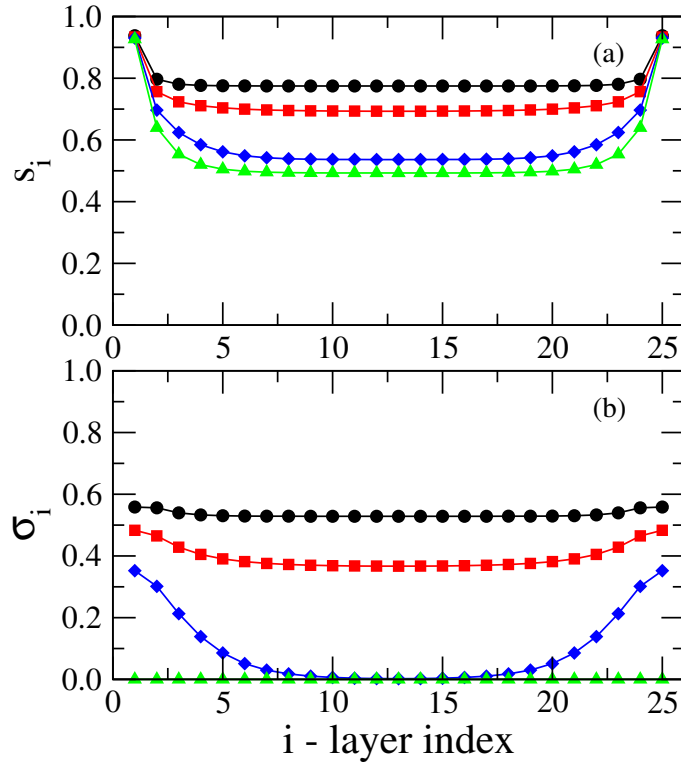
Source: Author, 2021.

4.3 Extended Molecular Model for Free-Standing Smectic-C Films

We have seen that the model proposed by Mirantsev satisfactorily extends McMillan's model for the smectic-A phase by considering a set of discrete smectic layers and an orientational field in the film's surface layers. However, Mirantsev's model is as limited as McMillan's original model, as it cannot distinguish between different smectic phases. In the following, we will introduce a model similar to Mirantsev's to extend the model introduced in section 3.2 for free-standing films.

4.3.1 Our Model and Formalism

An extended version of McMillan-Mirantsev's model [55] is used to describe phase transitions in free-standing smectic-C films, which includes an effective tilting potential. We assume a

stratified film of N discrete layers, where each has its own set of orientational, s_i, translational, σ_i, and tilt, η_i, order parameters.

Figure 4.7: Schematic representation of the Sm–C system. A Cartesian coordinate system whose z-axis is normal to the smectic layer plane is used.
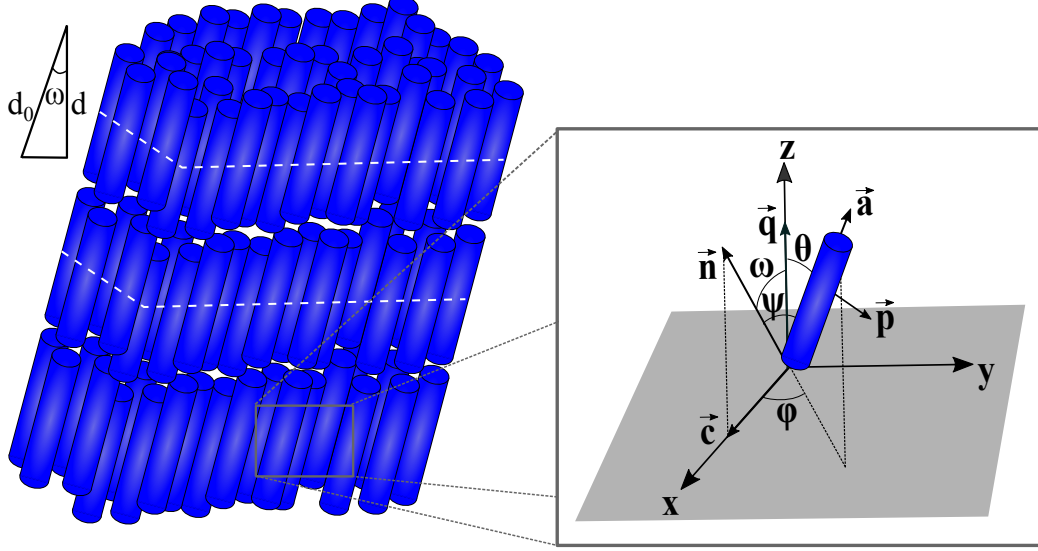
Source: Author, 2021.

Once the molecular orientation is defined via the polar and azimuthal angles θ_i and ϕ_i, the effective one-particle mean-field potential of the layer positioned at z_i is:

$$
\begin{aligned}
V_1(z_1,\theta_1,\phi_1) = \quad & - \quad \frac{V_0}{3}\left\{ P_2\left(\cos\psi_1\right)\left[s_1 + s_2 + \frac{3W_0}{V_0} + \alpha_1 \cos\left(\frac{2\pi z_1}{d_1}\right)(\sigma_1 + \sigma_2)\right] + \right. \\
& + \quad \left. \alpha_1 \beta \left(\frac{\sigma_1 + \sigma_2}{3}\right)^2 (\eta_1 + \eta_2)\sin 2\theta_1 \cos\phi_1 \right\},
\end{aligned}
$$

$$
\begin{aligned}
V_{2\leq i\leq N-1}(z_i,\theta_i,\phi_i) = \quad & - \quad \frac{V_0}{3}\left\{ P_2\left(\cos\psi_i\right)\left[\sum_{j=i-1}^{i+1} s_j + \alpha_i \cos\left(\frac{2\pi z_i}{d_i}\right)\left(\sum_{j=i-1}^{i+1}\sigma_j\right)\right] + \right. \\
& + \quad \left. \alpha_i \beta \left(\frac{\sum_{j=i-1}^{i+1}\sigma_j}{3}\right)^2 \left(\sum_{j=i-1}^{i+1}\eta_j\right)\sin 2\theta_i \cos\phi_i \right\},
\end{aligned} \tag{4.9}
$$

$$
\begin{aligned}
V_N(z_N,\theta_N,\phi_N) = \quad & - \quad \frac{V_0}{3}\left\{ P_2\left(\cos\psi_N\right)\left[s_{N-1} + s_N + \frac{3W_0}{V_0} + \alpha_N \cos\left(\frac{2\pi z_N}{d_N}\right)(\sigma_{N-1} + \sigma_N)\right] + \right. \\
& + \quad \left. \alpha_N \beta \left(\frac{\sigma_{N-1} + \sigma_N}{3}\right)^2 (\eta_{N-1} + \eta_N)\sin 2\theta_N \cos\phi_N \right\},
\end{aligned}
$$

The quantity α_i is given by:

$$
\alpha_i = 2\left(\frac{\alpha_0}{2}\right)^{\sec^2\omega_i}, \tag{4.10}
$$

in which α_0 is the geometric parameter related to the length of alkyl chains of rod-like molecules, through the expression $\alpha_0 = 2\exp\left[-(\pi r_0/d_0)^2\right]$, as defined by McMillan. ω_i is the tilt angle in the ith layer, satisfying the relation:

$$\cos\psi_i = \cos\theta_i\cos\omega_i + \sin\theta_i\sin\omega_i\sin\phi_i. \tag{4.11}$$

The tilt angle ω_i leads to a contraction of the ith layer spacing, defined by:

$$d_i = d_0\cos\omega_i, \tag{4.12}$$

with d_0 denoting the layer spacing in the smectic-A phase. In this approach, the surface anchoring is represented by a surface orientational field of strength W_0.

For a free-standing smectic-C film, we assume that the surface ordering gives rise to the following tilt angle profile [123]

$$\omega_i = \omega_B + \frac{(\omega_S - \omega_B)\cosh\left[\frac{d_0(2i-N-1)}{2\xi}\right]}{\cosh\left[\frac{d_0(N-1)}{2\xi}\right]}, \tag{4.13}$$

where ω_B is the bulk tilt angle and ω_S is the tilt angle in the outermost layers. ξ is the surface penetration length, which delimits the range of anchoring effects on the tilt ordering along the film. As we consider a short-range surface contribution in the one-particle mean-field potential, we assume $\xi = 2d_0$. In fact, previous studies reported that the surface penetration length is of the order of the average smectic layer spacing d_0 [72, 115, 124], which does not exceed a few molecular layers.

Figure 4.8: Tilt angle profile for a temperature below the Sm-C–Sm-A transition ($T = 0.885T_{NI}$), for $\alpha = 0.33$, $\beta = 0.85$ and different values of film thickness: $N = 7$ (black circles), $N = 15$ (red squares), $N = 25$ (blue diamonds), $N = 45$ (green up triangles) and $N = 85$ (grey left triangles).
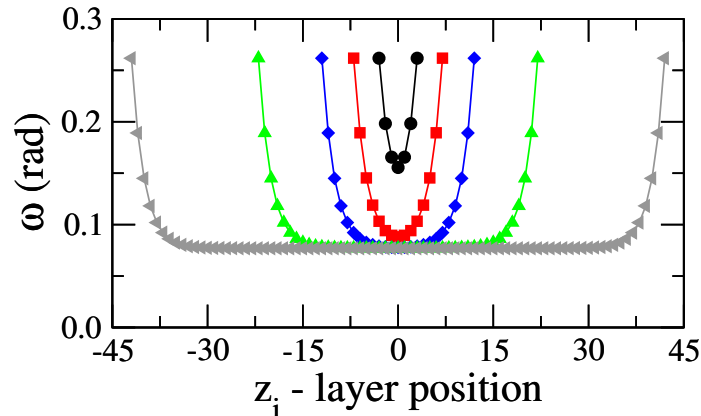
Source: Author, 2021.

It is important to highlight that the tilt angle profile defined by equation 4.13, and shown in figure 4.8, was introduced by Tweet and co-workers [123], using a simple phenomenological elastic model. However, experimental results indicate that the tilt angle disappears before the layered structure is disrupted when the film's temperature is increased [76, 125, 126]. In order to provide a better description of free-standing smectic-C films, we suppose that the surface tilt angle presents a typical temperature dependence of a mean-field model, that is,

$$\omega_S = \omega_0 \left(\frac{T_{AN} - T}{T_{AN} - T_{CA}} \right)^{\frac{1}{2}}. \tag{4.14}$$

T_{CA} and T_{AN} are the bulk Sm-C–Sm-A and Sm-A–N transition temperatures, respectively. In this model, ω_S vanishes as the smectic order is reduced. In what follows, we use $\omega_0 = 0.26$ ($\sim 15°$).

The local order parameters s_i, σ_i and η_i are defined as thermodynamical averages:

$$s_i = \langle P_2(\cos \psi_i) \rangle, \tag{4.15}$$

$$\sigma_i = \langle P_2(\cos \psi_i) \cos(2\pi z_i/d_i) \rangle, \tag{4.16}$$

and

$$\eta_i = \langle \sin 2\theta_i \cos \phi_i \rangle, \tag{4.17}$$

computed from the following one-particle distribution function in the i-th smectic layer:

$$\mathscr{Z}_i \propto \exp[-V_i/k_B T]. \tag{4.18}$$

The total Helmholtz free energy is then given by

$$\frac{F}{N_0 V_0} = \sum_{i=1}^{N} F_i, \tag{4.19}$$

with

$$\begin{aligned} F_i &= \frac{1}{2} \left(s_i \bar{s}_i + \alpha_i \sigma_i \bar{\sigma}_i + \alpha_i \beta \bar{\sigma}_i^2 \eta_i \bar{\eta}_i \right) - \\ &- \frac{k_B T}{V_0} \ln \left[\frac{1}{2\pi d_i} \int_{-1}^{1} d\cos\theta_i \int_{0}^{\pi} d\phi_i \int_{(i-1)d_{i-1}}^{id_i} dz_i \mathscr{Z}_i \right], \end{aligned} \tag{4.20}$$

where $\bar{s}_i$, $\bar{\sigma}_i$ and $\bar{\eta}_i$ are the average order parameters in i^{th} layer and its two neighbouring layers, given by

$$\bar{s}_i = \frac{(1 - \delta_{i-1,0})s_{i-1} + s_i + (1 - \delta_{i+1,N+1})s_{i+1}}{3}, \tag{4.21}$$

$$\overline{\sigma}_i = \frac{(1 - \delta_{i-1,0})\sigma_{i-1} + \sigma_i + (1 - \delta_{i+1,N+1})\sigma_{i+1}}{3}, \tag{4.22}$$

and

$$\overline{\eta}_i = \frac{(1 - \delta_{i-1,0})\eta_{i-1} + \eta_i + (1 - \delta_{i+1,N+1})\eta_{i+1}}{3}, \tag{4.23}$$

with $i = 1, 2, \ldots, N$, and δ_{ij} is the Kronecker's delta.

This model provides the order parameters' profile for different sets of free parameters in the single-particle mean-field potential: α_0, β and W_0. The tilt angle profile defined in equation 4.13 is used to obtain the order parameter profiles that minimise the Helmholtz free energy, thus yielding the equilibrium configuration of the system. It is important to highlight that the tilt angle profile given by equation 4.13 has been widely used in several experimental studies, leading to a reasonable description of the thermal and hydrodynamic properties of free-standing smectic-C films [85, 123, 125].

In combination with equation 4.14, the bulk values of ω_B are used to compute the tilt angle profile for distinct film temperatures, as shown in figure 4.9. We consider $N = 15$, $\omega_0 = 0.26$, $\alpha_0 = 0.85$ and $\beta = 0.33$, with a bulk transition temperature of $T_{CA} = 0.902T_{NI}$.

Figure 4.9: Tilt angle profile for a $N = 15$ layer film, for distinct temperatures: $T = 0.880T_{NI}$ (black circles) and $T = 0.906T_{NI}$ (red squares).
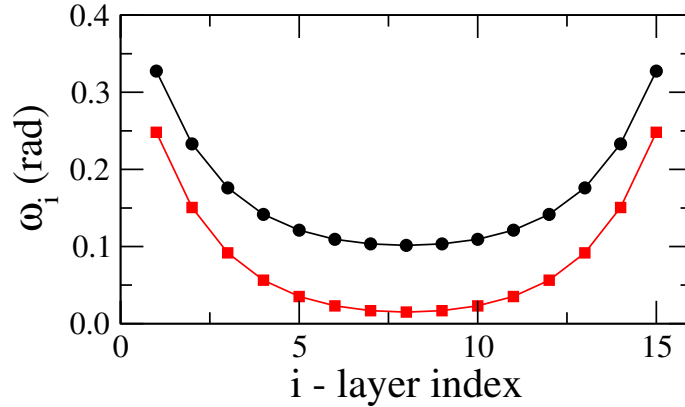
Source: Author, 2021.

We observe that equation 4.13 outputs a tilt profile with a positive curvature, where the outermost layers present tilt angles larger than the internal ones. For $T > T_{CA}$, a pronounced tilt reduction takes place at central layers as ω_B vanishes, while a non-vanishing tilt persists in outermost layers. Such a scenario is similar to experimental findings, where the surface layers exhibit a Sm-C–Sm-A transition well above the bulk transition temperature [76]. Besides, it is important to stress that the tilt angle profile is assumed to be independent of the surface anchoring, W_0.

4.3.2 Results

Figure 4.10 presents the profiles of the order parameters of a free-standing smectic film with $N = 15$ layers. We use the same model parameters as in figure 4.9 and $W_0/V_0 = 0.25$, which corresponds to the weak surface anchoring regime [90].

Figure 4.10: Profiles of (a) orientational, (b) translational and (c) tilt order parameters for a free-standing smectic film, around the bulk Sm-C–Sm-A transition temperature ($T_{CA} = 0.902T_{NI}$). We consider different film temperatures: $T = 0.880T_{NI}$ (black circles) and $T = 0.906T_{NI}$ (red squares). $W_0/V_0 = 0.25$, corresponding to the weak surface anchoring regime.
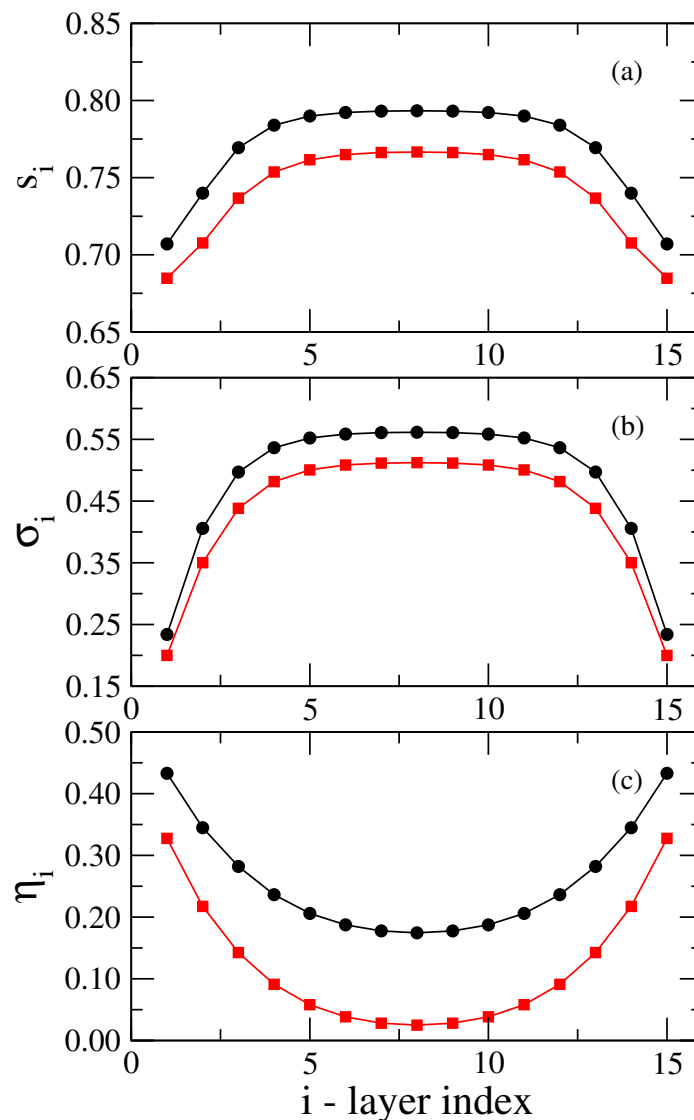
Source: Author, 2021.

For $T < T_{CA}$, the nematic and smectic order parameters present non-uniform profiles with negative curvature, where the central layers are more ordered than at the surface. More specifically, the weak anchoring leads to a small valued smectic order parameter at the surface layers.

On the other hand, the tilt order parameter exhibits a non-uniform profile with a positive curvature. This profile is characterised by a high tilt ordering in the surface layers, as defined by equation 4.13. This scenario holds for $T > T_{CA}$, with a small reduction in the nematic and smectic order parameters. However, the tilt order parameter becomes almost negligible in the central layers, while the surface layers present a finite tilt ordering. In this case, the surface layers remain in the Sm-C phase, while the central layers present the Sm-A phase. These results show that the tilt angle profile is the dominant effect in the weak surface anchoring regime.

Figure 4.11: Profiles of (a) orientational, (b) translational and (c) tilt order parameters for a free-standing smectic film, at the vicinity of bulk Sm-C–Sm-A transition temperature ($T_{CA} = 0.902T_{NI}$). We consider different film temperatures: $T = 0.880T_{NI}$ (black circles) and $T = 0.906T_{NI}$ (red squares). $W_0/V_0 = 2.50$, corresponding to the strong surface anchoring regime.
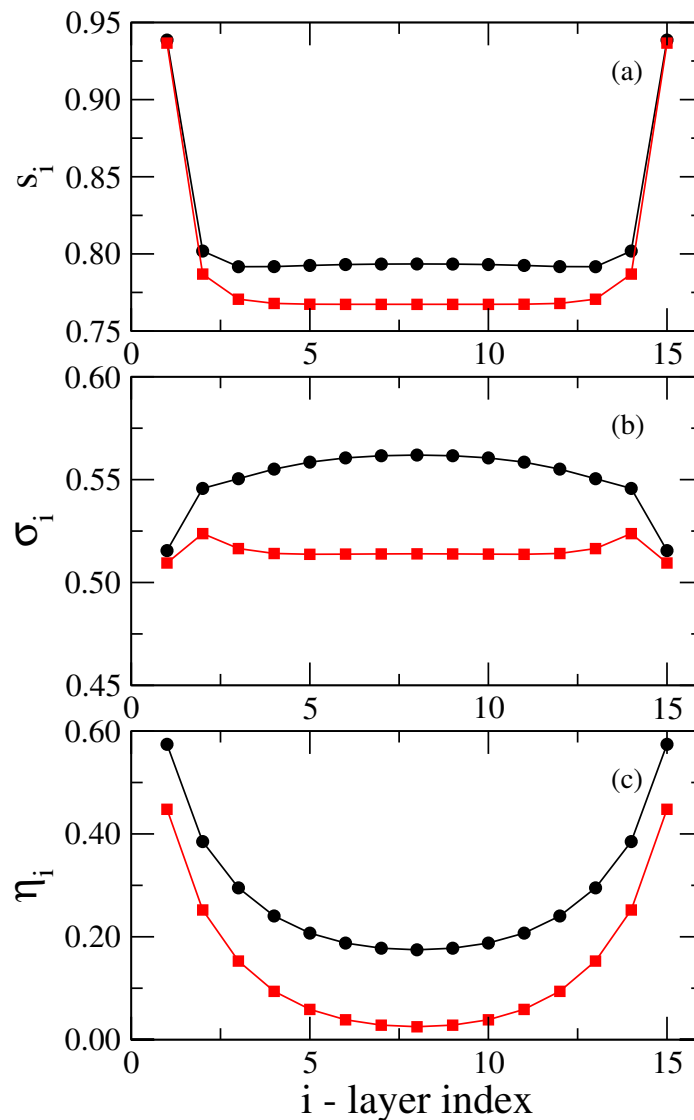
A distinct scenario emerges in the strong surface anchoring regime, where profound modifications in the order parameter profiles near the bulk Sm-C–Sm-A transition temperature are

exhibited in figure 4.11. Figure 4.11(a) shows the positive curvature of the nematic order parameter's profile, where the surface layers exhibit an almost saturated orientational ordering. The behaviour holds for $T > T_{CA}$, with a small reduction in the internal layers' nematic order parameter. Figure 4.11(b), shows that the smectic order parameter exhibits a non-uniform profile with a negative curvature for $T < T_{CA}$. In this case, the internal layers are more ordered than the outermost ones. For $T > T_{CA}$, the smectic order parameter exhibits a very small positive curvature. Although W_0/V_0 is not directly coupled to the tilt ordering, the strong anchoring condition leads to the enhancement of η_i along the whole film, specially in surface layers, as presented in figure 4.11c. For $T > T_{CA}$, a strong surface anchoring tends to stabilise the tilt order along the film, with the exception of the central layers where the tilt ordering is negligible.

Figure 4.12: Temperature dependence of (a) orientational, (b) translational and (c) tilt order parameters at the central layer in smectic films with $N = 15$ layers and different anchoring regimes: $W_0 = 0.25$ (black circles) and $W_0 = 2.50$ (red circles).
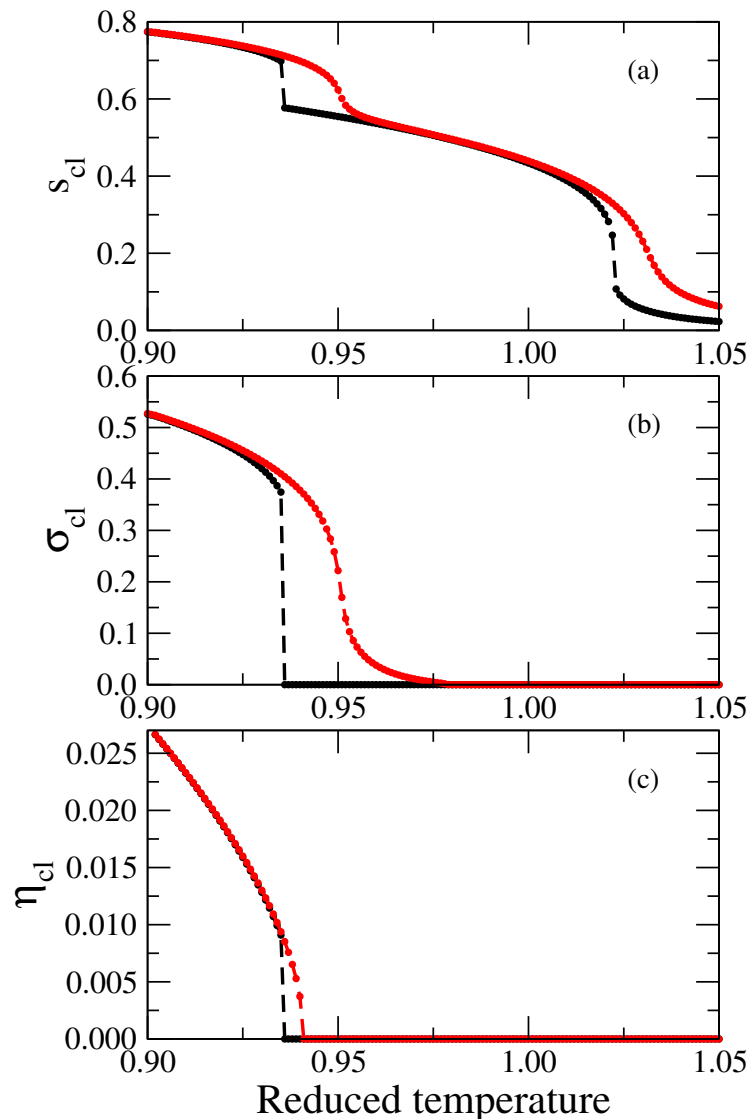
Figure 4.12 shows the order parameters' temperature dependence in the central layer for both weak and strong surface anchoring regimes. The former shows a competition between the surface-induced tilt and the thermal behaviour of the smectic order parameter near the Sm-A–N transition temperature, so that the centre of the film undergoes a first order Sm-C–N phase transition. In the latter, the film's centre undergoes a second-order Sm-C–Sm-A transition, while the orientational and translational order parameters vary continuously but remain finite at the transition.

Figure 4.13: Thickness dependence of (a) order parameters in the central layer and (b) average order parameter of free-standing smectic-C films: nematic (s - black circles), smectic (σ - red squares) and tilt (η - blue diamonds) order parameters. The tilt angle of central layer and average tilt angle are also shown (ω - green triangles). We consider a weak surface anchoring: $W_0 = 0.25$.
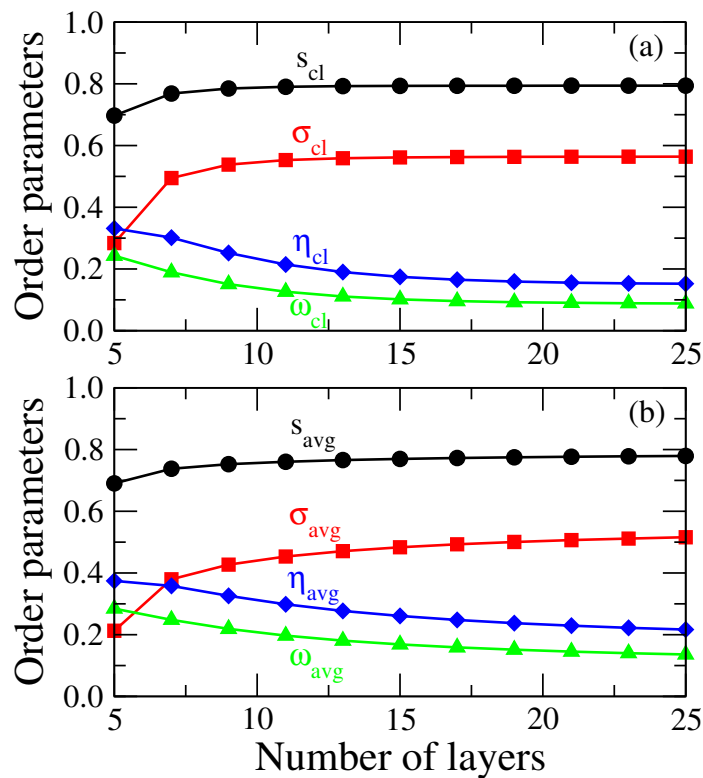
Source: Author, 2021.

The thickness dependence of the order parameters of free-standing films for distinct anchoring regimes was analysed to investigate the interplay of finite size effects and surface anchoring conditions, with a constant penetration surface length of $\xi = 2d_0$. In the regime of weak surface anchoring, as shown in figure 4.13(a), the nematic and smectic order parameters of the central layers increase rapidly with the film thickness, reaching their maximum values for $N = 15$. On the other hand, the tilt order parameter gradually decreases with increasing film thickness, thus reflecting the thickness dependence of tilt angle defined by equation 4.13. This result indicates that finite size effects govern the thermal behaviour of order parameters in the weak surface anchoring regime. The average order parameters across all layers are also shown in figure 4.13(b).

Figure 4.14 shows a distinct behaviour for strong surface anchoring. The nematic order parameter at the central layer is independent of the film thickness, while the smectic order parameter only slightly increases. The tilt order parameter, η_{cl}, is slightly larger in thin films due to the strong surface anchoring. However, the effects of the tilt angle's profile predominates as the film thickness is increased. It is assumed that the surface tilt amplitude ω_0 is independent of the surface anchoring W_0, as it is related to the molecular structure and excluded-volume contribution. More specifically, there is no experimental evidence supporting the dependence of surface tilt angle on the surrounding gas in free-standing films.

Figure 4.14: Thickness dependence of (a) order parameters in the central layer and (b) average order parameter of free-standing smectic-C films: nematic (s - black circles), smectic (σ - red squares) and tilt (η - blue diamonds) order parameters. The tilt angle of the central layer and its average tilt angle are also shown (ω - green triangles). We consider strong surface anchoring: $W_0 = 2.50$.
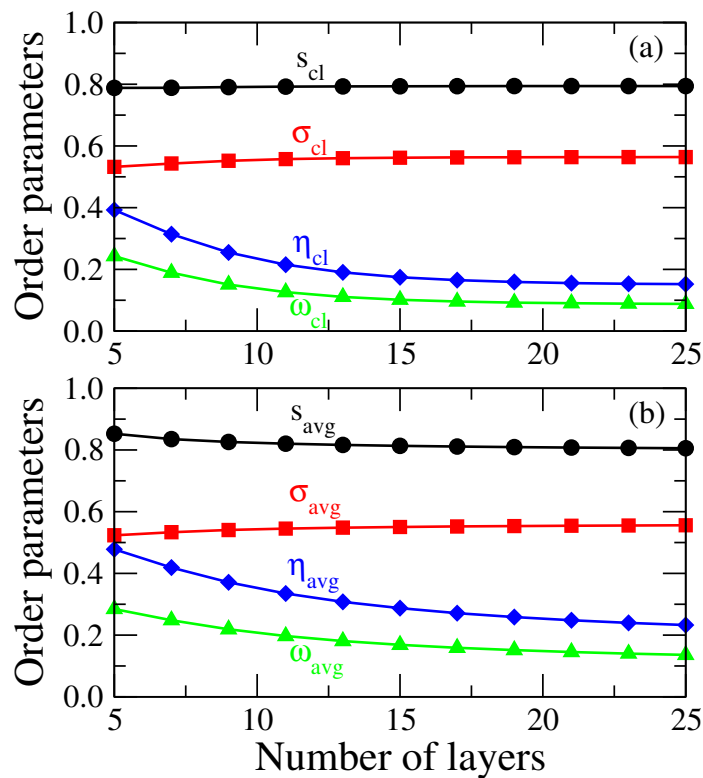
Source: Author, 2021.

Figure 4.15 illustrates the order parameters' temperature dependence at the central layer for different values of surface anchoring and film thickness. For a thin film with $N = 7$, a first order Sm-C–N occurs in the weak anchoring regime, while the nematic order vanishes smoothly with increasing temperature, as shown in figure 4.15(a). This result indicates the absence of the nematic–isotropic transition, even for small values of anchoring strength. However, the transition to the nematic phase in practice leads to the film thinning or rupturing. For a thin film with $N = 7$ and strong anchoring conditions, the first order Sm-C–N transition is replaced by a sequence of second order Sm-C–Sm-A and Sm-A–N transitions, occurring at higher temperatures than observed in bulk systems [see figure 3.17], as shown in figure 4.15(b).

Figure 4.15: Temperature dependence of order parameters at the central layer in smectic films with different thicknesses and anchoring conditions: (a) $N = 7$ and $W_0 = 0.25$, (b) $N = 7$ and $W_0 = 2.50$, (c) $N = 25$ and $W_0 = 0.25$ and (d) $N = 25$ and $W_0 = 2.50$. The grey areas represent the temperature regions where a drastic reduction in the smectic order takes place, corresponding to an unstable film.
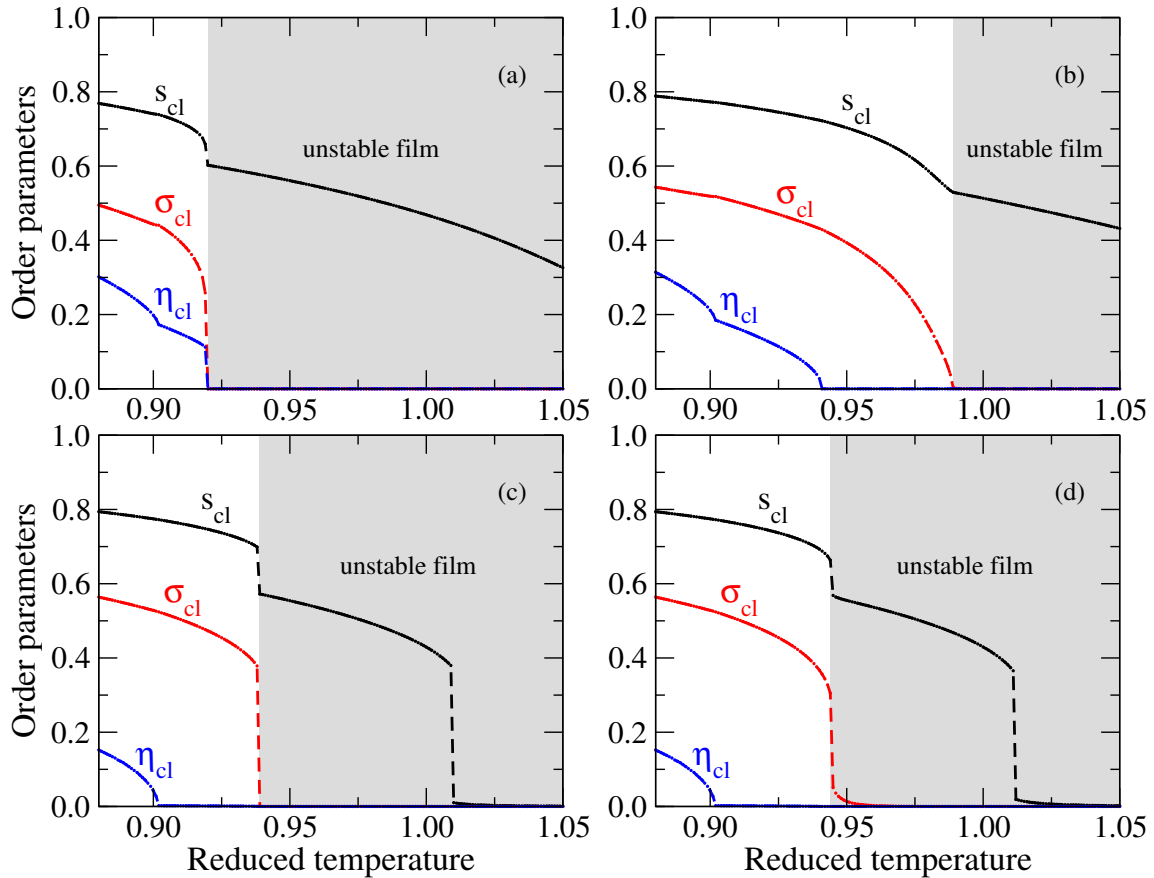
Source: Author, 2021.

For a thicker film ($N = 25$), a phase sequence similar to the bulk system is observed for even a weak anchoring strength, as shown in figure 4.15(c). Nevertheless, a residual smectic order parameter persists after the jump in Sm-A–N transition temperature for a 25-layer film under strong anchoring, as shown in figure 4.15(d). In this case, the nematic phase presents a residual smectic order, corresponding to a surface-induced smectic phase (si-Sm-A). A similar behaviour is observed above the nematic–isotropic transition temperature, where a residual nematic order is observed.

<div align="right">

V

</div>

ELECTRIC FIELD EFFECTS ON N–SM-A–SM-C PHASE TRANSITIONS

The effects of external fields on molecular ordering in liquid crystalline systems are an active research field [127–132] with major implications for developing new electro-optical devices [133–138]. In particular, the interplay of geometric anisotropy and different functional groups leads to anisotropic electromagnetic responses in thermotropic compounds [46, 139]. The system's molecular orientation depends on both the compound's dielectric anisotropy and the orientation of the applied external field, which in turn modifies the order parameters and liquid crystalline sequence phases. For example, an external field can give rise to ordered phases well above the nematic–isotropic and smectic–isotropic bulk transition temperatures [131, 132, 140]. Moreover, birefringence measurements close to the nematic–smectic–A transition temperature have shown that strong electric fields suppress the nematic fluctuations in systems with a positive dielectric anisotropy, causing the phase transition to cross from first to second order [141]. Concerning molecular reorientation, Wen and Rosenblatt have identified a crossover from a second to first order Fréedericksz transition in nematic liquid crystals with a negative dielectric anisotropy in the presence of a spatially homogeneous external field [142]. From a practical standpoint, external field induced director reorientation has proven crucial for developing fast response electro-optic modulators, switching devices and high-performance optical filters [133–138].

External field effects in the smectic–C phase were first considered by Rapini [143], which focused on phase stability and director reorientation. The discovery of different electric responses in the smectic-C phase, such as ferroelectricity [144–150] and antiferroelectricity [151], greatly encouraged further study of smectic phases, particularly under the influence of an external field. On the other hand, if the constituent molecules are chiral and possesses a permanent transversal dipole, each layer in the smectic–C phase exhibits a spontaneous polarisation. The coupling

between tilt angle and electric polarisation, which causes the spontaneous polarisation, can also occur at the smectic–A phase at high temperatures as the electroclinic effect [152]. In a bookshelf configuration, the director proportionally tilts perpendicular to the layers. Lee and Patel [153] studied the behaviour of a field-induced tilt angle in a ferroelectric liquid crystal. They observed that the molecular tilt crossed from a linear to a power law dependence with exponent $\nu \in (1/3, 1)$, near the Sm–A–Sm–C* transition, as seen in figure 5.1. The director field can deform due to the director's rotation around the normal to the smectic layers. As a result, the layers in most electroclinic materials contract and therefore buckle [114]. The electroclinic layer buckling can be observed in an optical microscope as periodic stripes and drastically reduces the high contrast ratio necessary for optical devices [154]. This effect has been considered theoretically [155–157] and observed experimentally [157, 158].

Figure 5.1: (a) Induced tilt angle θ vs applied field E. (b) Induced tilt angle θ in the limit of low field E. The cross, circle, triangle, and square symbols represent $T = 26.2, 27.8, 30.0$ and $35.0\ ^\circ C$, respectively.
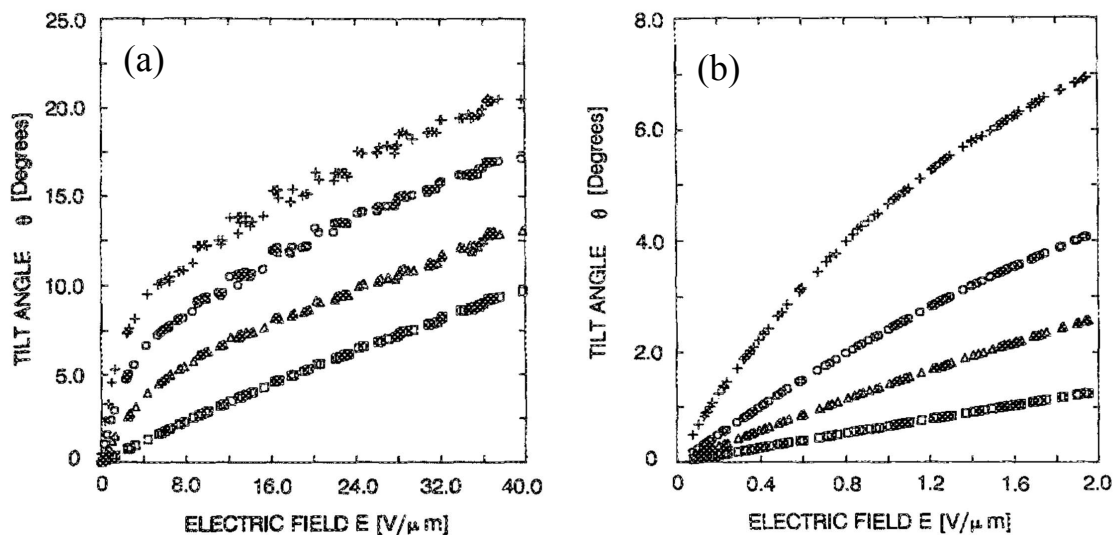
Source: Lee and Patel, 1989 [153].

The rich phenomenology of liquid crystal phase transitions under an external field have led to several proposed models. Despite the numerous aforementioned macroscopic experimental and theoretical studies of bulk smectic–C systems under external electric fields, a detailed microscopic approach is as yet lacking. We therefore investigate nematic–smectic–A–smectic–C phase transitions by extending the mean-field theory for smectic–C liquid crystals under an external electric field. The resulting effect on the thermal behaviour of the order parameters, and the nature of the phase transitions is analysed for both positive and negative polarisability anisotropies.

5.1 Microscopic Model for Transitions of Smectogenic Systems in the Smectic-C Phase Under the Influence of an Electric Field

A single component smectogenic system of rod-like molecules with a small or moderate transverse dipole moment [89], presents a layer contraction in the tilted smectic phase. To characterise the average molecular orientation inside the smectic layers, the relative orientation of the director $\vec{n}$ ($|\vec{n}| = 1$) and the smectic wave vector $\vec{q}$, represented by average tilt angle ω, as shown in figure 5.2 are considered. $\vec{q}$ is assumed to be normal to the smectic layer plane ($x - y$ plane), with a magnitude depending on the layer spacing d ($|\vec{q}| = 2\pi/d$). For convenience, the director $\vec{n}$ is assumed as restricted to the z–x plane, defined as the tilt plane. The orientation of the long molecular axis is defined by the polar and azimuthal angles θ and ϕ, respectively. ψ is the relative angle between the long molecular axis $\vec{a}$ and director $\vec{n}$.

Figure 5.2: Schematic representation of the smectic–C system, a Cartesian coordinate system whose z-axis is normal to the smectic layer plane is used. The external electric field is applied along the z axis, i.e. $\vec{E} = E\hat{z}$.
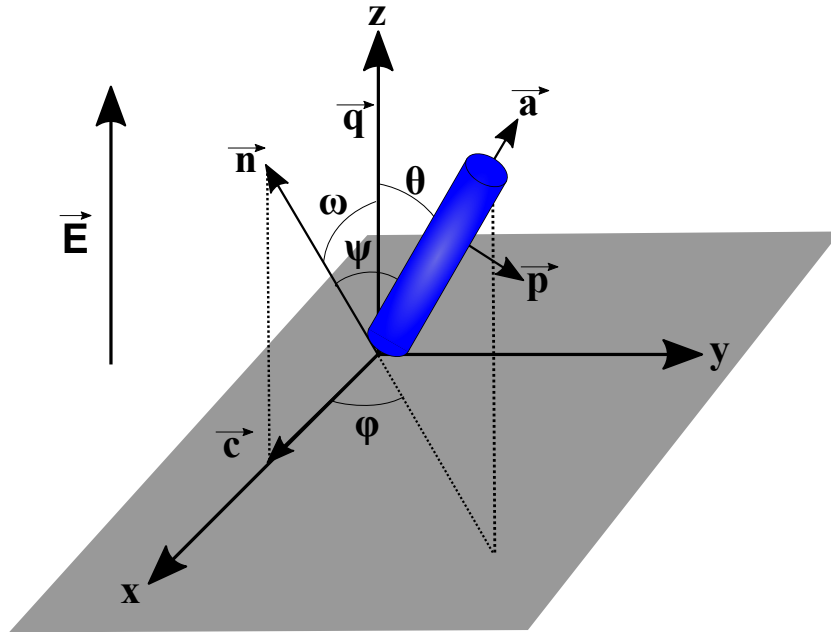
Source: Author, 2021.

5.1.1 Our Model and Formalism

We consider a single-particle mean-field potential that extends McMillan's model by including a tilting term and an external electric field along the z-axis. The tilt direction is assumed to

be constant for all smectic layers. Assuming that the liquid crystals molecules present a small transverse dipole, we consider two contributions due to the electric field: a linear term associated with the field-transverse dipole interaction, $V_{dip} = pE\sin\theta$, and a dielectric term associated with the molecular polarisability anisotropy, $V_{die} = -\frac{1}{3}\Delta\alpha_p E^2 P_2(\cos\theta)$. p is the dipolar moment and $\Delta\alpha_p$ is the molecular polarisability anisotropy. For calamitic molecules with a moderate or strong transverse dipole ($P > 5nC/cm^2$), the dipole-dipole interaction becomes relevant and a single-particle mean-field potential is not suitable to describe phase transitions involving such systems.

Aiming the analysis of electric field effects on phase transitions involving the smectic-C phase, the contributions of electric field must be added to the interaction potential introduced in chapter 3. Thus, the interaction potential accounting for the effect of the electric field is written as:

$$V = -\ V_0\Bigg\{\left[s + \alpha\sigma\cos\left(\frac{2\pi z}{d}\right)\right]P_2(\cos\psi) + \alpha\beta\eta\sigma^2\sin2\theta\cos\phi - $$
$$-\ \frac{pE}{V_0}\sin\theta + \frac{\Delta\alpha_p E^2}{3V_0}P_2(\cos\theta)\ \Bigg\}. \tag{5.1}$$

where V_0 is an interaction energy that determines the bulk sample's nematic-isotropic transition temperature. $P_2(\cos\psi)$ is the second order Legendre polynomial. The model parameters are α_0 and β. The former is a geometric parameter related to the length of alkyl chains of rod-like molecules, given by $\alpha_0 = 2\exp\left[-(\pi r_0/d)^2\right]$, where r_0 defines the characteristic length of the molecular rigid portion. The latter parameter depends on the spatial arrangement and strength of the dipoles in rod-like molecules.

A non-null average tilt contracts the layer spacing, as defined by $d = d_0\cos\omega$, where d_0 denotes the layer spacing in the smectic-A phase. We therefore define the quantity α in terms of the model parameter α_0 to account for the layer contraction due to tilting, as:

$$\alpha = 2\left(\frac{\alpha_0}{2}\right)^{\sec^2\omega}. \tag{5.2}$$

The orientation of the molecular long axis with respect to the director is represented by the angle ψ which satisfies the relation $\cos\psi = \cos\theta\cos\omega + \sin\theta\sin\omega\sin\phi$. The order parameters s, σ and η are defined by:

$$s = \langle P_2(\cos\psi)\rangle, \tag{5.3}$$

$$\sigma = \left\langle P_2(\cos\psi)\cos\left(\frac{2\pi z}{d}\right)\right\rangle, \tag{5.4}$$

and

$$\eta = \langle \sin 2\theta \cos \phi \rangle. \tag{5.5}$$

Where the thermodynamic averages, $\langle \cdots \rangle$, are computed from the following one-particle distribution function:

$$\mathscr{L}(z, \theta, \phi) \propto \exp\left[-V/k_B T\right], \tag{5.6}$$

k_B is the Boltzmann constant and T is the temperature. The equilibrium order parameters are solutions of self-consistent equations, found at extreme values of the following Helmholtz free energy:

$$\frac{F}{N_0 V_0} = \frac{1}{2}\left(s^2 + \alpha\sigma^2 + \alpha\beta\sigma^2\eta^2\right) + \frac{1}{2}\left(-\frac{pE}{V_0}\langle\sin\theta\rangle + \frac{\Delta\alpha E^2}{3V_0}\langle P_2(\cos\theta)\rangle\right) -$$
$$- \frac{k_B T}{V_0}\ln\left(\frac{1}{2\pi d}\int_{-1}^{1} d\cos\theta \int_{0}^{\pi} d\phi \int_{0}^{d} dz\mathscr{L}\right), \tag{5.7}$$

where, for $\omega = 0$, $s = \langle P_2(\cos\theta)\rangle$.

The order parameters are numerically determined using the self-consistent equations for different values of the tilt angle ω, and fixed values of T, α_0 and β. The equilibrium configuration corresponds to the Helmholtz free energy minimum with respect to ω. The solutions corresponding to the different phases are

- $s = \sigma = \eta = 0 \rightarrow$ Isotropic;

- $s \neq 0$ and $\sigma = \eta = 0 \rightarrow$ Nematic;

- $s \neq 0$, $\sigma \neq 0$ and $\eta = 0 \rightarrow$ Smectic-A;

- $s \neq 0$, $\sigma \neq 0$ and $\eta \neq 0 \rightarrow$ Smectic-C.

The model parameters are henceforth $\alpha_0 = 0.84$ and $\beta = 0.31$ which gives a good representation of the nonchiral liquid-crystalline compound p-decyloxybenzoic acid p-n-hexyphenyl ester (DOBHOP). This compound exhibits the following phase transition sequence: Sm–C - 77.5 - Sm–A - 83.3 - N - 88.9 - Iso. We then have the following important parameters: transversal dipole moment $p = 1.16 \times 10^{-29} \cdot m$, polarisability anisotropy $|\Delta\alpha_p| = 2.03 \times 10^{-29}$ m^3 and characteristic potential $V_0 = k_B T_{NI}/0.2202 = 2.3 \times 10^{-20}$ J [32].

Although this specific compound presents a negative polarisability, it is useful to analyse a similar compound that presents an opposite polarisability. For that reason, we are going to present the results for both polarisabilities: $\Delta\alpha_p^* = \pm|\Delta\alpha_p|$.

5.1.2   Results

Negative Polarisability

To investigate how the smectic–C order can be favoured by an electric field, we consider a negative polarisability anisotropy ($\Delta\alpha_p^* < 0$). In fact, the negative polarisability anisotropy favours the reorientation of calamitic molecules along the perpendicular direction to the external field.

Figure 5.3: Helmholtz free energy as a function of the tilt angle ω for different values of applied electric field: $E = 0$ kV/cm (solid black line), $E = 4$ kV/cm (dashed red line), $E = 8$ kV/cm (dotted blue line) and $E = 12$ kV/cm (dashed-dotted green line). We use representative values of the model parameters $\alpha_0 = 0.84$ and $\beta = 0.31$, $\Delta\alpha_p^* < 0$ and fixed temperature $T/T_{CA} = 0.8$.
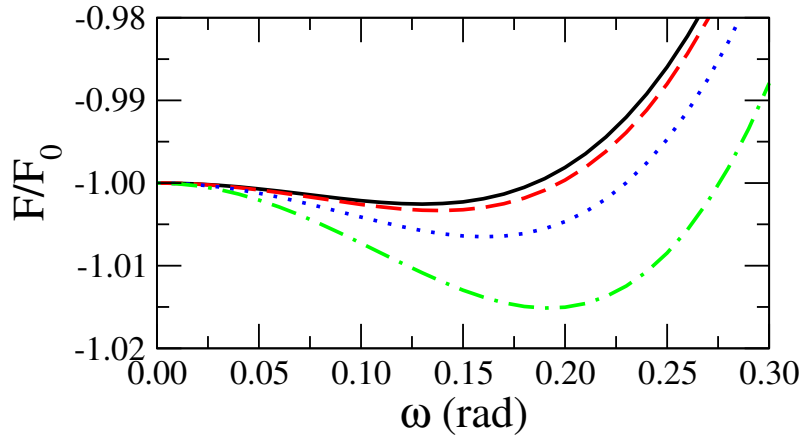
Source: Author, 2021.

In order to characterise the stability of the smectic-C phase, we present the Helmholtz free energy as a function of the average tilt angle for different values of external electric field, as shown in figure 5.3. The temperature was fixed at $T/T_{CA} = 0.8$, where T_{CA} is the temperature at which the Sm–C order disappears in the absence of an external field. To aid visualisation, the free energy axis is normalised to F_0, corresponding to the absolute value of Helmholtz free energy for $\omega = 0$. For $E = 0$, we observe that the Helmholtz free energy presents a minimum at non-null value of tilt angle, confirming that the smectic-C phase corresponds to the equilibrium phase at $T/T_{CA} = 0.8$. As the external electric field is raised, we notice that the energy minimum becomes more pronounced, taking place at higher values of the tilt angle. Such a result indicates that the electric field favours the tilt ordering inside the smectic layers, thus increasing the stability of the smectic-C. In particular, molecules presenting a negative polarisability tend to align themselves perpendicular to the external field, similar to the contribution of field-transverse dipole interaction. As a consequence, a gradual increase of the tilt angle is expected as field amplitude is enhanced, for $T < T_{CA}$.

Figure 5.4 shows the temperature dependence of s, σ and η order parameters, for different electric fields. Figure 5.4(a) shows the bulk order parameters, without an external electric field, presenting a second order Sm–C–Sm–A phase transition, followed by first-order Sm–A–N and N–Iso phase transitions. We note that even for a small electric field the isotropic phase is suppressed, giving rise to a field-induced nematic phase, with negative orientational order parameter, as shown in figure 5.4(b). Additionally, the temperature-range of the Sm–A phase is reduced, while the Sm–C phase is favoured by the external field. Figure 5.4(c) shows a small-range Sm–A phase followed by a first-order Sm–A–fi-N phase transition, completely suppressing the nematic phase with positive order parameter. Moreover, we notice a pronounced increase in the transition discontinuity between conventional and field-induced nematic phases. We also verify a gradual increase in the Sm-A-Sm-C transition temperature as the electric field is enhanced, being accompanied by a raise in the tilt order parameter increases at $T < T_{CA}$. Sufficiently strong electric fields induce a first order Sm–C–fi-N phase transition, where the Sm–A phase is completely suppressed, as seen in figure 5.4(d).

Figure 5.4: Variation of the orientational s, translational σ, and tilt η order parameters as a function of the reduced temperature for $\Delta\alpha_p^* < 0$ and different values of electric field: (a) $E = 0$ kV/cm, (b) $E = 4$ kV/cm, (c) $E = 12$ kV/cm and (d) $E = 16$ kV/cm.
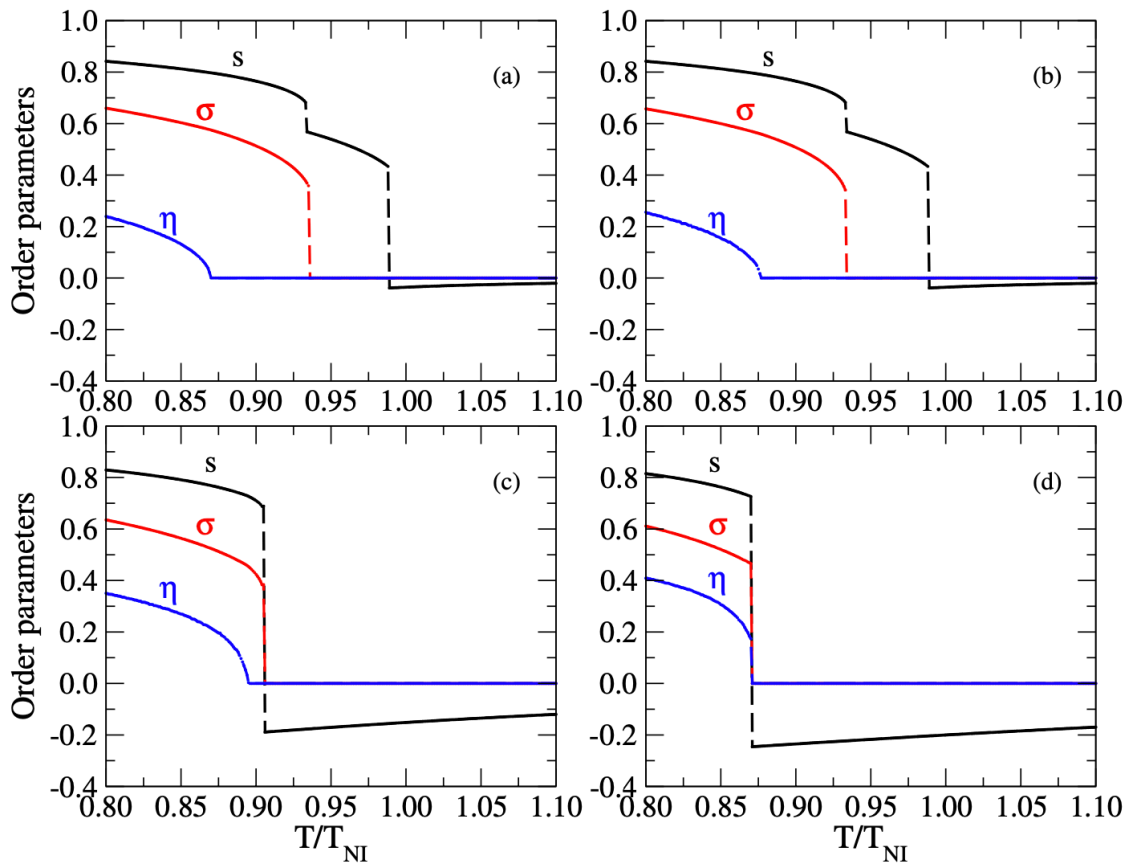
Source: Author, 2021.

The temperature dependence of tilt angle for different values of electric field was analysed

to characterise the electric field's effects on the phase transitions, shown in figure 5.5. For
convenience, we rescaled the temperature by T_C, corresponding to the temperature at which
the η order parameter vanishes. For $T < T_C$, we observe that the tilt angle increases with the
electric field. Additionally, the continuous decay of the tilt angle is replaced by a jump at $T =
T_C$, which suggests that sufficiently strong electric fields affect the nature of phase transitions
involving the smectic–C phase, even though the model parameters are kept constant. Since we
are considering a negative polarisability, this result is in agreement with experimental studies,
given that sufficiently strong electric fields suppresses the Sm–A phase [114, 141, 152–154].

Figure 5.5: Variation of the tilt angle ω as a function of the reduced temperature, which is normalised by
the temperature at which the η order parameter vanishes, for $\Delta\alpha_p^* < 0$ and different electric field values:
$E = 0$ kV/cm (solid black line), $E = 8$ kV/cm (dashed red line), $E = 12$ kV/cm (dotted blue line) and
$E = 16$ kV/cm (dashed-dotted green line).
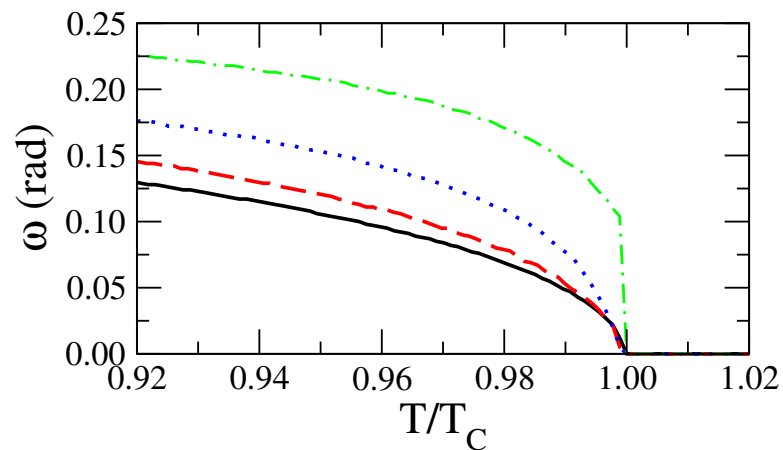
Source: Author, 2021.

In figure 5.6, we present the variation of the tilt angle ω as a function of the electric field,
for different values of temperature. In figure 5.6(a), for $T < T_{CA}$, which corresponds to the
temperature at which the η order parameter vanishes, we observe an monotonic increase of
tilt angle under the influence of an external electric field, reflecting the increase in the order
parameter η. More specifically, an almost quadratic growth with the applied field is observed,
indicating that the contribution associated with the anisotropy in polarisability predominates
over the contribution of the transverse dipole. This behaviour persists at temperatures where
the smectic-C phase is well established. As the temperature approaches T_{CA}, ω saturates at a
maximum value as the field strength increases. This is due to the fact that the second-order
Sm-A-Sm-C transition is suppressed at high fields when $T \to T_{CA}$, giving way to the Sm-C-N
transition, as shown in figure 5.4(d).

The dependence of the tilt angle on the external field exhibits a distinct behaviour when $T > T_{CA}$.
In particular, the tilt angle remains null until the electric field reaches a threshold value due to
the competition between thermal and field effects. This is associated with the molecule's small
dipole moment, requiring a stronger electric field to overcome the thermal effects and thus

induce tilting. For increasing field strength, the tilt angle is favoured up to a certain point. When approaching the smectic–C–nematic phase transition, there is a continuous reduction on the tilt angle, thus representing a reentrant-like behaviour.

Figure 5.6: Variation of the tilt angle ω as a function of the electric field, for different temperatures, with $\Delta\alpha_p^* < 0$. Temperatures (a) below T_{CA} and (b) above T_{CA}.
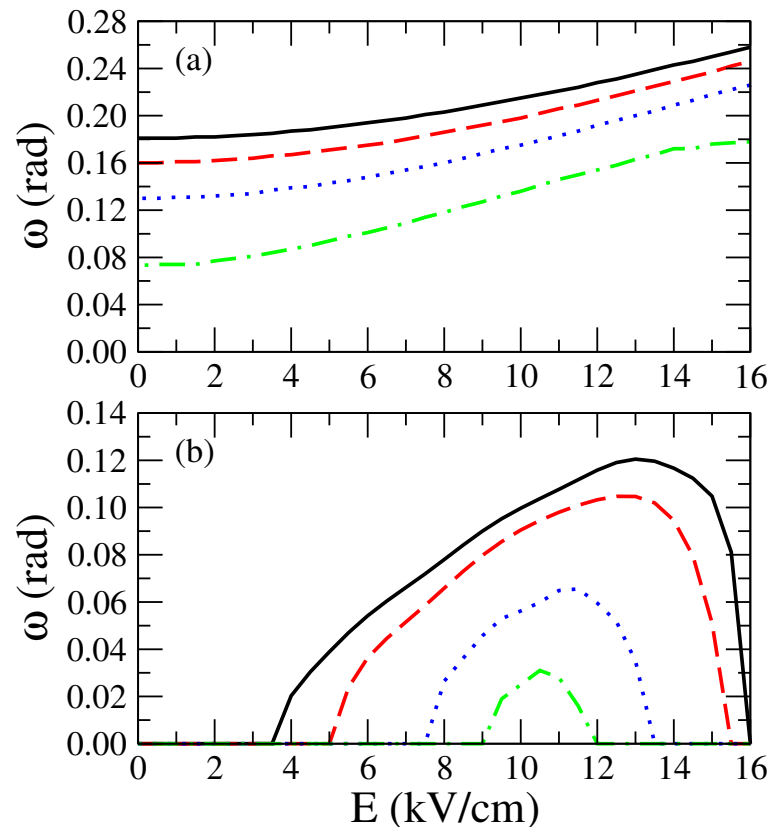
Source: Author, 2021.

Figure 5.7 presents the phase diagram of temperature versus the applied electric field. The temperature is rescaled by the nematic–isotropic transition temperature, T_{NI}. For low fields, a second-order Sm–C–Sm–A, followed by a Sm–A–N phase transition is present. As the applied field increases, the Sm–A phase is suppressed, due to the reduction in the Sm–A–N and the increase in the Sm–C–Sm–A transition temperatures. Additionally, the representation range of the nematic phase induced by the external field increases. For $E = 15$ kV/cm, a second-order Sm–C–Sm–A phase transition is present, while a first-order Sm–C–fi–N phase transition only takes place for $E > 15$ kV/cm. This indicates that $E = 15$ kV/cm is a critical end point, which corresponds to where the line of continuous Sm–C–Sm–A transition encounters the coexistence line between the Sm–C and the nematic phase.

Figure 5.7: Phase diagram of the reduced temperature as a function of the applied electric field for $\Delta\alpha_p^* < 0$. The dashed line represents a second order phase transition, and the filled line describes a first order phase transition.
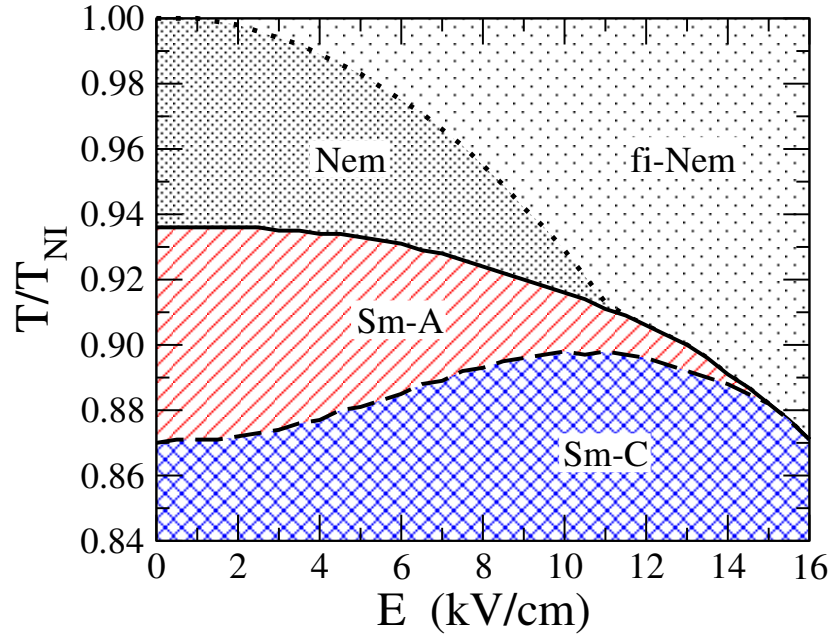
Source: Author, 2021.

Positive Polarisability

Now, we consider a positive polarisability anisotropy ($\Delta\alpha_p^* > 0$). In this configuration, we have opposite contributions associated with the external field: (i) the positive polarisability anisotropy favours molecular alignment along the external field; (ii) the field-dipole interaction tends to reorient molecules perpendicular to the electric field. Such opposite trends may lead to different scenarios for transitions involving the smectic-*C*.

Figure 5.8 presents the variation of the tilt angle ω as a function of electric field, for different temperatures. We note that, differently than for the case of negative polarisability anisotropy, the tilt angle ω decreases under the influence of an external field for a given temperature, with a reduction of its maximum value when the applied electric field increases. This happens because the molecules' major axis tend to align parallel to the field, since the contribution associated with the polarisability anisotropy overcomes the contribution of the transverse dipole.

Figure 5.9 shows the temperature dependence of s, σ and η order parameters, for different values of the electric field strength. For $E = 4$ kV/cm (figure 5.9(b)), the electric field suppresses the isotropic phase, giving rise to an field-induced nematic phase. Additionally, the temperature-range of the smectic–*C* phase reduces, while the smectic–*A* phase is favoured by the external field. For increasing field strength, we notice a reduction in the nematic-isotropic transition dis-

Figure 5.8: Variation of the tilt angle ω as a function of the electric field, for $\Delta\alpha_p^* > 0$ and different temperatures: $T/T_{NI} = 0.80$ (solid black line), $T/T_{NI} = 0.81$ (dashed red line), $T/T_{NI} = 0.82$ (dotted blue line) and $T/T_{NI} = 0.85$ (dashed-dotted green line).
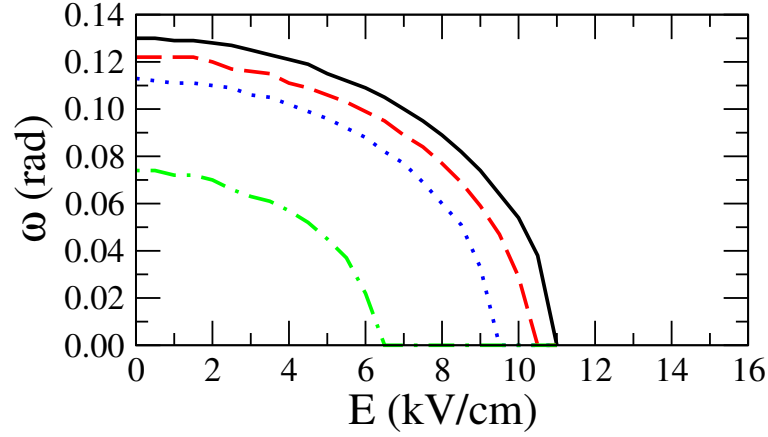
Source: Author, 2021.

Figure 5.9: Variation of the orientational s, translational σ, and tilt η order parameters as a function of the reduced temperature for $\Delta\alpha_p^* > 0$ and different values of electric field: (a) $E = 0$ kV/cm, (b) $E = 4$ kV/cm, (c) $E = 6$ kV/cm and (d) $E = 8$ kV/cm.
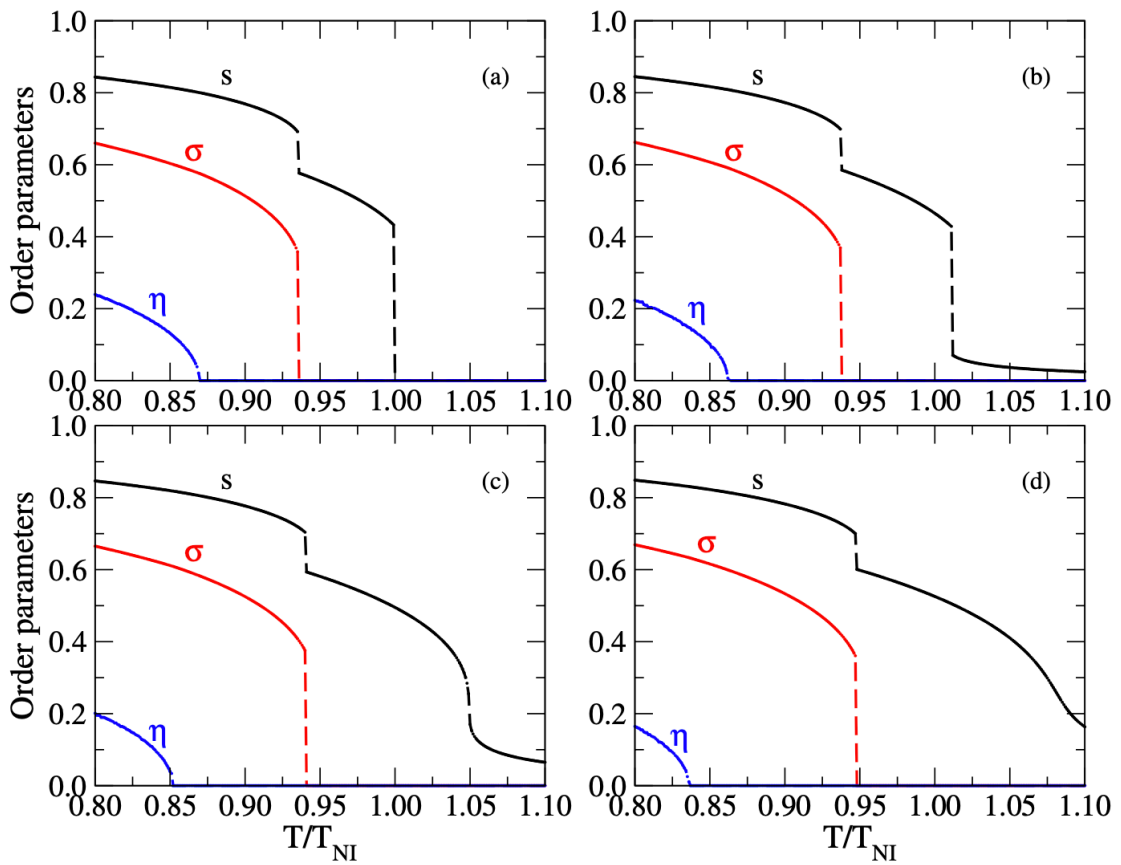
Source: Author, 2021.

continuity (figure 5.9(c)). In this case, the nature of the Sm–*C*–Sm–*A* and Sm–*A*–N transitions
remain the same, as second and first order transitions, respectively. For a sufficiently high field
strength (figure 5.9(d)), the discontinuity in the orientational order parameter disappears, due to
the suppression of the liquid isotropic phase. Moreover, we can see that the tilt angle assumed
by the smectic–*C* phase decreases as the electric field increase, contrary to the behaviour for
$\Delta\alpha_p^* < 0$.

Finally, figure 5.10 presents the phase diagram for $\Delta\alpha_p^* > 0$. We note that the smectic–*A* phase
is favoured, while the smectic–*C* phase is suppressed with increasing field strength. Under the
influence of an external electric field, a residual nematic phase appears, favouring the phase for
increasing field, while suppressing the isotropic phase. However, the liquid isotropic phase is
present for low field strengths. The phase diagram permits the characterisation of the phase tran-
sitions, where a second-order smectic-C–smectic-A phase transition and a first-order smectic-
A–nematic phase transition is present for all values of the external electric field strength.

Figure 5.10: Phase diagram of the reduced temperature as a function of the applied electric field for
$\Delta\alpha_p^* > 0$. The dashed line represents a second order transition, and the filled line represents the first
order transition.

Source: Author, 2021.

VI
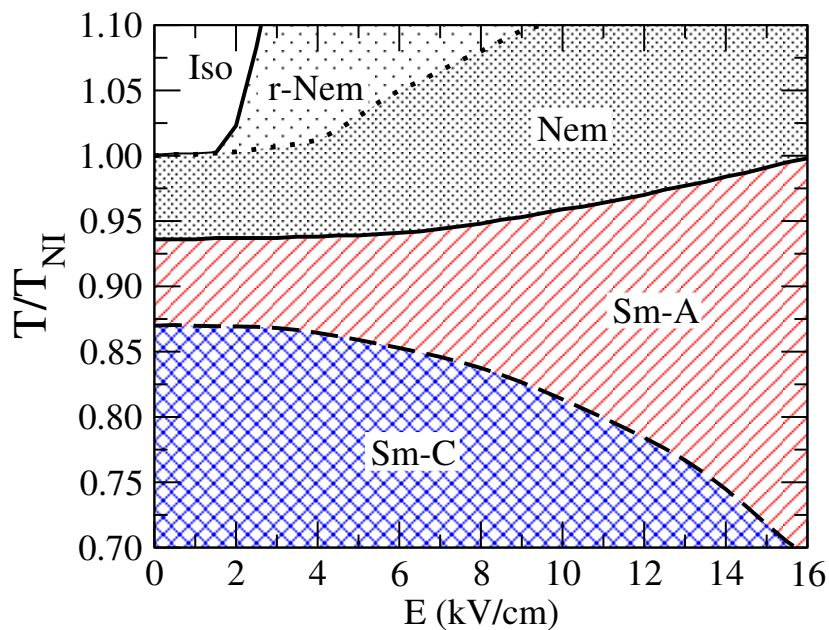
CONCLUDING REMARKS AND PERSPECTIVES

This thesis investigated surface and finite size effects in freely suspended films and electric field effects in the bulk of smectogenic systems presenting the smectic-C phase.

Initially, a review of existing models describing bulk phase transitions involving nematic, smectic-A and smectic-C phases was given. The model proposed by Govind and Madhusudana was shown to be a satisfactory extension of the well-established Maier-Saupe and McMillan models for the nematic and smectic-A phases. While it satisfactorily describes transitions involving the smectic-C phase, the need for an extra parameter to include an excluded volume contribution makes the model more computationally demanding, especially for studying surface and external field effects.

Phase transitions in bulk systems presenting a smectic-C phase were studied using a single-particle mean-field potential similar to that introduced by Govind and Madhusudana. The phase diagrams of smectogenic compounds with a small transverse dipole can be reasonably described when the tilt-induced contraction of smectic layers is considered. This approach eliminates the need to introduce an additional excluded-volume contribution to stabilise the smectic-A phase, thus reducing the model's free parameters.

Varying the model parameter associated with the transverse dipoles in rod-like molecules led to a rich variety of phase diagrams. In particular, a NAC critical end point was identified which corresponds to where the line of continuous transition between the smectic-C and smectic-A phases encounters the coexistence line between the smectic-C and the nematic phases. Moreover, the triple point marking the coexistence of nematic, smectic-A and isotropic phases was determined. Finally, the NA tricritical point (already predicted by McMillan) and the NAC crit-

ical end point were observed to merge with increasing β, giving rise to a NC tricritical point, delimiting the regions of continuous and discontinuous smectic-C–nematic transitions. Despite not being explicitly calculated, the existence of a multicritical point in the phase diagrams of compounds with short alkyl chains and large transverse dipole moment could, in principle, be predicted.

The previous model was extended to study phase transitions in free-standing films presenting a smectic-C phase. Our results showed that the interplay of finite size effects and surface anchoring conditions affects the phase diagrams of thin films. A discrete version of the single-particle mean-field potential as well as a tilt angle profile induced by the surface ordering were considered. The profiles of order parameters of free-standing films were computed under different anchoring regimes. Surface effects were observed to stabilise the tilt order parameter in outermost layers of films above the bulk smectic-C–smectic-A transition temperature. As a consequence, surface layers may remain in the smectic-C phase, while the central layers undergo a smectic-C–smectic-A transition. Such coexisting smectic-C and smectic-A phases in free-standing films have been reported in previous experimental studies [81, 116]. Our results were published on August 19, 2020, in Physical Review E **102**, 022702. A copy of the article can be found in appendix A.

The model for bulk phase transitions was extended by a collaborative work analysing the effects of applying external fields. For this, an electric field contribution must be added to the interaction potential, which is composed of two terms: A linear term, $V_{dip} = pE\sin\theta$, and a dielectric term, $V_{die} = -\frac{1}{3}\Delta\alpha_p E^2 P_2(\cos\theta)$, where p is the dipole moment and $\Delta\alpha_p$ is the molecular polarisability anisotropy. This work is in the final stages of writing for submission to a journal yet to be decided (a preliminary version can be found in appendix B). The results obtained encourage the further study of external field effects in smectic-C free-standing films by including the electric field term in the discrete interaction potential introduced in this thesis.

As previously stated, free-standing smectic films are very suitable for determining the surface properties of liquid crystals. In particular, surface tension is the main contributing factor as it is responsible for the film's stability. It restricts fluctuations in the smectic order on the film's surface, enabling the production of free-standing films of up to thousands of molecular layers. Therefore, it is interesting to investigate its dependence on the film's thickness and temperature, especially near phase transitions. Experiments have previously established that surface tension depends very little on film thickness. However, the thickness of thin films may become important when phase sequences or transition temperatures change with respect to the bulk phase. The surface tension's thermal and film thickness dependence is given by: $\gamma = \gamma_{iso} + \sum_{I=1}^{N} f_i - f_b$, where f_i and f_b are the free energy per unit area of the ith layer and bulk respectively, and γ_{iso} is the isotropic surface tension contribution. This work is in its

initial phase, with the potential of experimental collaboration to enable qualitative comparisons between theoretical and experimental results for different phase transition sequences.

The study of the film's surface tension under an external electric field is also of great scientific interest. The order imposed by the surface tension and by the external field results in the existence of a characteristic thickness, where a crossover from surface-induced to field-induced ordering is observed.

We hope that the results presented here will stimulate further investigations and experimental efforts aiming to probe the rich scenarios predicted by the extended version of the molecular theory for smectic-C free-standing films.

BIBLIOGRAPHY

[1] F. Reinitzer, "Beiträge zur kenntniss des cholesterins", Monatsh. Chem. **9**, 421 (1888) (cited on page 2).

[2] F. Reinitzer, "Contributions to the knowledge of cholesterol", Liq. Cryst. **5**, 7 (1989) (cited on page 2).

[3] O. Lehmann, "Über fliessende krystalle", Z. Phys. Chem. **4**, 462 (1889) (cited on page 2).

[4] O. Lehmann, *Flüssige Kristalle* (Wilhelm Engelmann, Leipzig, 1904) (cited on page 2).

[5] D. Vorländer, "Einfluß der molekularen gestalt auf den krystallinisch-flüssigen zustand", Ber. Dtsch. Chem. Ges. **40**, 1970 (1907) (cited on page 2).

[6] D. Vorländer, "Die erforschung der molekularen gestalt mit hilfe der kristallinischen flüssigkeiten", Z. Phys. Chem. **105U**, 211 (1923) (cited on page 2).

[7] G. Friedel, "Les états mésomorphes de la matière", Ann. Phys. **9**, 273 (1922) (cited on pages 2, 59).

[8] V. Fréedericksz and V. Zolina, "Forces causing the orientation of an anisotropic liquid", Trans. Faraday Soc. **29**, 919 (1933) (cited on page 2).

[9] C. W. Oseen, *Die anisotropen Flüssigkeiten: Tatsachen und Theorien* (Gebrüder Borntraeger, Berlin, 1929) (cited on page 3).

[10] C. W. Oseen, "The theory of liquid crystals", Trans. Faraday Soc. **29**, 883 (1933) (cited on page 3).

[11] H. Zocher, "The effect of a magnetic field on the nematic state", Trans. Faraday Soc. **29**, 945 (1933) (cited on page 3).

[12] F. C. Frank, "I. Liquid crystals. On the theory of liquid crystals", Discuss. Faraday Soc. **25**, 19 (1958) (cited on page 3).

[13] V. N. Tsvetkov, "On molecular order in the anisotropic liquid phase", Acta Physicochim. URSS **16**, 132 (1942) (cited on page 3).

[14] W. Maier and A. Saupe, "Eine einfache molekulare theorie des nematischen kristallinflüssigen zustandes", Z. Naturforsch. **A 13**, 564 (1958) (cited on pages 3, 23).

[15] W. Maier and A. Saupe, "Eine einfache molekular-statistische theorie der nematischen kristallinflüssigen phase. teil i", Z. Naturforsch. **A 14**, 882 (1959) (cited on pages 3, 23).

[16] W. Maier and A. Saupe, "Eine einfache molekular-statistische theorie der nematischen kristallinflüssigen phase. teil ii", Z. Naturforsch. **A 15**, 287 (1960) (cited on pages 3, 23).

[17] J. F. Dreyer, *3rd Int. Liquid Crystal Conf.* (Berlin, Germany, 1970) (cited on page 3).

[18] P. Sheng, "Phase Transition in Surface-Aligned Nematic Films", Phys. Rev. Lett. **37**, 1059 (1976) (cited on page 3).

[19] P. Sheng, "Boundary-layer phase transition in nematic liquid crystals", Phys. Rev. A **26**, 1610 (1982) (cited on pages 3, 30).

[20] P. Pieranski and B. Jérôme, "Adsorption-induced anchoring transitions at nematic-liquid-crystal–crystal interfaces", Phys. Rev. A **40**, 317 (1989) (cited on page 3).

[21] B. Jérôme and P. Pieranski, "Depth of Interaction of Nematic Liquid Crystals with Crystalline Substrates", Europhys. Lett. **13**, 55 (1990) (cited on page 3).

[22] B. Jerome, J. Bechhoefer, A. Bosseboeuf, and P. Pieranski, "On the Anchoring of Nematics on Silicon Surfaces", Mol. Cryst. Liq. Cryst. Inc. Nonlinear Opt. **192**, 69 (1990) (cited on page 3).

[23] B. Jerome, "Surface effects and anchoring in liquid crystals", Rep. Prog. Phys. **54**, 391 (1991) (cited on pages 3, 26, 30).

[24] B. Jérôme and Y. R. Shen, "Anchoring of nematic liquid crystals on mica in the presence of volatile molecules", Phys. Rev. E **48**, 4556 (1993) (cited on page 3).

[25] R. de Oliveira, B. H. G. Lourenço, J. S. Jr., N. P. Andery, and L. S. Jr., "Termômetro de Cristal Líquido Colestérico", (2008) (cited on page 3).

[26] I. Chuang, T. Durrer R., and B. N. Yurke, "Cosmology in the Laboratory: Defect Dynamics in Liquid Crystals", Science **251**, 1336 (1991) (cited on page 4).

[27] I. C. Khoo, D. H. Werner, X. Liang, A. Diaz, and B. Weiner, "Nanosphere dispersed liquid crystals for tunable negative–zero–positive index of refraction in the optical and terahertz regimes", Opt. Lett. **31**, 2592 (2006) (cited on page 4).

[28] D. F. Gardner, J. S. Evans, and I. I. Smalyukh, "Towards Reconfigurable Optical Metamaterials: Colloidal Nanoparticle Self-Assembly and Self-Alignment in Liquid Crystals", Mol. Cryst. Liq. Cryst. **545**, 3 (2011) (cited on page 4).

[29] F. Kahn, "Smectic liquid crystal storage displays for high resolution graphics applications", in 1972 International Electron Devices Meeting (1972), page 72 (cited on page 4).

[30] R. Virchow, "Ueber das ausgebreitete vorkommen einer dem nervenmark analogen substanz in den thierischen geweben", Archiv f. pathol. Anat. 6, 562 (1854) (cited on page 6).

[31] A. M. F. Neto, "Fluidos complexos na matéria condensada:os cristais líquidos", Rev. Bras. Ensino Fís. 43, 10 . 1590 / 1806 − 9126 − rbef − 2020 − 0300 (2021) (cited on page 8).

[32] S. Pestov, *Physical Properties of Liquid Crystals*, Advanced Materials and Technologies 5A (Springer-Verlag Berlin Heidelberg, 2003) (cited on pages 10–12, 53, 81).

[33] I. Dierking, "Color Plates", in *Textures of Liquid Crystals* (John Wiley & Sons, Ltd, 2004), pages 167–212 (cited on pages 13, 15–17).

[34] I. C. Khoo, *Liquid Crystals* (John Wiley & Sons, New Jersey, 2007) (cited on pages 14, 31).

[35] M. Schadt, "The twisted nematic effect: liquid crystal displays and liquid crystal materials", Mol. Cryst. Liq. Cryst. Inc. Nonlinear Opt. 165, 405 (1988) (cited on page 14).

[36] B. R. Acharya, K. W. Baldwin, R. A. MacHarrie, J. A. Rogers, C. C. Huang, and R. Pindak, "In-fiber nematic liquid crystal optical modulator based on in-plane switching with microsecond response time", Appl. Phys. Lett. 81, 5243 (2002) (cited on page 14).

[37] J. A. Castellano and E. F. Pasierb, "Electronically-tuned optical filters utilizing nematic liquid crystals", in 1969 International Electron Devices Meeting (1969), page 94 (cited on page 14).

[38] J. Schmidtke, W. Stille, and H. Finkelmann., "Defect mode emission of a dye doped cholesteric polymer network", Phys. Rev. Lett 90, 083902 (2003) (cited on page 15).

[39] N. Y. Ha, Y. Ohtsuka, S. M. Jeonh, S. Nishimura, S. G., Y. Takanishi, K. Ishikawa, and H. Takezoe, "Fabrication of a simultaneous red–green–blue reflector using single-pitched cholesteric liquid crystals", Nat. Mater. 7, 43 (2008) (cited on page 15).

[40] D. Andrienko, *Introduction to Liquid Crystal*, Advanced Materials and Technologies (International Max Planck Research School, Bad Marienberg, 2006) (cited on page 15).

[41] C. Y. Chao, C. F. Chou, J. T. Ho, S. W. Hui, A. J. Jin, and C. C. Huang, "Electron-Diffraction Studies of Phase Transitions in 40.8 Free-Standing Thin Films", Mol. Cryst. Liq. Cryst. 301, 123 (1997) (cited on page 17).

[42] W. L. McMillan, "Simple Molecular Theory of the Smectic *C* Phase", Phys. Rev. A 8, 1921 (1973) (cited on pages 18, 38).

[43] B. W. V. der Meer and G. Vertogen, "An induced dipole model of the smectic C phase", J. Phys. Colloq. **40**, C3–222 (1979) (cited on pages 18, 33).

[44] A. S. Govind and N. V. Madhusudana, "A simple molecular theory of smectic-C liquid crystals", Europhys. Lett. **55**, 505 (2001) (cited on pages 18, 32–33, 49, 57).

[45] J. W. Goodby, G. W. Gray, and D. G. McDonnell, "Dipole Moments and the Smectic C Phase", Mol. Cryst. Liq. Cryst. **34**, 183 (1977) (cited on page 18).

[46] P. G. de Gennes and J. Prost, *The Physics of Liquid Crystals*, International Series of Monographs on Physics (Clarendon Press, 1993) (cited on pages 19–20, 24–25, 77).

[47] K. Huang, *Statistical mechanics*, 2nd edition (Wiley, 1987) (cited on page 21).

[48] C. Domb and M. S. Green, 1st edition, Vol. 6, Phase Transitions and Critical Phenomena (Academic Press Inc., 1976) (cited on page 21).

[49] L. Landau and E. Lifshitz, *Statistical physics*, 1st edition, Vol. 5, Course of Theoretical Physics (Elsevier Science, 1980) (cited on page 23).

[50] P. G. de Gennes, "Short range order effects in the isotropic phase of nematics and cholesterics", Mol. Cryst. Liq. Cryst. **12**, 193 (1971) (cited on page 23).

[51] L. Onsager, "The effects of shape on the interaction of colloidal particles", Ann. NY Acad. Sci., 627 (1949) (cited on page 23).

[52] T. Stoebe, P. Mach, and C. C. Huang, "Unusual Layer-Thinning Transition Observed near the Smectic-*A*-Isotropic Transition in Free-Standing Liquid-Crystal Films", Phys. Rev. Lett. **73**, 1384 (1994) (cited on pages 25, 30, 58, 62).

[53] S. Pankratz, P. M. Johnson, R. Hołyst, and C. C. Huang, "Thinning transitions in free-standing liquid-crystal films as the successive formation of dislocation loops", Phys. Rev. E **60**, R2456 (1999) (cited on page 25).

[54] P. M. Johnson, P. Mach, E. D. Wedell, F. Lintgen, M. Neubert, and C. C. Huang, "Layer thinning transition above the bulk smectic-a–isotropic transition in free-standing liquid-crystal films", Phys. Rev. E **55**, 4386 (1997) (cited on page 25).

[55] M. V. Mirantsev, "Theoretical description of layer-thinning transitions in free-standing smectic-A films", Phys. Lett. A **205**, 412 (1995) (cited on pages 25, 62, 66).

[56] L. V. Mirantsev, "Influence of external field on layer-thinning transitions in free-standing smectic-a films", Phys. Rev. E **55**, 4816 (1997) (cited on page 25).

[57] A. A. Canabarro, I. N. de Oliveira, and M. L. Lyra, "Homeotropic surface anchoring and the layer-thinning transition in free-standing films", Phys. Rev. E **77**, 011704 (2008) (cited on page 25).

[58] D. Brisbin, D. L. Johnson, H. Fellner, and M. E. Neubert, "Universality of Phase Diagrams near the Nematic, Smectic-*A*, Smectic-*C* Multicritical Point", Phys. Rev. Lett. **50**, 178 (1983) (cited on pages 26, 32).

[59] R. Shashidhar, B. R. Ratna, and S. K. Prasad, "Nematic-Smectic-*A*-Smectic-*C* Multi-critical Point in a Single-Component System", Phys. Rev. Lett. **53**, 2141 (1984) (cited on pages 26, 32).

[60] S. Chandrasekhar, *Liquid crystals*, 2nd edition (Cambridge University Press, 1992) (cited on page 26).

[61] C. Mauguin, "Orientation of liquid crystals by mica sheets", CR Acad. Sci. Paris **156**, 1246 (1913) (cited on page 27).

[62] J. L. Janning, "Thin film surface orientation for liquid crystals", Appl. Phys. Lett. **21**, 173 (1972) (cited on page 28).

[63] S. Singh, "Phase transitions in liquid crystals", Phys. Rep. **324**, 107 (2000) (cited on page 29).

[64] Y. Ouchi, J. Lee, H. Takezoe, A. Fukuda, K. Kondo, T. Kitamura, and A. Mukoh, "Smectic layer structure of thin ferroelectric liquid crystal cells aligned by SiO oblique evaporation technique", Jpn. J. Appl. Phys. **27**, L1993 (1988) (cited on page 29).

[65] Y. Ouchi, J. Lee, H. Takezoe, A. Fukuda, K. Kondo, T. Kitamura, and A. Mukoh, "Smectic c* chevron layer structure studied by x-ray diffraction", Jpn. J. Appl. Phys. **27**, L725 (1988) (cited on page 29).

[66] R. Lucht, C. Bahr, G. Heppke, and J. W. Goodby, "Variety of wetting behaviors at the free surface of isotropic liquid crystals", J. Chem. Phys. **108**, 3716 (1998) (cited on page 30).

[67] R. Lucht and C. Bahr, "Wetting phenomena at the free surface of the isotropic phase of a smectic liquid crystal", Phys. Rev. Lett. **78**, 3487 (1997) (cited on page 30).

[68] J. Als-Nielsen, F. Christensen, and P. S. Pershan, "Smectic-*A* Order at the Surface of a Nematic Liquid Crystal: Synchrotron X-Ray Diffraction", Phys. Rev. Lett. **48**, 1107 (1982) (cited on pages 30, 58).

[69] F. Batalioto, L. Evangelista, and G. Barbero, "Effect of the incomplete interaction on the nematic–isotropic transition at the nematic–wall interface", Phys. Lett. A **324**, 198 (2004) (cited on page 30).

[70] L. R. E. G. Barbero, "Local self-consistent approach to the phase transition at the nematic liquid-crystal-wall interface", Phys. Rev. E **65**, 031708 (2002) (cited on page 30).

[71] Z. Pawlowska, G. F. Kventsel, and T. J. Sluckin, "Theory of smectic wetting and layering", Phys. Rev. A **36**, 992 (1987) (cited on page 30).

[72] J. V. Selinger and D. R. Nelson, "Density-functional theory of nematic and smectic-A order near surfaces", Phys. Rev. A **37**, 1988 (1736) (cited on pages 30, 68).

[73] A. A. Sonin, *The surface physics of liquid crystals*, 1st edition (Gordon and Breach, 1995) (cited on page 30).

[74] S. Kumar, "High-resolution x-ray measurements of the smectic phases of terephthal-bis-(4n)-alkylanilines", Phys. Rev. A **23**, 3207 (1981) (cited on pages 32, 55–56).

[75] J. Morikawa, T. Hashimoto, A. Kishi, Y. Shinoda, K. Ema, and H. Takezoe, "Critical anomalies in thermal diffusivity of liquid-crystalline terephthal-bis-(4-*n*-butylaniline)", Phys. Rev. E **87**, 022501 (2013) (cited on pages 32, 58).

[76] S. Heinekamp, R. A. Pelcovits, E. Fontes, E. Y. Chen, R. Pindak, and R. B. Meyer, "Smectic-C^* to Smectic-A Transition in Variable-Thickness Liquid-Crystal Films: Order-Parameter Measurements and Theory", Phys. Rev. Lett. **52**, 1017 (1984) (cited on pages 32, 58, 69–70).

[77] C. C. Huang and J. M. Viner, "Nature of the smectic-A–smectic-C phase transition in liquid crystals", Phys. Rev. A **25**, 3385 (1982) (cited on page 32).

[78] C. Y. Chao, C. R. Lo, P. J. Wu, Y. H. Liu, D. R. Link, J. E. Maclennan, N. A. Clark, M. Veum, C. C. Huang, and J. T. Ho, "Unusual Thickness-Dependent Thermal Behavior and Anticlinic Coupling in Chiral Smectic Free-Standing Liquid-Crystal Films", Phys. Rev. Lett. **86**, 4048 (2001) (cited on pages 32, 58–59).

[79] T. Stoebe, L. Reed, M. Veum, and C. C. Huang, "Nature of the smectic-A –smectic-C transition of a partially perfluorinated compound", Phys. Rev. E **54**, 1584 (1996) (cited on pages 32, 58).

[80] K. Ema and H. Yao, "Crossover from XY critical to tricritical behavior of heat capacity at the smectic-A–chiral-smectic-C liquid-crystal transition", Phys. Rev. E **57**, 6677 (1998) (cited on pages 32, 58).

[81] C.-Y. Chao, S. W. Hui, and J. T. Ho, "Layer-Dependent Surface-Induced Tilt, Hexatic, and Positional Orders in Free-Standing 7O.7 Films", Phys. Rev. Lett. **78**, 4962 (1997) (cited on pages 32, 58–59, 90).

[82] M. R. M, K. P. Zuhail, A. Roy, and S. Dhara, "$N-\mathrm{Sm}A-\mathrm{Sm}C$ phase transitions probed by a pair of elastically bound colloids", Phys. Rev. E **97**, 032702 (2018) (cited on page 32).

[83] C. C. Huang and S. C. Lien, "Effect of the smectic-A temperature range on the behavior of the smectic-A–smectic-C (or –chiral-smectic-C) transition", Phys. Rev. A **31**, 2621 (1985) (cited on page 32).

[84] C. Bahr and D. Fliegner, "Behavior of a first-order smectic-A–smectic-C transition in free-standing liquid-crystal films", Phys. Rev. A **46**, 7657 (1992) (cited on pages 32, 58–59).

[85] L. Reed, T. Stoebe, and C. C. Huang, "Critical fluctuations near the smectic-A–smectic-C transition of a partially perfluorinated compound", Phys. Rev. E **52**, R2157 (1995) (cited on pages 32, 70).

[86] H. Y. Liu, C. C. Huang, T. Min, M. D. Wand, D. M. Walba, N. A. Clark, C. Bahr, and
      G. Heppke, "Effect of the transverse dipole moment on the smectic-A–smectic-C (or
      –chiral-smectic-C) transition", Phys. Rev. A **40**, 6759 (1989) (cited on page 32).

[87] R. G. Priest, "Molecular statistical model of the smectic A and smectic C phases", J.
      Chem. Phys. **65**, 408 (1976) (cited on page 32).

[88] F. Gieβelmann and P. Zugenmaier, "Molecular-statistical description of the smectic-A–
      smectic-C phase transition", Phys. Rev. E **55**, 5613 (1997) (cited on page 32).

[89] A. S. Govind and N. V. Madhusudana, "A molecular theory of smectic C liquid crystals
      made of rod-like molecules", Eur. Phys. J. E **9**, 107 (2002) (cited on pages 32–33,
      43–44, 47–49, 57, 79).

[90] K. Saunders, "de Vries behavior in smectic liquid crystals near a biaxiality-induced
      smectic-*A*–smectic-*C* tricritical point", Phys. Rev. E **77**, 061708 (2008) (cited on
      pages 32, 71).

[91] M. Osipov and G. Pająk, "Molecular theory of the tilting transition in smectic liquid
      crystals with weak layer contraction and diffused cone orientational distribution", Phys.
      Rev. E **85**, 021701 (2012) (cited on pages 32–33).

[92] G. Pajak and M. A. Osipov, "Unified molecular field theory of nematic, smectic-*A*, and
      smectic-*C* phases", Phys. Rev. E **88**, 012507 (2013) (cited on pages 32–33).

[93] A. V. Emelyanenko and A. R. Khokhlov, "Simple theory of transition between smectic,
      nematic, and isotropic phases", J. Chem. Phys. **142**, 204905 (2015) (cited on page 32).

[94] M. V. Gorkunov, M. A. Osipov, J. P. F. Lagerwall, and F. Giesselmann, "Order-disorder
      molecular model of the smectic-*A*–smectic-*C* phase transition in materials with conven-
      tional and anomalously weak layer contraction", Phys. Rev. E **76**, 051706 (2007) (cited
      on page 33).

[95] M. V. Gorkunov and M. A. Osipov, "Molecular theory of layer contraction in smectic
      liquid crystals", J. Phys.: Condens. Matter **20**, 465101 (2008) (cited on page 33).

[96] M. V. Gorkunov, F. Giesselmann, J. P. F. Lagerwall, T. J. Sluckin, and M. A. Osipov,
      "Molecular model for de Vries type smectic-*A*–smectic-*C* phase transition in liquid crys-
      tals", Phys. Rev. E **75**, 060701(R) (2007) (cited on page 33).

[97] P. O. Andreeva, V. K. Dolganov, C. Gors, R. Fouret, and E. I. Kats, "Nonchiral ferro-
      electric smectic-C films", JETP Lett. **67**, 856 (1998) (cited on page 53).

[98] N. Kapernaum, C. S. Hartley, J. C. Roberts, F. Schoerg, D. Krueerke, R. P. Lemieux, and
      F. Giesselmann, "Systematic Variation of Length Ratio and the Formation of Smectic A
      and Smectic C Phases", ChemPhysChem **11**, 2099 (2010) (cited on pages 55–56).

[99] W. L. McMillan, "Simple Molecular Model for the Smectic *A* Phase of Liquid Crystals",
      Phys. Rev. A **4**, 1238 (1971) (cited on page 56).

[100] C. W. Garland and G. Nounesis, "Critical behavior at nematic–smectic-A phase transitions", Phys. Rev. E **49**, 2964 (1994) (cited on page 58).

[101] T. Jin, G. P. Crawford, R. J. Crawford, S. Zumer, and D. Finotello, "Surface Ordering Transitions at a Liquid Crystal–Solid Interface above the Isotropic Smectic-*A* Transition", Phys. Rev. Lett. **90**, 015504 (2003) (cited on page 58).

[102] L. D. Pan, B. K. McCoy, S. Wang, W. Weissflog, and C. C. Huang, "Surface and Bulk Uniaxial to Biaxial Smectic-*A* Transition in a Bent Core Liquid Crystal", Phys. Rev. Lett. **105**, 117802 (2010) (cited on page 58).

[103] R. Geer, T. Stoebe, and C. C. Huang, "Thickness dependence of the interior smectic-A–hexatic-B transition temperatures in liquid-crystal films", Phys Rev B **45**, 13055 (1992) (cited on page 58).

[104] Z. Li and O. D. Lavrentovich, "Surface Anchoring and Growth Pattern of the Field-Driven First-Order Transition in a Smectic-*A* Liquid Crystal", Phys. Rev. Lett. **73**, 280 (1994) (cited on page 58).

[105] M. S. S. Pereira, M. L. Lyra, and I. N. de Oliveira, "Field-Induced Layer Thinning Transition on Free-Standing Smectic Films", Phys. Rev. Lett. **103**, 177801 (2009) (cited on page 58).

[106] O. Francescangeli, F. Vita, F. Fauth, and E. T. Samulski, "Extraordinary Magnetic Field Effect in Bent-Core Liquid Crystals", Phys. Rev. Lett. **107**, 207801 (2011) (cited on page 58).

[107] W. H. de Jeu, B. I. Ostrovskii, and A. N. Shalaginov, "Structure and fluctuations of smectic membranes", Rev. Mod. Phys. **75**, 181 (2003) (cited on page 58).

[108] R. Hołyst, D. J. Tweet, and L. B. Sorensen, "Fluctuations in thin smectic-a films", Phys. Rev. Lett. **65**, 2153 (1990) (cited on page 58).

[109] C. Barh, "Influence of dimensionality and surface ordering on phase transitions: studies of freely-suspended liquid-crystal films", Int. J. Mod. Phys. B **8**, 3051 (1994) (cited on pages 58, 62).

[110] F. Bougrioua, P. Cluzeau, P. Dolganov, G. Joly, H. T. Nguyen, and V. Dolganov, "Light-Induced Layer by Layer Thickening in Photosensitive Liquid Crystal Membranes", Phys. Rev. Lett. **95**, 027802 (2005) (cited on page 58).

[111] E. S. Pikina, B. I. Ostrovskii, and W. H. de Jeu, "Thinning and thickening of free-standing smectic films revisited", Eur. Phys. J. E **38**, 13 (2015) (cited on page 58).

[112] Z. H. Nguyen, M. Atkinson, C. S. Park, J. Maclennan, M. Glaser, and N. Clark, "Crossover between 2D and 3D Fluid Dynamics in the Diffusion of Islands in Ultrathin Freely Suspended Smectic Films", Phys. Rev. Lett. **105**, 268304 (2010) (cited on page 58).

[113] V. K. Dolganov, E. I. Demikhov, R. Fouret, and C. Gors, "Surface ordering near the smectic-A-smectic-C transition in thin, free-standing, liquid-crystal films", J. Exp. Theor. Phys. **84**, 522 (1997) (cited on page 58).

[114] M. S. Spector, P. A. Heiney, J. Naciri, B. T. Weslowski, D. B. Holt, and R. Shashidhar, "Electroclinic liquid crystals with large induced tilt angle and small layer contraction", Phys. Rev. E **61**, 1579 (2000) (cited on pages 58, 78, 84).

[115] A. Fera, R. Opitz, W. H. de Jeu, B. I. Ostrovskii, D. Schlauf, and C. Bahr, "Structure of freely suspended chiral smectic films as determined by x-ray reflectivity and optical ellipsometry", Phys. Rev. E **64**, 021702 (2001) (cited on pages 58–59, 68).

[116] I. Kraus, P. Pieranski, E. Demikhov, H. Stegemeyer, and J. Goodby, "Destruction of a first-order smectic-A→smectic-C^* phase transition by dimensional crossover in free-standing films", Phys. Rev. E **48**, 1916 (1993) (cited on pages 58–59, 90).

[117] C. Y. Young, R. Pindak, N. A. Clark, and R. B. Meyer, "Light-Scattering Study of Two-Dimensional Molecular-Orientation Fluctuations in a Freely Suspended Ferroelectric Liquid-Crystal Film", Phys. Rev. Lett. **40**, 773 (1978) (cited on page 59).

[118] P. Pieranski, L. Beliard, J.-P. Tournellec, X. Leoncini, C. Furtlehner, H. Dumoulin, E. Riou, B. Jouvin, J.-P. Fénerol, P. Palaric, J. Heuving, B. Cartier, and I. Kraus, "Physics of smectic membranes", Physica A **194**, 364 (1993) (cited on pages 59, 61–62).

[119] E. B. Sirota, P. S. Pershan, L. B. Sorensen, and J. Collett, "X-ray and optical studies of the thickness dependence of the phase diagram of liquid-crystal films", Phys. Rev. A **36**, 2890 (1987) (cited on page 60).

[120] P. Mach, C. C. Huang, T. Stoebe, E. D. Wedell, T. Nguyen, W. H. de Jeu, F. Guittard, J. Naciri, R. Shashidhar, N. Clark, I. M. Jiang, F. J. Kao, H. Liu, and H. Nohira, "Surface tension obtained from various smectic free-standing films: the molecular origin of surface tension", Langmuir **14**, 4330 (1998) (cited on page 62).

[121] T. Stoebe, P. Mach, S. Grantz, and C. C. Huang, "Surface tension of freestanding partially fluorinated liquid-crystal films", Phys. Rev. E **53**, 1662 (1996) (cited on page 62).

[122] W. H. De Jeu, A. Fera, and B. I. Ostrovskii, "Thickening of a smectic membrane in an evanescent X-ray beam", Eur. Phys. J. E **15**, 61 (2004) (cited on page 62).

[123] D. J. Tweet, R. Hołyst, B. D. Swanson, H. Stragier, and L. B. Sorensen, "X-ray determination of the molecular tilt and layer fluctuation profiles of freely suspended liquid-crystal films", Phys. Rev. Lett. **65**, 2157 (1990) (cited on pages 68–70).

[124] C. Bahr, C. J. Booth, D. Fliegner, and J. W. Goodby, "Behavior of a surface phase transition in freely suspended liquid-crystal films", Phys. Rev. E **52**, R4612 (1995) (cited on page 68).

[125] P. O. Andreeva, V. K. Dolganov, C. Gors, R. Fouret, and E. I. Kats, "Polarization in free standing chiral and nonchiral smectic films", Phys. Rev. E **59**, 4143 (1999) (cited on pages 69–70).

[126] D. Schlauf, C. Bahr, and C. C. Huang, "Ellipsometric study of freely suspended smectic films of a partially fluorinated compound", Phys. Rev. E **55**, R4885 (1997) (cited on page 69).

[127] C. Rosenblatt, "Magnetically induced nematic-smectic A tricritical point", J. Physique Lett. **42**, 9 (1981) (cited on page 77).

[128] C. Rosenblatt, "Magnetically induced nematic phase at a smectic A-isotropic transition", Phys. Lett. A **83**, 221 (1981) (cited on page 77).

[129] H. Hama, "Effects of a Magnetic Field on the Nematic-Smectic A Transition in Liquid Crystals", J. Phys. Soc. Jpn. **54**, 2204 (1985) (cited on page 77).

[130] I. Lelidis, M. Nobili, and G. Durand, "Electric-field-induced change of the order parameter in a nematic liquid crystal", Phys. Rev. E **48**, 3818 (1993) (cited on page 77).

[131] I. Lelidis and G. Durand, "Electric-field-induced isotropic-nematic phase transition", Phys. Rev. E **48**, 3822 (1993) (cited on page 77).

[132] I. Lelidis and G. Durand, "Electrically Induced Isotropic-Nematic-Smectic-*A* Phase Transitions in Thermotropic Liquid Crystals", Phys. Rev. Lett. **73**, 672 (1994) (cited on page 77).

[133] A. Mochizuki, "Molecular tilting effect on smectic liquid crystal sub-phase stability from its retardation switching behavior", J. Mol. Liq. **267**, 456 (2018) (cited on page 77).

[134] L. Sirleto, G. Coppola, A. D'Agata, G. Breglio, and A. Cutolo, "Optoelectronic switch and continuously tunable filter based on a liquid crystal waveguide", in Integrated optics devices v, Vol. 4277 (International Society for Optics and Photonics, 2001), page 320 (cited on page 77).

[135] R. Cassano, R. Dąbrowski, J. Dziaduszek, S. Trombino, F. Iemma, F. P. Nicoletta, G. D. Filpo, and N. Picci, "New ferroelectric liquid crystals for high-performance optical devices", Liq. Cryst. **35**, 625 (2008) (cited on page 77).

[136] A. Nagai, H. Kondo, Y. Miwa, T. Kondo, S. Kutsumizu, Y. Yamamura, and K. Saito, "Optical switching between liquid-crystalline assemblies with different structural symmetries and molecular orders", B. Chem. Soc. Jpn. **91**, 1652 (2018) (cited on page 77).

[137] V. G. Guimarães, J. Wang, S. Planitzer, K. Fodor-Csorba, R. S. Zola, and A. Jákli, "Fast electro-optical switching of dichroic dye-doped antiferroelectric liquid crystals without polarizers", Phys. Rev. Appl. **10**, 064008 (2018) (cited on page 77).

[138] L. Sirleto, G. Coppola, G. C. Righini, and G. Abbate, "Photonics devices based on hybrid approach combining liquid crystals and sol-gel waveguides", Fiber Integrated Opt. **25**, 175 (2006) (cited on page 77).

[139] I. Khoo and S. Wu, *Optics and nonlinear optics of liquid crystals* (World Scientific, 1993) (cited on page 77).

[140] T. Ostapenko, D. B. Wiant, S. N. Sprunt, A. Jákli, and J. T. Gleeson, "Magnetic-Field Induced Isotropic to Nematic Liquid Crystal Phase Transition", Phys. Rev. Lett. **101**, 247801 (2008) (cited on page 77).

[141] I. Lelidis, "Experimental Evidence of the Halperin-Lubensky-Ma Effect in Liquid Crystals", Phys. Rev. Lett. **86**, 1267 (2001) (cited on pages 77, 84).

[142] B. Wen and C. Rosenblatt, "First-Order Fréedericksz Transition Above the Nematic–Smectic-*A* Phase Transition", Phys. Rev. Lett. **89**, 195505 (2002) (cited on page 77).

[143] A. Rapini, "Instabilités magnétiques d'un smectique C", J. Phys. France **33**, 237 (1972) (cited on page 77).

[144] R. B. Meyer, L. Liebert, L. Strzelecki, and P. Keller, "Ferroelectric liquid crystals", J. Physique Lett. **36**, 69 (1975) (cited on page 77).

[145] R. B. Meyer, "Ferroelectric liquid crystals; a review", Mol. Cryst. Liq. Cryst. **40**, 33 (1977) (cited on page 77).

[146] S. T. Lagerwall and I. Dahl, "Ferroelectric liquid crystals", Mol. Cryst. Liq. Cryst. **114**, 151 (1984) (cited on page 77).

[147] L. A. Beresnev, L. M. Blinov, M. A. Osipov, and S. A. Pikin, "Ferroelectric liquid crystals", Molecular Crystals and Liquid Crystals Incorporating Nonlinear Optics **158**, 1 (1988) (cited on page 77).

[148] F. Tournilhac, L. M. Blinov, J. Simon, and S. V. Yablonsky, "Ferroelectric liquid crystals from achiral molecules", Nature **359**, 621 (1992) (cited on page 77).

[149] T. Niori, T. Sekine, J. Watanabe, T. Furukawa, and H. Takezoe, "Distinct ferroelectric smectic liquid crystals consisting of banana shaped achiral molecules", J. Mater. Chem. **6**, 1231 (1996) (cited on page 77).

[150] M. Hird, "Ferroelectricity in liquid crystals—materials, properties and applications", Liq. Cryst. **38**, 1467 (2011) (cited on page 77).

[151] S. T. Lagerwall, "Ferroelectric and antiferroelectric liquid crystals", Ferroelectrics **301**, 15 (2004) (cited on page 77).

[152] S. Garoff and R. B. Meyer, "Electroclinic effect at the $A-C$ phase change in a chiral smectic liquid crystal", Phys. Rev. A **19**, 338 (1979) (cited on pages 78, 84).

[153] S.-D. Lee and J. S. Patel, "Nonlinear behavior of the field-induced molecular tilt near the smectic A-C* transition", Appl. Phys. Lett. **54**, 1653 (1989) (cited on pages 78, 84).

[154] K. Skarp, G. Andersson, T. Hirai, A. Yoshizawa, K. Hiraoka, H. Takezoe, and A. Fukuda, "Investigations of Soft-Mode and Electroclinic Response in a Ferroelectric Liquid Crystal with Ps≈5 mC/m2", Jpn. J. Appl. Phys. **31**, 1409 (1992) (cited on pages 78, 84).

[155] E. Meirovitch, Z. Luz, and S. Alexander, "Magnetic instabilities of smectic-*C* liquid crystals", Phys. Rev. A **15**, 408 (1977) (cited on page 78).

[156] P. Schiller and G. Pelzl, "Discontinuous Freedericksz transition in the smectic C phase", Crystal Res. Technol. **18**, 923 (1983) (cited on page 78).

[157] G. Pelzl, P. Schiller, and D. Demus, "Freedericksz transition of planar oriented smectic C phases", Liq. Cryst. **2**, 131 (1987) (cited on page 78).

[158] E. Meirovitch, Z. Luz, and S. Alexander, "Magnetic instabilities of smectic C liquid crystals studied by electron spin resonance spectroscopy", Mol. Phys. **37**, 1489 (1979) (cited on page 78).

SURFACE AND FINITE-SIZE EFFECTS ON N–SM-A–SM-C PHASE TRANSITIONS IN FREE-STANDING FILMS

Surface and finite-size effects on $N-$Sm-$A-$Sm-C phase transitions in free-standing films

E. J. L. de Oliveira [ORCID],[1] D. C. S. de Melo,[1] Maria S. S. Pereira,[1] L. R. Evangelista,[2] and I. N. de Oliveira [ORCID][1]

[1]*Instituto de Física, Universidade Federal de Alagoas 57072-970 Maceió-AL, Brazil*
[2]*Departamento de Física, Universidade Estadual de Maringá 87020-900 Maringá-PR, Brazil*

The present study is devoted to the investigation of surface anchoring and finite-size effects on nematic–smectic-A–smectic-C ($N-$Sm-$A-$Sm-C) phase transitions in free-standing films. Using an extended version of the molecular theory for smectic-C liquid crystals, we analyze how surface anchoring and film thickness affect the thermal behavior of the order parameters in free-standing smectic films. In particular, we determine how the transition temperature depends on the surface ordering and film thickness. We show that the additional orientational order imposed by the surface anchoring may lead to a stabilization of order parameters in central layers, thus modifying the nature of the phase transitions. We compare our results with experimental findings for typical thermotropic compounds presenting a $N-$Sm-$A-$Sm-C phase sequence.

I. INTRODUCTION

The comprehension of phase transitions involving smectic liquid crystals is a long standing issue. In these systems, a very rich phenomenology can be observed due to the interplay of anisotropic critical behavior [1,2], surface ordering [3–5], finite-size effects [6,7], and external fields [8–10]. In particular, smectic samples have a unique ability of forming freely suspended films, also termed as free-standing films, which correspond to a stack of smectic layers confined in a surrounding gas [11]. Due to the absence of a solid substrate, the equilibrium configuration is determined by the film holder, with the surface tension reducing the thermal fluctuations at the film surface [12]. In fact, surface anchoring conditions at the gas/film interface can lead to the stabilization of the smectic ordering even above the bulk transition temperatures [13]. As a consequence, a large variety of unusual physical phenomena can be observed in free-standing smectic films, such as layer thinning and thickening transitions [14–16], anomalies on the specific heat [2,17,18], thickness dependence of the transition temperature [6], as well as surface-induced biaxiliaty [5]. Since the film thickness can vary from a few nanometers to several micrometers, free-standing films constitute a suitable experimental setup for understanding how changes in the system dimensionality affect the thermodynamic behavior of the smectic phase [13,19].

Over the past decades, a remarkable amount of interest has been devoted to phase transitions involving smectic liquid crystals with a tilted molecular alignment [2,7,17,18,20–25]. Different experimental techniques have been employed to determine the nature of smectic-$C-$smectic-A (Sm-$C-$Sm-A) and smectic-$C-$nematic (Sm-$C-N$) phase transitions [17,20–23,26–29]. In rodlike compounds presenting a small or moderate transverse dipole moment ($P \leqslant 20$ nC/cm^2), it has been verified that the Sm-$C-$Sm-A phase transition has a second-order character [20,22], while the Sm-$C-N$ phase

transition exhibits a first-order behavior with a small latent heat [20]. Moreover, the analysis of heat-capacity measurements in several compounds revealed that the temperature range of the Sm-A phase plays an important role to the behavior of continuous Sm-$C-$Sm-A phase transition [26], delimiting the crossover between the mean-field tricritical and the ordinary mean-field character of this transition [17]. However, a first-order Sm-$C-$Sm-A phase transition has been reported in smectogenic compounds presenting a large transverse dipole moment ($P > 50$ nC/cm^2) [27], with a large Sm-A temperature range [17]. Besides, a nematic–smectic-A–smectic-C ($N-$Sm-$A-$Sm-C) multicritical point has been reported in binary liquid-crystal mixtures [30], as well as in single component systems under high pressures [23].

Motivated by the rich phenomenology observed in the experimental results, several theoretical studies have been performed to better describe transitions involving Sm-C liquid-crystal phase [31–38]. In fact, a large variety of microscopic models have been introduced to characterize intermolecular interactions in smectogenic systems. Assuming a bilinear mean-field potential for the tilt angle distribution, Gieβelman and Zugenmeier provided an equation of state for the Sm-C phase [32], consisting in a Langevin function of the reduced tilt angle and the reduced temperature. Despite the good description of the temperature dependence of tilt angle, such an oversimplified model cannot reproduce the variety of experimental phase diagrams. Considering a system of rodlike molecules with a perfect orientational order, van deer Meer and Vertogen analyzed how a dipole-induced interaction leads to the emergence of a tilted smectic phase [39], in which the Sm-$C-$Sm-A transition does not correspond to the usual order-disorder type. Based on molecular interactions between rodlike molecules with off-axis dipoles, Govind and Madhusudana have developed a modified version of McMillan's model for Sm-A–N-Iso

systems, being successful in the description of experimental phase diagrams presenting the Sm-*C* phase [33,34]. However, such a model requires the introduction of an excluded-volume contribution to stabilize the Sm-*A* phase, thus leading to a large number of free parameters. Using a complete set of orientational- and translational-order parameters, recent studies have introduced different pair-interaction potentials for polar and nonpolar molecules, to reproduce phase diagrams containing conventional or "de Vries-type" Sm-*C* phases [36,37,40–42]. Nevertheless, the use of a complete set of order parameters implies a large number of free parameters in these molecular models, making difficult their comparison with the typical characteristic of liquid-crystalline compounds.

Tilting transitions in free-standing smectic films may exhibit a distinct behavior in relation to those observed in bulk systems [7,21,24,27,43–46]. In fact, surface anchoring conditions and finite size effects tend to affect the thermal behavior of orientational- and translational-order parameters in thin free-standing smectic films. From monitoring the transmittance of such systems close to a second-order Sm-*C*−Sm-*A* phase transition, an unusual thickness dependence has been reported for the thermal behavior of the average tilt angle [21], with the transition temperature in thin films being higher than that of a bulk system. Optical ellipsometry measurements have revealed that a finite average tilt may remain in the surface layers of free-standing films, well above the bulk transition temperature [27]. Such a scenario has been supported by electron diffraction measurements in thin film [24], where a surface-induced phase sequence is identified. Moreover, surface-effects may lead to changes in the nature of Sm-*C*−Sm-*A* phase transition [27,46], especially in films with a few layers. For compounds presenting a first-order Sm-*C*−Sm-*A* bulk phase transition, the discontinuous jump in the tilt angle is replaced by a continuous behavior at the transition temperature, when the film thickness is lower than a characteristic thickness [27,46]. Furthermore, surface anchoring and finite size effects give rise to a nonuniform tilt profile in free-standing Sm-*C* films [45], with the outermost layers being more tilted than the inner layers. In chiral smectic samples, a series of discrete transitions has been reported [7], where a reentrant synclinic-anticlinic-synclinic ordering sequence takes place at the surface film in the presence of an external electric field.

Although several studies have been devoted to the theoretical description of phase transitions in bulk Sm-*C* systems, microscopic models for free-standing films have not been exploited so far. In the present study, we investigate *N*−Sm-*A*−Sm-*C* phase transitions by using an extended version of the mean-field theory for Sm-*C* liquid crystals. We analyze how the interplay of surface anchoring and finite size effects affect the thermal behavior of the order parameters in free-standing smectic films. In particular, we show that the additional orientational order imposed by the surface anchoring may lead to a stabilization of order parameters in central layers, thus modifying the nature of the phase transitions. We compare our results with experimental findings for typical thermotropic compounds presenting a *N*−Sm-*A*−Sm-*C* phase sequence.
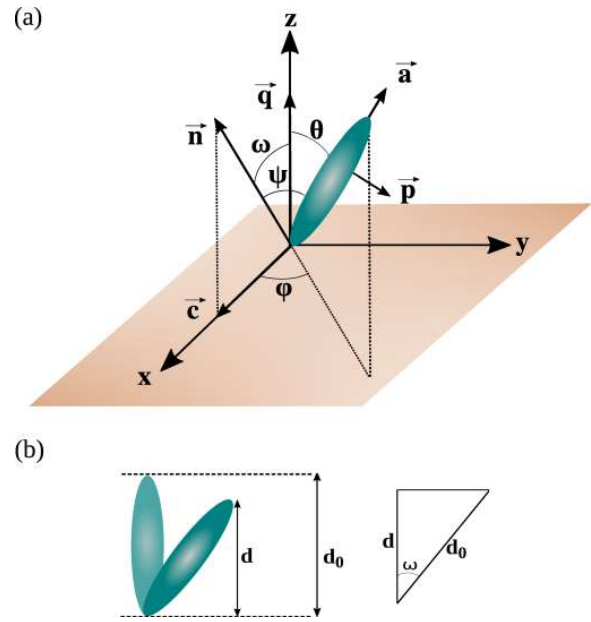
FIG. 1. (a) Schematic representation of the long molecular axis $\vec{a}$ in the Sm-*C* phase, for a Cartesian coordinate system with the *z* axis being normal to the smectic layer plane. For convenience, we assume that the director $\vec{n}$ is restricted to the *z*-*x* plane, defined as the tilt plane. Here, the vector $\vec{c}$ corresponds to the projection of the director in the *x* axis, while ω represents the tilt angle of the director $\vec{n}$ in relation to the smectic wave vector $\vec{q}$. The orientation of the long molecular axis is defined by polar and azimuthal angles θ and ϕ, respectively. ψ is the relative angle between the long molecular axis $\vec{a}$ and director $\vec{n}$. (b) Representation of the layer contraction induced by the molecular tilt, with d_0 being the layer spacing in the Sm-*A* phase.

II. MICROSCOPIC MODEL FOR BULK TRANSITIONS

We investigate a single component smectogenic system of rodlike molecules with a small or moderate transverse dipole moment [34], which presents a layer contraction in the tilted smectic phase. To characterize the average molecular orientation inside the smectic layers, we consider the relative orientation of the director $\vec{n}$ ($|\vec{n}| = 1$) and the smectic wave vector $\vec{q}$, which is represented by average tilt angle ω, as shown in Fig. 1(a), where $\vec{q}$ is assumed to be normal to the smectic layer plane (*x*-*y* plane), with a magnitude depending on the layer spacing *d* ($|\vec{q}| = 2\pi/d$). Moreover, we assume that the director $\vec{n}$ is fixed at the *z*-*x* plane for convenience. Considering the Cartesian coordinate system where the *z* axis is parallel to $\vec{q}$, the orientation of the molecular long axis $\vec{a}$ is defined in terms of polar and azimuthal angles θ and ϕ, respectively. Besides, the orientation of molecular long axis in relation to the director is represented by the angle ψ, which satisfies the relation

$$\cos \psi = \cos \theta \cos \omega + \sin \theta \sin \omega \sin \phi. \tag{1}$$

In what follows, we assume that the average tilt direction is the same for all smectic layers and the molecular centers are randomly distributed inside the smectic layers. Furthermore,

we consider that a nonnull average tilt leads to a contraction of the layer spacing, being defined by $d = d_0 \cos \omega$, with d_0 denoting the layer spacing in the Sm-A phase, as represented in Fig. 1(b).

Using Govind and Madhusudana's approach [33,34], we consider a single-particle mean-field potential that corresponds to an extension of McMillan's model with the inclusion of a tilting term, written as

$$V = - V_0 \left\{ \left[s + \alpha \sigma \cos \left(\frac{2\pi z}{d} \right) \right] P_2(\cos \psi) \right.$$
$$\left. + \alpha \beta \sigma^2 \eta \sin 2\theta \cos \phi \right\}. \quad (2)$$

In Eq. (2), V_0 is a typical interaction energy that determines the scale of the nematic-isotropic transition temperature of bulk sample; $P_2(\cos \psi)$ is the second-order Legendre polynomial, with ψ being the angle between the molecular long axis and the director $\vec{n}$; s, σ and η are orientational, translational and tilt-order parameters, respectively, and β is a constant associated with the geometrical arrangement and amplitude of the dipoles in rodlike molecules. The quantity α is given by

$$\alpha = 2 \left(\frac{\alpha_0}{2} \right)^{\sec^2 \omega}, \quad (3)$$

in which α_0 is the geometric parameter related to the length of alkyl chains of rodlike molecules, through the expression $\alpha_0 = 2 \exp[-(\pi r_0 / d)^2]$, with r_0 being a characteristic length associated with the molecular rigid part.

The order parameters s, σ, and η are defined by

$$s = \langle P_2(\cos \psi) \rangle, \quad (4)$$

$$\sigma = \langle P_2(\cos \psi) \cos(2\pi z/d) \rangle, \quad (5)$$

and

$$\eta = \langle \sin(2\theta) \cos \phi \rangle. \quad (6)$$

The thermodynamical averages, $\langle \cdots \rangle$, are computed from the one-particle distribution function, that is,

$$\mathcal{Z}(z, \theta, \phi) \propto \exp[-V/k_B T], \quad (7)$$

in which k_B is the Boltzmann constant and T is the temperature. The equilibrium order parameters are solutions of the self-consistent equations, corresponding to the extreme values of the Helmholtz free energy, given by

$$\frac{F}{N_0 V_0} = \frac{1}{2} (s^2 + \alpha \sigma^2 + \alpha \beta \sigma^2 \eta^2)$$
$$- \frac{k_B T}{V_0} \ln \left[\frac{1}{2\pi d} \int_{-1}^{1} d\cos(\theta) \int_0^\pi d\phi \int_0^d dz \mathcal{Z} \right], \quad (8)$$

where N_0 is the number of molecules. The equilibrium state is determined from the global minimum of the Helmholtz free energy. The solutions corresponding to the different phases are

(1) $s = \sigma = \eta = 0 \rightarrow$ Isotropic;
(2) $s \neq 0$ and $\sigma = \eta = 0 \rightarrow$ Nematic;
(3) $s \neq 0$, $\sigma \neq 0$ and $\eta = 0 \rightarrow$ Sm-A;
(4) $s \neq 0$, $\sigma \neq 0$ and $\eta \neq 0 \rightarrow$ Sm-C.
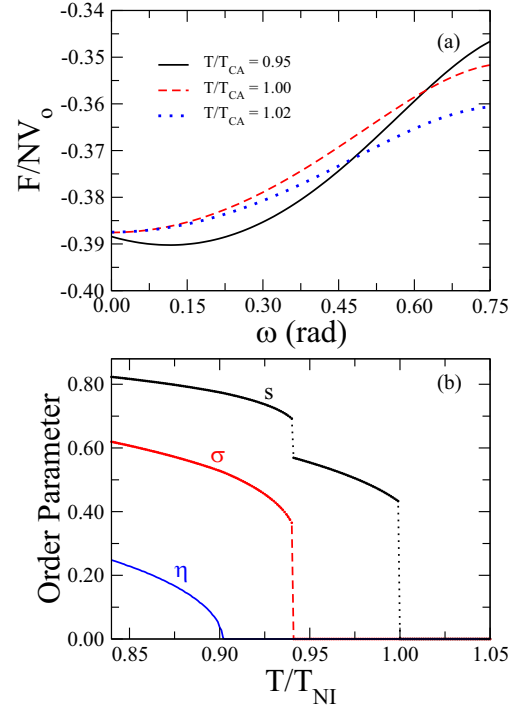
FIG. 2. (a) Helmholtz free energy as a function of the tilt angle ω, at the vicinity of the Sm-C−Sm-A transition temperature, T_{CA}. We use representative values of the model parameters: $\alpha_0 = 0.85$ and $\beta = 0.33$. Notice that a nonnull tilt angle corresponds to a minimum of the Helmholtz free energy for $T < T_{CA}$. (b) Temperature dependence of tilt, η, translational, σ, and orientational, s, order parameters for $\alpha_0 = 0.85$ and $\beta = 0.33$. We observe that η decays continuously as the system temperature is increased, while σ and s stay finite, signaling a second-order Sm-C−Sm-A phase transition.

In the present model, the order parameters are numerically determined using the self-consistent equations for different values of the tilt angle ω, for fixed values of T, α_0, and β. The equilibrium configuration is determined from the minimum value of the Helmholtz free energy with respect to ω.

In Fig. 2(a), we present the Helmholtz free energy as a function of the average tilt angle, at the vicinity of the Sm-C−Sm-A transition temperature, T_{CA}. We consider as representative values of the model parameters $\alpha_0 = 0.85$ and $\beta = 0.33$. For $T > T_{CA}$, we notice that the null tilt angle corresponds to the only minimum of the Helmholtz free energy, which excludes the possibility of a coexistence of Sm-C and Sm-A phases at $T = T_{CA}$. Such a scenario is typical of a second-order phase transition, where the energy minimum in the disordered phase becomes a local maximum in the ordered one. In fact, a nonnull value of the tilt angle becomes the minimum of the Helmholtz free energy when $T < T_{CA}$. In Fig. 2(b), we show the temperature dependence of s, σ and η order parameters. The system temperature is normalized by the nematic-isotropic transition temperature, $T_{NI} = 0.2202 V_0 / k_B$. The tilt-order parameter η decays continuously as the system temperature is raised, while the

Instituto de Física - UFAL
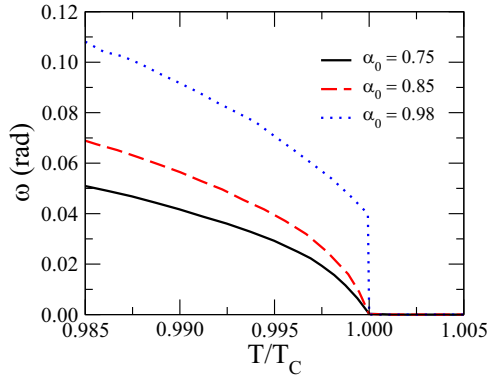
FIG. 3. The tilt angle as a function of T/T_C for $\beta = 0.33$ and three representative values of the geometric parameter α_0: $\alpha_0 = 0.75$ (black solid line), $\alpha_0 = 0.85$ (red dashed line), and $\alpha_0 = 0.98$ (blue dotted line), where T_C represents the temperature where η order parameter vanishes. Notice that the continuous decay of the tilt angle is replaced by a discontinuous behavior as the parameter α_0 is increased.

FIG. 4. The phase diagram in the reduced temperature vs α_0 plane for different values of the parameter β. (a) $\beta = 0.30$, (b) $\beta = 0.33$, (c) $\beta = 0.40$, and (d) $\beta = 0.70$. Solid (dotted) lines corresponds to first-order (second-order) transitions. As the parameter β increases, the Sm-A phase disappears.

orientational- and translational-order parameters stay finite, characterizing a second-order Sm-C−Sm-A phase transition at $T/T_{NI} = 0.902$. For $\eta = 0$, the single-particle potential is reduced to that of McMillan's model, which predicts that a first-order Sm-A–N phase transition takes place for $\alpha_0 > 0.70$. We notice that the translational-order parameter σ develops a discontinuity at $T/T_{NI} = 0.941$, which is accompanied by an abrupt reduction of the orientational order parameter s, signaling a first-order Sm-A–N phase transition. Moreover, we can use T_{CA}/T_{NI} and T_{AN}/T_{NI} ratios to compare the present results with experimental findings for smectogenic compounds with a small transverse dipole moment. We recall that the nonchiral liquid-crystalline compound p-decyloxybenzoic acid p-n-hexyphenyl ester (DOBHOP) exhibits a second-order Sm-C−Sm-A phase transition, followed by a first-order Sm-A–N phase transition, with $T_{CA}/T_{NI} = 0.872$ and $T_{AN}/T_{NI} = 0.937$ [47]. As the DOBHOP molecules present a small transverse dipole moment ($P \approx 4$ nC/cm^2) [48], the present results indicate that the single-particle molecular potential of Eq. (2) provides a reasonable description of the phase sequence of DOBHOP compound, with $\alpha_0 = 0.85$ and $\beta = 0.33$.

To characterize the effects of molecular structure on the tilt behavior of Sm-C phase, we analyze the temperature dependence of tilt angle for $\beta = 0.33$ and distinct values of the parameter α_0, as shown in Fig. 3. For the sake of convenience, the system temperature was rescaled by T_C, which corresponds to the temperature at which the η order parameter vanishes. As the parameter α_0 is increased, we observe that the continuous decay of the tilt angle is replaced by a discontinuous jump at $T = T_C$. Such a behavior suggests that the value of the parameter α_0 affects the nature of the phase transitions involving Sm-C phase, even though β is kept constant. Since α_0 is associated with the length of alkyl-chain in rodlike molecules, this result is in agreement with experimental findings for different homologous series [20,49], where the molecular rigid part is kept constant and the length of alkyl-chain is varied. For $T < T_C$, we notice that the tilt
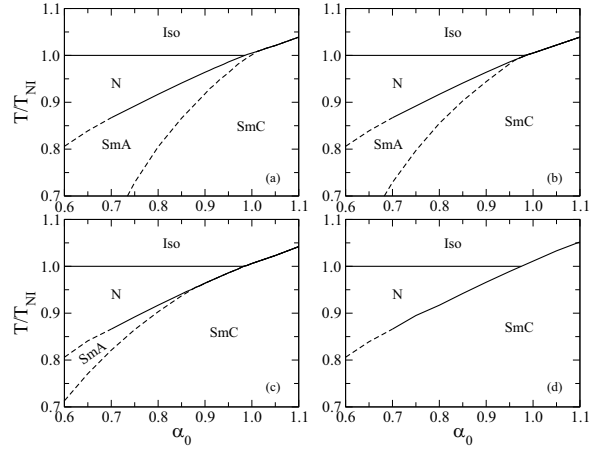
angle is favored as the value of the parameter α_0 is raised, with the layer contraction becoming more pronounced.

In Fig. 4, we present the phase diagrams, temperature versus the parameter α_0, considering different values for the parameter β. The temperature is rescaled by nematic-isotropic transition temperature, T_{NI}. For $\beta = 0.30$, we observe a second-order Sm-C−Sm-A phase transition for $\alpha_0 < 1.01$, while a first-order Sm-C−Iso phase transition takes place for $\alpha_0 > 1.01$, as shown in Fig. 4(a). This indicates that $\alpha_0 = 1.01$ is a critical end point, which corresponds to the position where the line of continuous Sm-C−Sm-A transition encounters the coexistence line between the Sm-C and the isotropic phase. Similar to McMillan's model [50], we observe a tricritical point at $\alpha_0 = 0.70$, delimiting the regions of continuous and discontinuous Sm-A–N transitions. Moreover, one can note the triple point at $\alpha_0 = 0.98$, which determines the coexistence of nematic, Sm-A and isotropic phases. This phase behavior is in agreement with experimental findings for terephthal-bis-(4n)-alkylaniline (TBnA) [20] and 2-(4-alkyloxyphenyl)-5-alkyloxypyrimidines (PhPn) [49] homologous series. In Fig. 4(b), we show the T-α_0 phase diagram for $\beta = 0.33$, where a critical end point is observed for $\alpha_0 = 0.96$. However, the line of continuous Sm-C−Sm-A transition reaches the coexistence line of discontinuous Sm-A–N transition, thus corresponding to a N−Sm-A−Sm-C critical end point. A similar scenario is observed for $\beta = 0.40$, as presented in Fig. 4(c). It is remarkable that the N−Sm-A−Sm-C critical end point is displaced to lower values of α_0 as β is increased, which is accompanied by a reduction in the Sm-A temperature range. For $\beta = 0.70$, the Sm-A phase is suppressed and a tricritical point at $\alpha_0 = 0.70$ delimits the regions of continuous and discontinuous Sm-C−N transitions, as shown in Fig. 4(d). We notice that the NA tricritical point and the N−Sm-A−Sm-C critical end point tend to merge as the parameter β is increased, thus giving rise to a NC tricritical point. It is important to emphasize that

Instituto de Física - UFAL

the Sm-A phase is stabilized by the layer contraction, without the need to introduce an excluded-volume contribution, as suggested by Govind and Madhusudana [33,34]. In this case, the single-particle mean-field potential introduced in Eq. (2) captures the main features of the phase transitions involving Sm-C phase, with a reduced number of free parameters.

III. EXTENDED MOLECULAR MODEL FOR FREE-STANDING FILMS

Let us now describe phase transitions in free-standing Sm-C films. We consider an extended version of McMillan-Mirantsev's model [51], by inserting the effective tilting potential. We assume a stratified film with N discrete layers, where each layer has its own set of orientational, s_i, translational, σ_i, and tilt, η_i, order parameters. Considering the layer located at the position z_i and the molecular orientation defined by polar and azimuthal angles, θ_i and ϕ_i, respectively, the effective one-particle mean-field potential can be written as

$$V_i = -V_0\big\{P_2(\cos\psi_i)[\bar{s}_i + \alpha_i\bar{\sigma}_i\cos(2\pi z_i/d_i)]$$
$$+ \alpha_i\beta\bar{\sigma}_i^2\bar{\eta}_i\sin(2\theta_i)\cos\phi_i\big\}, \tag{9}$$

in which $\alpha_i = 2(\alpha_0/2)^{\sec^2\omega_i}$, $d_i = d_0\cos\omega_i$, and ω_i is the tilt angle in the ith layer, satisfying the angular relation $\cos\psi_i = \cos\theta_i\cos\omega_i + \sin\theta_i\sin\omega_i\sin\phi_i$. In addition, $\bar{s}_i$, $\bar{\sigma}_i$, and $\bar{\eta}_i$ are the average order parameters in ith layer and its two neighboring layers, being given by

$$\bar{s}_i = \frac{(1 - \delta_{i-1,0})s_{i-1} + s_i + (1 - \delta_{i+1,N+1})s_{i+1}}{3}$$
$$+ \frac{W_0(\delta_{i,1} + \delta_{i,N})}{V_0}, \tag{10}$$

$$\bar{\sigma}_i = \frac{(1 - \delta_{i-1,0})\sigma_{i-1} + \sigma_i + (1 - \delta_{i+1,N+1})\sigma_{i+1}}{3}, \tag{11}$$

and

$$\bar{\eta}_i = \frac{(1 - \delta_{i-1,0})\eta_{i-1} + \eta_i + (1 - \delta_{i+1,N+1})\eta_{i+1}}{3}, \tag{12}$$

with $i = 1, 2, \ldots, N$, and δ_{ij} is the Kronecker's δ. In this approach, the surface anchoring is represented by a surface orientational field of strength W_0. For free-standing Sm-C film, we assume that the surface ordering gives rise to a tilt angle profile as follows [52]:

$$\omega_i = \omega_B + \frac{(\omega_S - \omega_B)\cosh[d_0(2i - N - 1)/2\xi]}{\cosh[d_0(N - 1)/2\xi]}, \tag{13}$$

where ω_B is the bulk tilt angle and ω_S is the tilt angle in outermost layers. ξ is the surface penetration length, which delimits the range of anchoring effects on the tilt ordering along the film. As we consider a short-range surface contribution in the one-particle mean-field potential, we assume $\xi = 2d_0$. In fact, previous studies reported that the surface penetration length is of the order of the average smectic layer spacing d_0 [45,53,54], not exceeding a few molecular layers. It is important to highlight that the tilt angle profile defined by Eq. (13) was introduced by Tweet and co-workers [52], using a simple phenomenological elastic model. However, experimental results indicate that the tilt angle disappears before the layered structure is disrupted when the film temperature is

increased [21,55,56]. To provide a better description of free-standing Sm-C films, we consider that the surface tilt angle presents a typical temperature dependence of a mean-field model, that is,

$$\omega_S = \omega_0\left(\frac{T_{AN} - T}{T_{AN} - T_{CA}}\right)^{\frac{1}{2}}. \tag{14}$$

In Eq. (14), T_{CA} and T_{AN} are the bulk Sm-C−Sm-A and Sm-A–N transition temperatures, respectively. In this model, ω_S vanishes as the smectic order is reduced. In what follows, we use $\omega_0 = 0.26$ ($\sim15°$).

The local order parameters s_i, σ_i, and η_i are defined as the thermodynamical averages

$$s_i = \langle P_2(\cos\psi_i)\rangle, \tag{15}$$

$$\sigma_i = \langle P_2(\cos\psi_i)\cos(2\pi z_i/d_i)\rangle, \tag{16}$$

and

$$\eta_i = \langle\sin(2\theta_i)\cos\phi_i\rangle, \tag{17}$$

being computed from the one-particle distribution function in the ith smectic layer, that is,

$$\mathcal{Z}_i \propto \exp[-V_i/k_BT]. \tag{18}$$

The total Helmholtz free energy is then given by

$$\frac{F}{N_0V_0} = \sum_{i=1}^{N} F_i, \tag{19}$$

with

$$F_i = \frac{1}{2}(s_i\bar{s}_i + \alpha_i\sigma_i\bar{\sigma}_i + \alpha_i\beta\bar{\sigma}_i^2\eta_i\bar{\eta}_i)$$
$$- \frac{k_BT}{V_0}\ln\left[\frac{1}{2\pi d_i}\int_{-1}^{1}d\cos(\theta_i)\int_0^{\pi}d\phi_i\int_{(i-1)d_{i-1}}^{id_i}dz_i\mathcal{Z}_i\right]. \tag{20}$$

From this model, we can compute the profile of the order parameters for different sets of free parameters in the single-particle mean-field potential: α_0, β, and W_0. Indeed, we use the tilt angle profile defined in Eq. (13) to obtain the actual profiles of order parameters that minimize the Helmholtz free energy, thus yielding the equilibrium configuration of the system. It is important to highlight that the tilt angle profile of Eq. (13) has been widely used in several experimental studies, leading to a reasonable description of the thermal and hydrodynamic properties of free-standing Sm-C films [28,52,55].

In combination with Eq. (14), we use the bulk values of ω_B to compute the tilt angle profile for distinct film temperatures, as shown in Fig. 5. We consider $N = 15$, $\omega_0 = 0.26$, $\alpha_0 = 0.85$, and $\beta = 0.33$. We observe that Eq. (13) provides a tilt profile with a positive curvature, where the outermost layers present tilt angles larger than the internal ones. For $T > T_{CA}$, a pronounced tilt reduction takes place at central layers as ω_B vanishes, while a non vanishing tilt persists in outermost layers. Such a scenario is similar to the experimental findings, where the surface layers exhibit a Sm-C−Sm-A transition well above the bulk transition temperature [21]. Besides, it
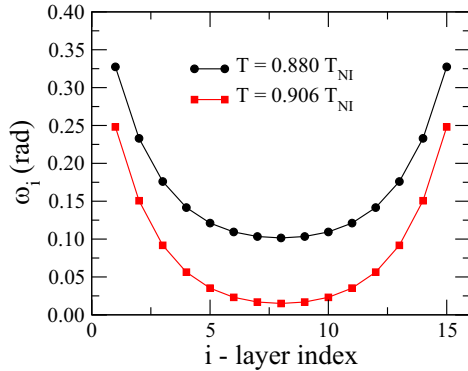
FIG. 5. Tilt angle profile for a $N = 15$ layer film, for distinct temperatures: $T = 0.880T_{NI}$ (black circles) and $T = 0.906T_{NI}$ (red squares). We consider $\omega_0 = 0.26$, $\alpha_0 = 0.85$, and $\beta = 0.33$. For these parameters, bulk Sm-C−Sm-A transition temperature is estimated as $T_{CA} = 0.902T_{NI}$. Notice that a pronounced reduction takes place in the tilt angle of central layers when $T > T_{CA}$, while a nonnull tilt persists in outermost layers.

is important to stress that the tilt angle profile is assumed to be independent of the surface anchoring, W_0.

In Fig. 6, we present the profiles of order parameters for a free-standing smectic film with $N = 15$ layers. We use the same model parameters of Fig. 5. Furthermore, we consider $W_0/V_0 = 0.25$, which corresponds to the regime of weak surface anchoring [35]. For $T < T_{CA}$, we observe that nematic and smectic order parameters present nonuniform profiles with a negative curvature, where central layers are more ordered than the surface. More specifically, the weak anchoring leads to a small value of smectic order parameter in surface layers. However, the tilt-order parameter exhibits a nonuniform profile with a positive curvature. This profile is characterized by a high tilt ordering in surface layers, due to the tilt angle profile defined in Eq. (13). Such a scenario holds for $T > T_{CA}$, with a small reduction in the nematic and smectic order parameters. However, the tilt-order parameter becomes almost negligible in central layers, while surface layers present a finite tilt ordering. In this case, surface layers remain in the Sm-C phase, with the central layers being in the Sm-A phase. These results show that the tilt angle profile is the dominant effect in the regime of weak surface anchoring.

A distinct scenario emerges in the regime of strong surface anchoring, where profound modifications can be observed in the profiles of order parameters near the bulk Sm-C−Sm-A transition temperature, as exhibited in Fig. 7. Figure 7(a) shows that the profile of the nematic order parameter presents a positive curvature, with surface layers exhibiting an almost saturated orientational ordering. Such a behavior holds for $T > T_{CA}$, with a small reduction in the nematic order parameter of internal layers. In Fig. 7(b), we observe that the smectic order parameter exhibits a nonuniform profile with a negative curvature for $T < T_{CA}$. In this case, internal layers are more ordered than the outermost ones. For $T > T_{CA}$, the smectic order parameter exhibits a nearly flat profile, in which a small positive curvature can be verified. Although W_0/V_0 is not directly coupled to the tilt ordering, we notice that the
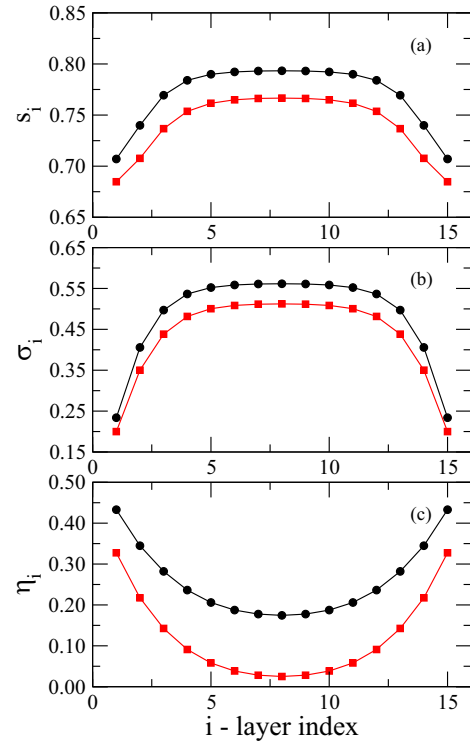
FIG. 6. Profiles of (a) orientational, (b) translational, and (c) tilt-order parameters for a free-standing film with $N = 15$, at different temperatures: $T = 0.880T_{NI}$ (black circles) and $T = 0.906T_{NI}$ (red squares). The model parameters are the same used in Fig. 5, where the bulk Sm-C−Sm-A transition temperature takes place at $T_{CA} = 0.902T_{NI}$. We use $W_0/V_0 = 0.25$, corresponding to the regime of weak anchoring condition. Notice that the tilt-order parameter stays finite in the surface layers above the bulk Sm-C−Sm-A transition temperature, even in the regime of weak surface anchoring.

strong anchoring condition leads to the enhancement of η_i along the whole film, specially in surface layers, as presented in Fig. 7(c). For $T > T_{CA}$, a strong surface anchoring tends to stabilize the tilt order along the film, with exception of the central layers where tilt ordering is negligible.

To investigate the interplay of finite size effects and surface anchoring conditions, in Fig. 8 we analyze the thickness dependence of order parameters at the central layer of free-standing films for distinct anchoring regimes. The penetration surface length is kept constant, with $\xi = 2d_0$. In the regime of weak surface anchoring, the nematic and smectic order parameters of central layer increase rapidly as the film thickness is enhanced, reaching their maximum values for $N = 15$. However, the tilt-order parameter exhibits a gradual reduction as the film thickness increases, thus reflecting the thickness dependence of tilt angle defined by Eq. (13). This result indicates that the finite size effects govern the thermal behavior of order parameters in the regime of weak surface anchoring. A distinct behavior is observed for strong surface anchoring, as shown in Fig. 8(b). The nematic order parameter at the central layer is independent of the film thickness, while
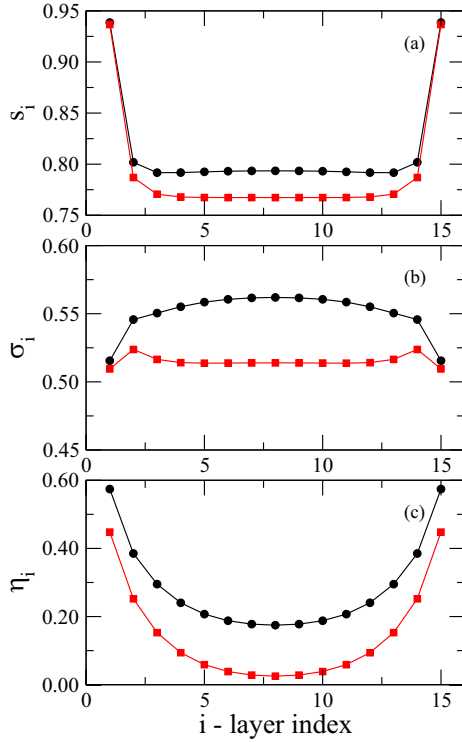
FIG. 7. Profiles of (a) orientational, (b) translational, and (c) tilt-order parameters for a free-standing smectic film, at the vicinity of bulk Sm-C−Sm-A transition temperature ($T_{CA} = 0.902T_{NI}$). We consider different film temperatures: $T = 0.880T_{NI}$ (black circles) and $T = 0.906T_{NI}$ (red squares). The model parameters are $\alpha_0 = 0.85$, $\beta = 0.33$, $\omega_0 = 0.26$, $N = 15$, and $W_0/V_0 = 2.5$. We notice an enhancement in the tilt-order parameter due to the strong anchoring condition.

a very small increase is observed in the smectic order parameter. Concerning the tilt-order parameter, we notice that η_{cl} is slightly larger in thin films due to the strong surface anchoring. However, the effects of tilt angle profile predominates as the film thickness is increased. In fact, we have assumed that the surface tilt amplitude ω_0 is independent of the surface anchoring W_0, as it is related to the molecular structure and excluded-volume contribution. More specifically, there is no experimental evidence supporting the dependence of surface tilt angle on the surrounding gas in free-standing films.

Figure 9 exhibits the temperature dependence of the order parameters at the central layer for different values of surface anchoring ($W_0/V_0 = 0.25$ and $W_0/V_0 = 2.5$) and two representative film thicknesses ($N = 7$ and $N = 25$). For a thin film with $N = 7$, we observe that a first-order Sm-C−N transition takes place in the regime of weak anchoring conditions, while the nematic order vanishes smoothly as the temperature is raised, as shown in Fig. 9(a). This result indicates the absence of the nematic-isotropic transition, even for small values of the anchoring strength. However, the transition to the nematic phase leads in practice to the film thinning or to the film rupture. For a thin film with $N = 7$ and strong anchoring con-
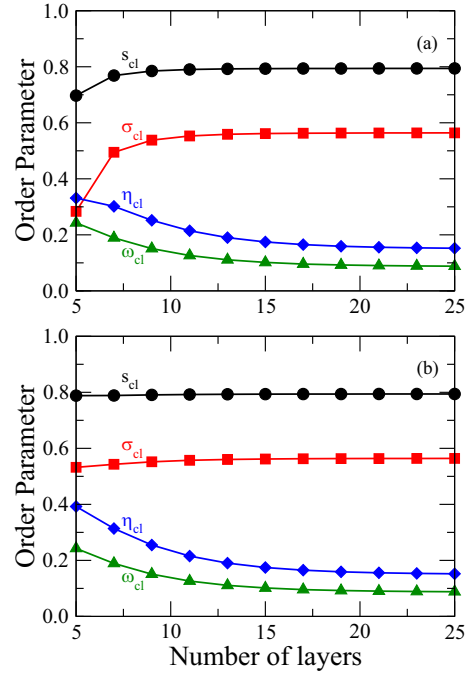
FIG. 8. Thickness dependence of order parameters in central layer of free-standing Sm-C films: nematic (s_{cl}, black circles), smectic (σ_{cl}, red squares), and tilt (η_{cl}, blue diamonds) order parameters. The tilt angle of central layer is also shown (ω_{cl}, green triangles). Different regimes of surface anchoring are considered: (a) $W_0 = 0.25$ and (b) $W_0 = 2.50$. The model parameters are $\alpha_0 = 0.85$, $\beta = 0.33$, and $\omega_0 = 0.26$. Notice that the surface anchoring plays an important role in central order parameters of thin films.
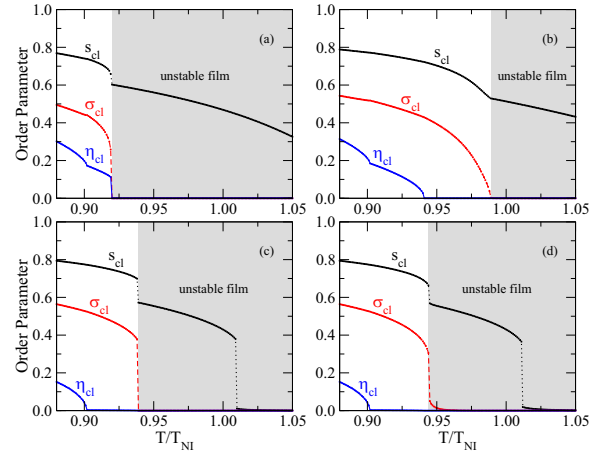
FIG. 9. Temperature dependence of order parameters at the central layer in smectic films with different thicknesses and anchoring conditions: (a) $N = 7$ and $W_0 = 0.25$, (b) $N = 7$ and $W_0 = 2.50$, (c) $N = 25$ and $W_0 = 0.25$, and (d) $N = 25$ and $W_0 = 2.50$. Notice that the interplay of finite size effects and surface anchoring may change the phase diagram of free-standing films. The gray areas represent the temperature regions where a dramatic reduction in the smectic order takes place, corresponding to an unstable film.

ditions, one can note that the first-order Sm-C−N transition is replaced by a sequence of second-order Sm-C–Sm-A and Sm-A–N transitions, occurring in higher temperatures than that observed in bulk systems [see Fig. 2(b)]. For the thicker film ($N = 25$), we observe a phase sequence similar to the bulk system, even for a weak anchoring strength, as observed in Fig. 9(c). Nevertheless, a residual smectic order parameter persists after the jump in Sm-A–N transition temperature for a 25-layer film under strong anchoring, as shown in Fig. 9(d). In this case, the nematic phase presents a residual smectic order, corresponding to a surface-induced smectic phase (si–Sm-A). A similar behavior is observed above the nematic-isotropic transition temperature, where a residual nematic order is observed.

IV. SUMMARY AND CONCLUSIONS

In summary, we have studied the phase transitions in bulk systems and free-standing films presenting a Sm-C phase. Using a single-particle mean-field potential introduced by Govind and Madhusudana [33], we have shown that the phase diagram of smectogenic compounds with a small transverse dipole can be reasonably described when the tilt-induced contraction of smectic layers is considered. This approach eliminates the need to introduce an additional excluded-volume contribution to stabilize the Sm-A phase, thus reducing the number of free parameters of the model. By varying the model parameter associated with the transverse dipoles in rodlike molecules, a rich variety of phase diagrams have been observed. In particular, we have identified a N−Sm-A−Sm-C critical end point, corresponding to the position at which the line of continuous transition between the Sm-C and Sm-A phases encounters the coexistence line between the Sm-C and the nematic phases. Concerning free-standing Sm-C films, our results showed that the interplay of finite size effects and surface anchoring conditions affects the phase diagrams of thin films. Considering a tilt angle profile and a discrete version of single-particle mean-field potential, we have computed the profiles of order parameters of free-standing films under different anchoring regimes. We have observed that surface effects stabilize the tilt-order parameter in outermost layers of films above the bulk Sm-C−Sm-A transition temperature. As a consequence, surface layers may remain in the Sm-C phase, while the central layers are in the -Sm-A phase. Such a coexistence of Sm-C and -Sm-A phases in a free-standing film has been reported in previous experimental studies [24,46]. However, some questions still remain open, such as the possible connection between the surface anchoring strength and surface tilt angle. From a practical point of view, the control of the anchoring strength may be a challenging task. Although free-standing smectic films under strong anchoring condition have been widely probed, the scenario of films with a weak anchoring is very difficult to be realized. However, recent studies of free-standing smectic films immersed in aqueous solutions of surfactants revealed a reduction of anisotropic contribution of the surface tension [57,58], indicating a reduction of the orientational order at the surface layers. Furthermore, the effective control of surface anchoring has been realized in the study of spherical smectic shells [59], where an aqueous solution of an amphiphilic triblock copolymer was used to induce a weak homeotropic anchoring. Considering the status of the experiments nowadays, the present results may stimulate experimental efforts aiming to probe the rich scenario predicted by the extended version of the molecular theory for Sm-C liquid crystals.

[1] C. W. Garland and G. Nounesis, Phys. Rev. E **49**, 2964 (1994).

[2] J. Morikawa, T. Hashimoto, A. Kishi, Y. Shinoda, K. Ema, and H. Takezoe, Phys. Rev. E **87**, 022501 (2013).

[3] J. Als-Nielsen, F. Christensen, and P. S. Pershan, Phys. Rev. Lett. **48**, 1107 (1982).

[4] T. Jin, G. P. Crawford, R. J. Crawford, S. Zumer, and D. Finotello, Phys. Rev. Lett. **90**, 015504 (2003).

[5] L. D. Pan, B. K. McCoy, S. Wang, W. Weissflog, and C. C. Huang, Phys. Rev. Lett. **105**, 117802 (2010).

[6] R. Geer, T. Stoebe, and C. C. Huang, Phys Rev B **45**, 13055 (1992).

[7] C. Y. Chao, C. R. Lo, P. J. Wu, Y. H. Liu, D. R. Link, J. E. Maclennan, N. A. Clark, M. Veum, C. C. Huang, and J. T. Ho, Phys. Rev. Lett. **86**, 4048 (2001).

[8] Z. Li and O. D. Lavrentovich, Phys. Rev. Lett. **73**, 280 (1994).

[9] M. S. S. Pereira, M. L. Lyra, and I. N. de Oliveira, Phys. Rev. Lett. **103**, 177801 (2009).

[10] O. Francescangeli, F. Vita, F. Fauth, and E. T. Samulski, Phys. Rev. Lett. **107**, 207801 (2011).

[11] W. H. de Jeu, B. I. Ostrovskii, and A. N. Shalaginov, Rev. Mod. Phys. **75**, 181 (2003).

[12] R. Hołyst, D. J. Tweet, and L. B. Sorensen, Phys. Rev. Lett. **65**, 2153 (1990).

[13] C. Bahr, Int. J. Mod. Phys. **8**, 3051 (1994).

[14] T. Stoebe, P. Mach, and C. C. Huang, Phys. Rev. Lett. **73**, 1384 (1994).

[15] F. Bougrioua, P. Cluzeau, P. Dolganov, G. Joly, H. T. Nguyen, and V. Dolganov, Phys. Rev. Lett. **95**, 027802 (2005).

[16] E. S. Pikina, B. I. Ostrovskii, and W. H. de Jeu, Eur. Phys. J. E **38**, 13 (2015).

[17] T. Stoebe, L. Reed, M. Veum, and C. C. Huang, Phys. Rev. E **54**, 1584 (1996).

[18] K. Ema and H. Yao, Phys. Rev. E **57**, 6677 (1998).

[19] Z. H. Nguyen, M. Atkinson, C. S. Park, J. Maclennan, M. Glaser, and N. Clark, Phys. Rev. Lett. **105**, 268304 (2010).

[20] S. Kumar, Phys. Rev. A **23**, 3207 (1981).

[21] S. Heinekamp, R. A. Pelcovits, E. Fontes, E. Y. Chen, R. Pindak, and R. B. Meyer, Phys. Rev. Lett. **52**, 1017 (1984).

Instituto de Física - UFAL

[22] C. C. Huang and J. M. Viner, Phys. Rev. A **25**, 3385 (1982).

[23] R. Shashidhar, B. R. Ratna, and S. K. Prasad, Phys. Rev. Lett. **53**, 2141 (1984).

[24] C.-Y. Chao, S. W. Hui, and J. T. Ho, Phys. Rev. Lett. **78**, 4962 (1997).

[25] M. R. M, K. P. Zuhail, A. Roy, and S. Dhara, Phys. Rev. E **97**, 032702 (2018).

[26] C. C. Huang and S. C. Lien, Phys. Rev. A **31**, 2621 (1985).

[27] C. Bahr and D. Fliegner, Phys. Rev. A **46**, 7657 (1992).

[28] L. Reed, T. Stoebe, and C. C. Huang, Phys. Rev. E **52**, R2157 (1995).

[29] H. Y. Liu, C. C. Huang, T. Min, M. D. Wand, D. M. Walba, N. A. Clark, C. Bahr, and G. Heppke, Phys. Rev. A **40**, 6759 (1989).

[30] D. Brisbin, D. L. Johnson, H. Fellner, and M. E. Neubert, Phys. Rev. Lett. **50**, 178 (1983).

[31] R. G. Priest, J. Chem. Phys. **65**, 408 (1976).

[32] F. Gieβelmann and P. Zugenmaier, Phys. Rev. E **55**, 5613 (1997).

[33] A. S. Govind and N. V. Madhusudana, Europhys. Lett. **55**, 505 (2001).

[34] A. S. Govind and N. V. Madhusudana, Eur. Phys. J. E **9**, 107 (2002).

[35] K. Saunders, Phys. Rev. E **77**, 061708 (2008).

[36] M. Osipov and G. Pajak, Phys. Rev. E **85**, 021701 (2012).

[37] G. Pajak and M. A. Osipov, Phys. Rev. E **88**, 012507 (2013).

[38] A. V. Emelyanenko and A. R. Khokhlov, J. Chem. Phys. **142**, 204905 (2015).

[39] B. W. van der Meer and G. Vertogen, J. Phys. Colloq. **40**, C3-222 (1979).

[40] M. V. Gorkunov, M. A. Osipov, J. P. F. Lagerwall, and F. Giesselmann, Phys. Rev. E **76**, 051706 (2007).

[41] M. V. Gorkunov and M. A. Osipov, J. Phys.: Condens. Matter **20**, 465101 (2008).

[42] M. V. Gorkunov, F. Giesselmann, J. P. F. Lagerwall, T. J. Sluckin, and M. A. Osipov, Phys. Rev. E **75**, 060701(R) (2007).

[43] V. K. Dolganov, E. I. Demikhov, R. Fouret, and C. Gors, JETP **84**, 522 (1997).

[44] M. S. Spector, P. A. Heiney, J. Naciri, B. T. Weslowski, D. B. Holt, and R. Shashidhar, Phys. Rev. E **61**, 1579 (2000).

[45] A. Fera, R. Opitz, W. H. de Jeu, B. I. Ostrovskii, D. Schlauf, and C. Bahr, Phys. Rev. E **64**, 021702 (2001).

[46] I. Kraus, P. Pieranski, E. Demikhov, H. Stegemeyer, and J. Goodby, Phys. Rev. E **48**, 1916 (1993).

[47] S. Pestov and V. Vill, *Physical Properties of Liquid Crystals* (Springer-Verlag, Berlin, 2003).

[48] P. O. Andreeva, V. K. Dolganov, C. Gors, R. Fouret, and E. I. Kats, JETP Lett. **67**, 856 (1998).

[49] N. Kapernaum, C. S. Hartley, J. C. Roberts, F. Schoerg, D. Krueerke, R. P. Lemieux, and F. Giesselmann, ChemPhysChem **11**, 2099 (2010).

[50] W. L. McMillan, Phys. Rev. A **4**, 1238 (1971).

[51] M. V. Mirantsev, Phys. Lett. A **205**, 412 (1995).

[52] D. J. Tweet, R. Hołyst, B. D. Swanson, H. Stragier, and L. B. Sorensen, Phys. Rev. Lett. **65**, 2157 (1990).

[53] C. Bahr, C. J. Booth, D. Fliegner, and J. W. Goodby, Phys. Rev. E **52**, R4612 (1995).

[54] J. V. Selinger and D. R. Nelson, Phys. Rev. A **37**, 1736 (1988).

[55] P. O. Andreeva, V. K. Dolganov, C. Gors, R. Fouret, and E. I. Kats, Phys. Rev. E **59**, 4143 (1999).

[56] D. Schlauf, C. Bahr, and C. C. Huang, Phys. Rev. E **55**, R4885 (1997).

[57] Y. Iwashita, S. Herminghaus, R. Seemann, and C. Bahr, Phys. Rev. E **81**, 051709 (2010).

[58] K. Harth and R. Stannarius, Phys. Chem. Chem. Phys. **15**, 7204 (2013).

[59] H.-L. Liang, R. Zentel, P. Rudquist, and J. Lagerwall, Soft Matter **8**, 5443 (2012).

Instituto de Física - UFAL

ELECTRIC FIELD EFFECTS ON N–SM-A–SM-C PHASE TRANSITIONS

Electric field effects on N–Sm–A–Sm–C phase transitions

D. C. S. de Melo[1], E. J. L. de Oliveira[1], Maria S. S. Pereira[1], L. R. Evangelista[2] and I. N. de Oliveira[1]

[1]*Instituto de Física, Universidade Federal de Alagoas 57072-970 Maceió-AL, Brazil*
[2]*Departamento de Física, Universidade Estadual de Maringá 87020-900 Maringá-PR, Brazil*

The effects of external electric fields on nematic–smectic–A–smectic–C liquid crystal phase transitions are studied using a microscopic molecular theory of smectic–C liquid crystals. The resulting thermal behavior of the system's order parameters, in the smectic–C phase, are analyzed. We compare our results with experimental findings for typical thermotropic compounds presenting a nematic–smectic–A–smectic–C phase sequence.

I. INTRODUCTION

The effects of external fields on molecular ordering in liquid crystalline systems are an active research field [1–6] with major implications for developing new electro-optical devices [7–12]. In particular, the interplay of geometric anisotropy and different functional groups leads to anisotropic electromagnetic responses in thermotropic compounds [13, 14]. The system's molecular orientation depends on both the compound's dielectric anisotropy and the orientation of the applied external field, which in turn modifies the order parameters and liquid crystalline sequence phases. For example, an external field can give rise to ordered phases well above the nematic–isotropic and smectic–isotropic bulk transition temperatures [5, 6, 15]. Moreover, birefringence measurements close to the nematic–smectic–A transition temperature have shown that strong electric fields suppress the nematic fluctuations in systems with a positive dielectric anisotropy, causing a crossover from first to second order phase transition [16]. Concerning molecular reorientation, Wen and Rosenblatt have identified a crossover from second to first order Fréedericksz transition in nematic liquid crystals with a negative dielectric anisotropy in the presence of a spatially homogeneous external field [17]. From a practical standpoint, external field induced director reorientation has proven crucial for developing fast response electro-optic modulators, switching devices and high-performance optical filters [7–12].

External field effects in the smectic–C phase were first considered by Rapini [18], which focused on phase stability and director reorientation. The discovery of different electric responses in the smectic-C phase, such as ferroelectricity [19–25] and antiferroelectricity [26], greatly encouraged further study of smectic phases, particularly under the influence of an external field. On the other hand, if the constituent molecules are chiral and possesses a permanent transversal dipole, each layer in the smectic–C phase exhibits a spontaneous polarization. The coupling between tilt angle and electric polarization, which causes the spontaneous polarization, can also occur at the smectic–A phase at high temperatures as the electroclinic effect [27]. In a bookshelf configuration, the director proportionally tilts perpendicular to the layers. Lee and Patel [28] studied the behavior of a field-induced tilt angle in a ferroelectric liquid crystal. They observed that the molecular tilt crossed from a linear to a power law dependence with exponent $\nu \in (1/3, 1)$, near the Sm–A–Sm–C^* transition. The director field can deform due to the director's rotation around the normal to the smectic layers. As a result, the layers in most electroclinic materials contract and therefore buckle [29]. The electroclinic layer buckling can be observed in an optical microscope as periodic stripes and drastically reduces the high contrast ratio necessary for optical devices [30]. This effect has been considered theoretically [31–33] and observed experimentally [33, 34].

The rich phenomenology of liquid crystal phase transitions under an external field have led to several proposed models. Despite the numerous aforementioned macroscopic experimental and theoretical studies of bulk smectic–C systems under external electric fields, a detailed microscopic approach is as of yet lacking. We therefore investigate nematic–smectic–A–smectic–C phase transitions by extending the mean-field theory for smectic–C liquid crystals under an external electric field. The resulting effect on the thermal behaviour of the order parameters, and the nature of the phase transitions is analyzed for both positive and negative polarizability anisotropies.

II. MICROSCOPIC MODEL FOR BULK TRANSITIONS

We investigate a single component smectogenic system of rod-like molecules with a small or moderate transverse dipole moment [35], which presents a layer contraction in the tilted smectic phase. In order to characterize the average molecular orientation inside the smectic layers, we consider the relative orientation of the director $\vec{n}$ ($|\vec{n}| = 1$) and the smectic wave vector $\vec{q}$, which is represented by average tilt angle ω, as shown in Fig. 1, where $\vec{q}$ is assumed to be normal to the smectic layer plane ($x - y$ plane), with a magnitude depending on the layer spacing d ($|\vec{q}| = 2\pi/d$).

We consider a single-particle mean-field potential that extends McMillan's model by including a tilting term and an external electric field along the z-axis. The tilt direction is assumed to be constant for all smectic layers.
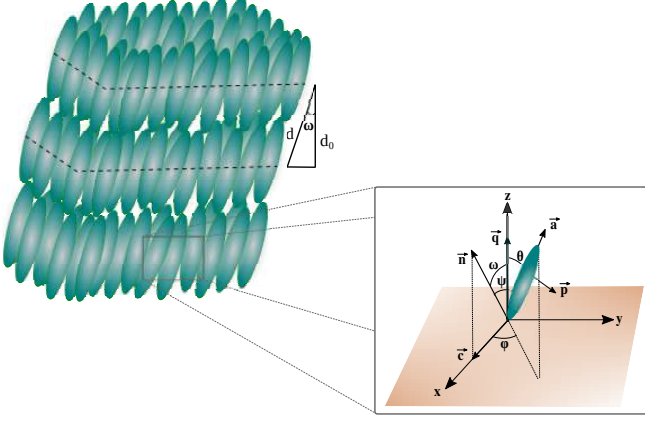
The contribution due to the electric field is given by

FIG. 1. Schematic representation of the Sm–C system, showing the layer contraction induced by the molecular tilt, where d_0 denotes the distance between layers in the Sm–A phase, d represents the molecular tilt in the Sm–C phase, and ω is the angle between d and d_0. A Cartesian coordinate system whose z-axis is normal to the smectic layer plane is used. For convenience, we assume that the director $\vec{n}$ is restricted to the z–x plane, defined as the tilt plane. Here, the vector $\vec{c}$ corresponds to the projection of the director in the x-axis, while ω represents the tilt angle of the director $\vec{n}$ with respect to the smectic wave vector $\vec{q}$. The orientation of the long molecular axis is defined by the polar and azimuthal angles θ and ϕ, respectively. ψ is the relative angle between the long molecular axis $\vec{a}$ and director $\vec{n}$. The external electric field is applied along the z axis, i.e. $\vec{E} = E\hat{z}$.

a linear term, $V_{dip} = pE\sin\theta$, and a dielectric term, $V_{die} = -\frac{1}{3}\Delta\alpha_p E^2 P_2\left(\cos\theta\right)$, where p is the dipolar moment and $\Delta\alpha_p$ is the molecular polarizability anisotropy. For calamitic molecules with a moderate or strong transverse dipole ($P > 5 nC/cm^2$), the dipole-dipole interaction becomes relevant and a single-particle mean-field potential is not suitable to describe phase transitions involving such systems.

Aiming the analysis of electric field effects on phase transitions involving the smectic-C phase, the contributions of electric field must be added to the single-particle mean-field potential. Thus, the interaction potential accounting for the effect of the electric field is written as:

$$V = -V_0 \left\{ \left[s + \alpha\sigma\cos\left(\frac{2\pi z}{d}\right) \right] P_2\left(\cos\psi\right) + \right.$$
$$+ \alpha\beta\eta\sigma^2\sin 2\theta\cos\phi - \frac{pE}{V_0}\sin\theta +$$
$$\left. + \frac{\Delta\alpha_p E^2}{3V_0} P_2\left(\cos\theta\right) \right\}. \tag{1}$$

where V_0 is an interaction energy that determines the scale of the bulk sample's nematic-isotropic transition temperature. $P_2(\cos\psi)$ is the second order Legendre polynomial. The model parameters are α_0 and β. The

former is a geometric parameter related to the length of alkyl chains of rod-like molecules, given by $\alpha_0 = 2\exp\left[-(\pi r_0/d)^2\right]$, where r_0 defines the characteristic length of the molecular rigid portion. The latter parameter depends on the spatial arrangement and strength of the dipoles in rod-like molecules.

A non-null average tilt contracts the layer spacing, as defined by $d = d_0\cos\omega$, where d_0 denotes the layer spacing in the smectic-A phase. We therefore define the quantity α in terms of the model parameter α_0 to account for the layer contraction due to tilting, as:

$$\alpha = 2\left(\frac{\alpha_0}{2}\right)^{\sec^2\omega}. \tag{2}$$

The orientation of the molecular long axis with respect to the director is represented by the angle ψ, as shown in the inset of Fig. 1, which satisfies:

$$\cos\psi = \cos\theta\cos\omega + \sin\theta\sin\omega\sin\phi. \tag{3}$$

The order parameters s, σ and η are defined by:

$$s = \langle P_2(\cos\psi)\rangle, \tag{4}$$

$$\sigma = \langle P_2(\cos\psi)\cos(2\pi z/d)\rangle, \tag{5}$$

and

$$\eta = \langle\sin 2\theta\cos\phi\rangle. \tag{6}$$

Where the thermodynamic averages, $\langle\cdots\rangle$, are computed from the following one-particle distribution function:

$$\mathcal{Z}(z,\theta,\phi) \propto \exp\left[-V/k_B T\right], \tag{7}$$

k_B is the Boltzmann constant and T is the temperature. The equilibrium order parameters are solutions of self-consistent equations, found at extreme values of the following Helmholtz free energy:

$$\frac{F}{N_0 V_0} = \frac{1}{2}\left(s^2 + \alpha\sigma^2 + \alpha\beta\sigma^2\eta^2\right) +$$
$$+ \frac{1}{2}\left(-\frac{pE}{V_0}\langle\sin\theta\rangle + \frac{\Delta\alpha_p E^2}{3V_0}\langle P_2\left(\cos\theta\right)\rangle\right) -$$
$$- \frac{k_B T}{V_0}\ln\left(\frac{1}{2\pi d}\int_{-1}^{1} d\cos\theta\int_0^\pi d\phi\int_0^d dz\mathcal{Z}\right), \tag{8}$$

where, for $\omega = 0$, $s = \langle P_2\left(\cos\theta\right)\rangle$.

The order parameters are numerically determined using the self-consistent equations for different values of the tilt angle ω, and fixed values of T, α_0 and β. The equilibrium configuration corresponds to the Helmholtz

	Order parameters		
Phases	s	σ	η
Isotropic	null	null	null
Nematic	non-null	null	null
Smectic–A	non-null	non-null	null
Smectic–C	non-null	non-null	non-null

TABLE I. Possible solutions corresponding to the different phases.

free energy minimum with respect to ω. The solutions corresponding to the different phases are shown in table I.

The model parameters are henceforth $\alpha_0 = 0.84$ and $\beta = 0.31$ which well represents the nonchiral liquid-crystalline compound p-decyloxybenzoic acid p-n-hexyphenyl ester (DOBHOP). This compound exhibits the following phase transition sequence: Sm–C - 77.5 - Sm–A - 83.3 - N - 88.9 - Iso. We then have the following important parameters: transversal dipole moment $p = 1.16 \times 10^{-29}$ Cm, polarizability anisotropy $|\Delta\alpha_p| = 2.03 \times 10^{-29}$ m^3 and characteristic potential $V_0 = k_B T_{NI}/0.2202 = 2.3 \times 10^{-20}$ J [36].

Although this specific compound presents a negative polarizability, it is usefull to analize a similar compound that presents an opposite polarizability. For that reason, we are going to present the results for both polarizabilities: $\Delta\alpha_p^* = \pm|\Delta\alpha_p|$.

A. Results - Negative Polarizability

To investigate how the smectic–C order can be favored by an electric field, we consider a negative polarizability anisotropy ($\Delta\alpha_p^* < 0$). In fact, the negative polarizability anisotropy favors the reorientation of calamitic molecules along the perpendicular direction to the external field.
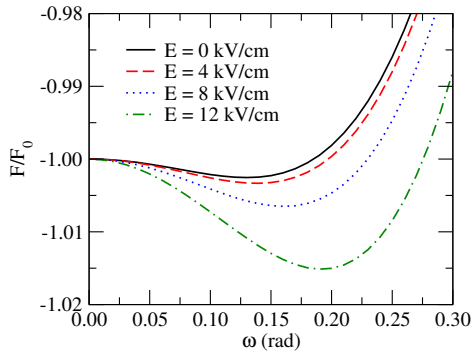

FIG. 2. Helmholtz free energy as a function of the tilt angle ω for different values of applied electric field. We use representative values of the model parameters $\alpha_0 = 0.84$ and $\beta = 0.31$. We use $\Delta\alpha_p^* < 0$ and fixed temperature $T/T_{CA} = 0.8$. We can notice that the minimum value of F/F_0 increasing in module implies a greater phase stability.

In order to characterize the stability of the smectic-C phase, we present the Helmholtz free energy as a function of the average tilt angle for different values of external electric field, as shown in Fig. 2. We fixed the temperature $T/T_{CA} = 0.8$, where T_{CA} is the temperature at which the Sm–C order disappears with no external field influence. To aid visualization, we normalized the free energy axis to F_0, the free energy corresponding to no field and $\omega = 0$. For $E = 0$, we observe that the Helmholtz free energy presents a minimum at non-null value of tilt angle, confirming that the smectic-C phase corresponds to the equilibrium phase at $T/T_{CA} = 0.8$. As the external electric field is raised, we notice that the energy minimum becomes more pronounced, taking place at higher values of the tilt angle. Such a result indicates that the electric field favors the tilt ordering inside the smectic layers, thus increasing the stability of the smectic-C. In particular, molecules presenting a negative polarizability tend to align themselves perpendicular to the external field, similar to the contribution of field-transverse dipole interaction. As a consequence, a gradual increase of the tilt angle is expected as field amplitude is enhanced, for $T < T_{CA}$.
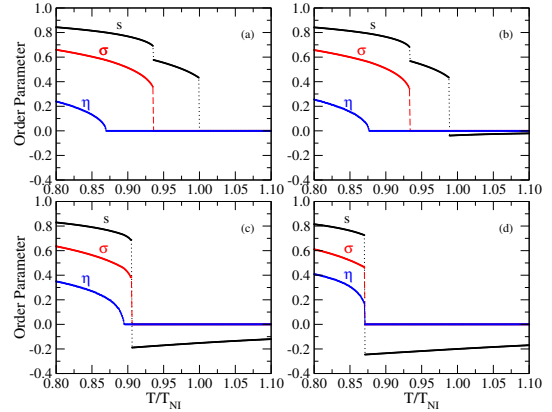

FIG. 3. Variation of the orientational s, translational σ, and tilt η order parameters as a function of the reduced temperature for different values of electric field and $\Delta\alpha_p^* < 0$. For (a) $E = 0$ kV/cm, we have the temperature dependence of order parameters on bulk. For (b) $E = 4$ kV/cm, we can already see the external field effects, where nematic order parameter start to have negative values. For (c) $E = 12$ kV/cm, we can notice that the Sm–A phase is being suppressed, where we have a first order Sm–A–fi–N phase transition. And for (d) $E = 16$ kV/cm, the Sm–A phase is completely suppressed and we have a Sm–C–fi–N phase transition.

Figure 3 shows the temperature dependence of s, σ and η order parameters, for different electric fields. Figure 3(a) shows the bulk order parameters, without an external electric field, presenting a second order Sm–C–Sm–A phase transition, followed by first-order Sm–A–N and N–Iso phase transitions. We note that even for a small electric field the isotropic phase is suppressed, giv-

ing rise to a field-induced nematic phase, with negative orientational order parameter, as shown in figure 3(b). Additionally, the temperature-range of the Sm–A phase is reduced, while the Sm–C phase is favoured by the external field. Figure 3(c) shows a small-range Sm–A phase followed by a first-order Sm–A–fi-N phase transition, completely suppressing the nematic phase with positive order parameter. Moreover, we notice a pronounced increase in the transition discontinuity between conventional and field-induced nematic phases. We also verify a gradual increase in the Sm-A-Sm-C transition temperature as the electric field is enhanced, being accompanied by a raise in the tilt order parameter increases at $T < T_{CA}$. Sufficiently strong electric fields induce a first order Sm–C–fi-N phase transition, where the Sm–A phase is completely suppressed, as seen in figure 3(d).

The temperature dependence of tilt angle for different values of electric field was analyzed to characterize the electric field's effects on the phase transitions, shown in Fig. 4. For convenience, we consider an reduced temperature, which is normalized by the temperature at which the η order parameter vanishes. For reduced temperature < 1, we observe that the tilt angle increases with the electric field. Additionally, the continuous decay of the tilt angle is replaced by a jump at reduced temperature $= 1$, which suggests that sufficiently strong electric fields affect the nature of phase transitions involving the smectic–C phase, even though the model parameters are kept constant. Since we are considering a negative polarizability, this result is in agreement with experimental studies, given that sufficiently strong electric fields suppresses the Sm–A phase [16, 27–30].
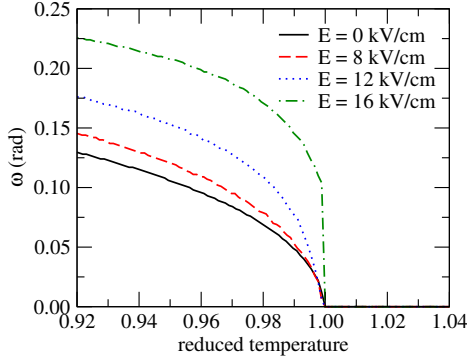

FIG. 4. Variation of the tilt angle ω as a function of the reduced temperature, which is normalized by the temperature at which the η order parameter vanishes, for different electric field values and $\Delta\alpha_p^* < 0$. We can observe that the assumed tilt angle increases as the electric field is applied. In addition, it's possible to notice that there is a change in the nature of the phase transition for high fields.

In Fig. 5, we present the variation of the tilt angle ω as a function of the electric field, for different values of temperature. In Fig. 5(a), for $T < T_{CA}$, which corresponds

to the temperature at which the η order parameter vanishes, we observe an monotonic increase of tilt angle under the influence of an external electric field, reflecting the increase in the order parameter η. More specifically, an almost quadratic growth with the applied field is observed, indicating that the contribution associated with the anisotropy in polarizability predominates over the contribution of the transverse dipole. This behavior persists at temperatures where the smectic-C phase is well established. As the temperature approaches T_{CA}, ω saturates at a maximum value as the field strength increases. This is due to the fact that the second-order Sm-A-Sm-C transition is suppressed at high fields when $T \to T_{CA}$, giving way to the Sm-C-N transition, as shown in Fig. 3(d).
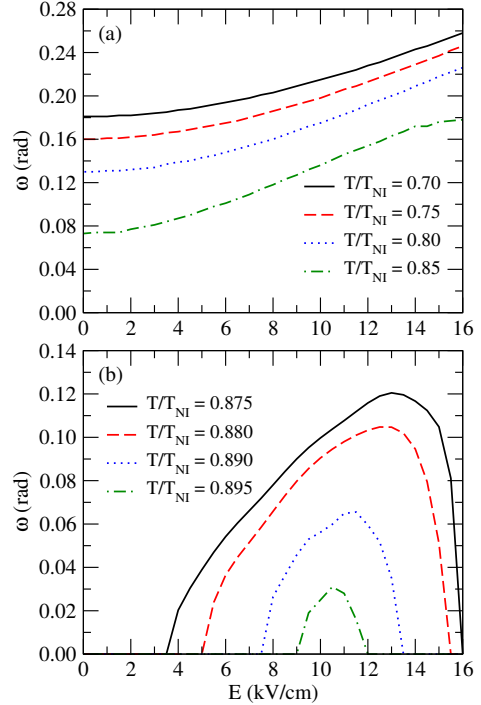

FIG. 5. Variation of the tilt angle ω as a function of the electric field, for different temperatures, with $\Delta\alpha_p^* < 0$. Temperatures (a) below T_{CA} and (b) above T_{CA}. Below T_{CA}, we notice that for smaller fields, the higher the temperature, the greater the variation in the tilt angle value. Above T_{CA}, it's important to notice the reentrant-like behavior around the smectic–C–nematic transition.

The dependence of the tilt angle on the external field exhibits a distinct behavior when $T > T_{CA}$. In particular, the tilt angle remains null until the electric field reaches a threshold value due to the competition between thermal and field effects. This is associated with the molecule's small dipole moment, requiring a stronger electric field to overcome the thermal effects and thus induce tilting. For increasing field strength, the tilt an-

gle is favored up to a certain point. When approaching the smectic–C–nematic phase transition, there is a continuous reduction on the tilt angle, thus representing a reentrant-like behavior.

Fig. 6 presents the phase diagram of temperature versus the applied electric field. The temperature is rescaled by the nematic–isotropic transition temperature, T_{NI}. For low fields, a second-order Sm–C–Sm–A, followed by a Sm–A–N phase transition is present. As the applied field increases, the Sm–A phase is suppressed, due to the reduction in the Sm–A–N and the increase in the Sm–C–Sm–A transition temperatures. Additionally, the representation range of the nematic phase induced by the external field increases. For $E = 15$ kV/cm, a second-order Sm–C–Sm–A phase transition is present, while a first-order Sm–C–fi–N phase transition only takes place for $E > 15$ kV/cm. This indicates that $E = 15$ kV/cm is a critical end point, which corresponds to where the line of continuous Sm–C–Sm–A transition encounters the coexistence line between the Sm–C and the nematic phase.
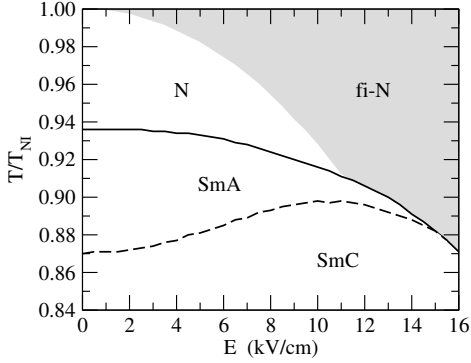

FIG. 6. Phase diagram of the reduced temperature as a function of the applied electric field for $\Delta\alpha_p^* < 0$. For low fields it's possible to notice a second order Sm–C–Sm–A phase transition. As the applied field increases, the Sm–A phase is suppressed, and we can see the representation range of the nematic phase induced by the external field increase. For $E > 15$ kV/cm, we have a continuous phase transition Sm–C–fi–N. Here, the dashed line represents a second order phase transition, and the filled line describes a first order phase transition. The painted part in the figure represents the field-induced nematic phase.

B. Results - Positive Polarizability

Now, we consider a positive polarizability anisotropy ($\Delta\alpha_p^* > 0$). In this configuration, we have opposite contributions associated with the external field: (i) the positive polarizability anisotropy favors molecular alignment along the external field; (ii) the field-dipole interaction tends to reorient molecules perpendicular to the electric field. Such opposite trends may lead to different scenarios for transitions involving the smectic-C.

Fig. 7 presents the variation of the tilt angle ω as a function of electric field, for different temperatures. We note that, differently than for the case of negative polarizability anisotropy, the tilt angle ω decreases under the influence of an external field for a given temperature, with a reduction of its maximum value when the applied electric field increases. This happens because the molecules' major axis tend to align parallel to the field, since the contribution associated with the polarizability anisotropy overcomes the contribution of the transverse dipole.
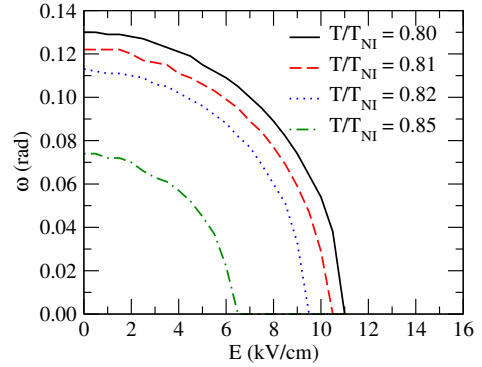

FIG. 7. Variation of the tilt angle ω as a function of the electric field, for different temperatures and $\Delta\alpha_p^* > 0$. We notice that the tilt angle decreases under the influence of the external electric field, and the maximum tilt angle assumed also decreases as the temperature approaches the transition temperature.

Fig. 8 shows the temperature dependence of s, σ and η order parameters, for different values of the electric field strength. For $E = 4$ kV/cm (Fig. 8(b)), the electric field suppresses the isotropic phase, giving rise to an field-induced nematic phase. Additionally, the temperature-range of the smectic–C phase reduces, while the smectic–A phase is favored by the external field. For increasing field strength, we notice a reduction in the nematic-isotropic transition discontinuity (Fig. 8(c)). In this case, the nature of the Sm–C–Sm–A and Sm–A–N transitions remain the same, as second and first order transitions, respectively. For a sufficiently high field strength (Fig. 8(d)), the discontinuity in the orientational order parameter disappears, due to the suppression of the liquid isotropic phase. Moreover, we can see that the tilt angle assumed by the smectic–C phase decreases as the electric field increase, contrary to the behavior for $\Delta\alpha_p^* < 0$.

Finally, Fig. 9 presents the phase diagram for $\Delta\alpha_p^* > 0$. We note that the smectic–A phase is favored, while the smectic–C phase is suppressed with increasing field strength. Under the influence of an external electric field, a residual nematic phase appears, favoring the phase for increasing field, while suppressing the isotropic phase. However, the liquid isotropic phase is present for low field strengths. The phase diagram permits the charac-
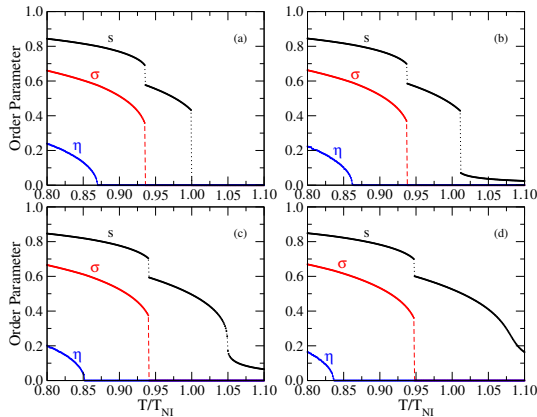
FIG. 8. Variation of the orientational s, translational σ, and tilt η order parameters as a function of the reduced temperature for different values of electric field and $\Delta\alpha_p^* > 0$. (a) $E = 0$ kV/cm, (b) $E = 4$ kV/cm, (c) $E = 6$ kV/cm and (d) $E = 8$ kV/cm. For $E = 4$ kV/cm, it's possible to notice the appearance of a nematic residual phase under the influence of the external electric field. For $E = 6$ kV/cm, we can already to observe the reduction of the smectic–C phase and an increase in the range of the smectic–A phase. It is important to notice that the nematic phase suppresses the liquid isotropic phase. Moreover, in 8(d), we can see that the tilt angle assumed by the smectic–C phase decrease as the electric field increase.

terization of the phase transitions, where a second-order smectic-C–smectic-A phase transition and a first-order smectic-A–nematic phase transition is present for all values of the external electric field strength.

III. SUMMARY AND CONCLUSIONS

ACKNOWLEDGMENTS

[1] C. Rosenblatt, J. Physique Lett. **42**, 9 (1981).
[2] C. Rosenblatt, Phys. Lett. A **83**, 221 (1981).
[3] H. Hama, J. Phys. Soc. Jpn. **54**, 2204 (1985).
[4] I. Lelidis, M. Nobili, and G. Durand, Phys. Rev. E **48**, 3818 (1993).
[5] I. Lelidis and G. Durand, Phys. Rev. E **48**, 3822 (1993).
[6] I. Lelidis and G. Durand, Phys. Rev. Lett. **73**, 672 (1994).
[7] A. Mochizuki, J. Mol. Liq. **267**, 456 (2018).
[8] L. Sirleto, G. Coppola, A. D'Agata, G. Breglio, and A. Cutolo, in Integrated Optics Devices V, Vol. 4277, International Society for Optics and Photonics (SPIE, 2001) pp. 320 – 327.
[9] R. Cassano, R. Dąbrowski, J. Dziaduszek, S. Trombino, F. Iemma, F. P. Nicoletta, G. D. Filpo, and N. Picci, Liq. Cryst. **35**, 625 (2008).
[10] A. Nagai, H. Kondo, Y. Miwa, T. Kondo, S. Kutsumizu, Y. Yamamura, and K. Saito, B. Chem. Soc. Jpn. **91**, 1652 (2018).
[11] V. G. Guimarães, J. Wang, S. Planitzer, K. Fodor-Csorba, R. S. Zola, and A. Jákli, Phys. Rev. Appl. **10**, 064008 (2018).
[12] L. Sirleto, G. Coppola, G. C. Righini, and G. Abbate, Fiber Integrated Opt. **25**, 175 (2006).
[13] P. de Gennes and J. Prost, The Physics of Liquid Crystals (Clarendon Press, 1993).
[14] I. Khoo and S. Wu, Optics and Nonlinear Optics of Liquid Crystals (World Scientific, 1993).

[15] T. Ostapenko, D. B. Wiant, S. N. Sprunt, A. Jákli, and J. T. Gleeson, Phys. Rev. Lett. **101**, 247801 (2008).
[16] I. Lelidis, Phys. Rev. Lett. **86**, 1267 (2001).
[17] B. Wen and C. Rosenblatt, Phys. Rev. Lett. **89**, 195505 (2002).
[18] A. Rapini, J. Phys. France **33**, 237 (1972).
[19] R. B. Meyer, L. Liebert, L. Strzelecki, and P. Keller, J. Physique Lett. **36**, 69 (1975).
[20] R. B. Meyer, Mol. Cryst. Liq. Cryst. **40**, 33 (1977).
[21] S. T. Lagerwall and I. Dahl, Mol. Cryst. Liq. Cryst. **114**, 151 (1984).
[22] L. A. Beresnev, L. M. Blinov, M. A. Osipov, and S. A. Pikin, Molecular Crystals and Liquid Crystals Incorporating Nonlinear Optics **158**, 1 (1988).
[23] F. Tournilhac, L. M. Blinov, J. Simon, and S. V. Yablonsky, Nature **359**, 621 (1992).
[24] T. Niori, T. Sekine, J. Watanabe, T. Furukawa, and H. Takezoe, J. Mater. Chem. **6**, 1231 (1996).
[25] M. Hird, Liq. Cryst. **38**, 1467 (2011).
[26] S. T. Lagerwall, Ferroelectrics **301**, 15 (2004).
[27] S. Garoff and R. B. Meyer, Phys. Rev. A **19**, 338 (1979).
[28] S.-D. Lee and J. S. Patel, Appl. Phys. Lett. **54**, 1653 (1989).
[29] M. S. Spector, P. A. Heiney, J. Naciri, B. T. Weslowski, D. B. Holt, and R. Shashidhar, Phys. Rev. E **61**, 1579 (2000).
[30] K. Skarp, G. Andersson, T. Hirai, A. Yoshizawa, K. Hiraoka, H. Takezoe, and A. Fukuda, Jpn. J. Appl. Phys.
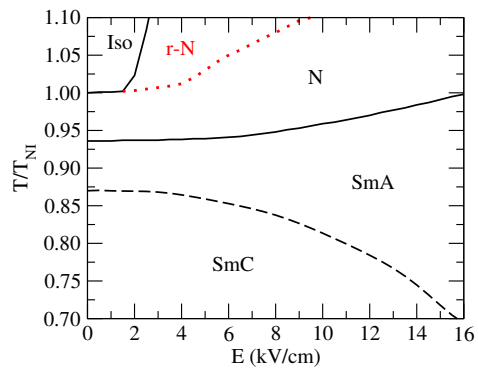
FIG. 9. Phase diagram of the reduced temperature as a function of the applied electric field for $\Delta\alpha_p^* > 0$. Here, it is possible to observe that for low fields we have the liquid isotropic phase present in the phase diagram. As the electric field increases, we notice the appearance of a nematic residual phase (r-N) represented by the dotted red line, causing the disappearance of the liquid isotropic phase for high fields. Moreover, the smectic–A phase suppresses the smectic–C phase as the applied electric field increases. Here, the dashed line represents a second order transition, and the filled line represents the first order transition.

31, 1409 (1992).

[31] E. Meirovitch, Z. Luz, and S. Alexander, Phys. Rev. A **15**, 408 (1977).

[32] P. Schiller and G. Pelzl, Cryst. Res. Technol. **18**, 923 (1983).

[33] G. Pelzl, P. Schiller, and D. Demus, Liq. Cryst. **2**, 131 (1987).

[34] E. Meirovitch, Z. Luz, and S. Alexander, Mol. Phys. **37**, 1489 (1979).

[35] A. S. Govind and N. V. Madhusudana, Eur. Phys. J. E **9**, 107 (2002).

[36] S. Pestov, Physical Properties of Liquid Crystals, Advanced Materials and Technologies (Springer-Verlag, 2003).